WASHINGTON UNIVERSITY
DEPARTMENT OF PHYSICS

Thesis Committee:

James G. Miller, Chairman
James H. Burgess
Edwin T. Jaynes
Robert A. King
James W. Mimbs
Richard E. Norberg
Lewis J. Thomas, Jr.

ELECTRON-PHONON INTERACTIONS IN PIEZOELECTRIC SEMICONDUCTORS FOR THE PHASE INSENSITIVE DETECTION OF ULTRASOUND

by

Lawrence J. Busse

A dissertation presented to the
Graduate School of Arts and Sciences
of Washington University in
partial fulfillment of the
requirement for the degree of
Doctor of Philosophy

December, 1979

Saint Louis, Missouri

TABLE OF CONTENTS

TABLE OF CONTENTS
(continued)

TABLE OF CONTENTS
(continued)

LIST OF FIGURES

LIST OF FIGURES
(continued)

LIST OF FIGURES
(continued)

LIST OF FIGURES
(continued)

LIST OF FIGURES
(continued)

LIST OF TABLES

ACKNOWLEDGMENTS

I would like to thank Professor James G. Miller for the total support and confidence he has shown towards me in my years of graduate study at Washington University. From a personal and professional point of view, I feel that the six years I have spent in St. Louis have been very rewarding and Jim has played a large role in providing a stimulating atmosphere in which to live and work. I am also indebted to all of the other member of the faculty and staff of the physics department for providing many interesting courses, discussions and a genuinely positive environment in which to work.

A special note of thanks is also extended to member of the faculty of the medical school, Drs. Sobel, Weiss and Mimbs. Their interest in ultrasound measurement and imaging problems provided the impetus for much of this work.

There are also many past and present members of the Laboratory for Ultrasonic to which I will always be grateful. Don Yuhas was very helpful in the early experimental attempts at observing and applying the acoustoelectric effect. The critical and constructive comments provided by Dennis Dietz at the outset of this project were also appreciated. Matt O'Donnell, John Klepper and Gary Brandenburger have all been valuable collaborators and have contributed greatly to every aspect of this work. I also wish to thank Tom Shoup, Jack Mottley and Tom Thomas for their assistance and patience when I was monopolizing the experimental equipment.

A note of thanks is extended to Pranoat Suntharothok-Priesmeyer for her expertise and professional support in the production of this and other manuscripts.

I owe so much to my parents, John and Grace, and I am truly indebted to them for their encouragement and support. To be curious, persistent, and to have a positive outlook on life are just a few of the many valuable lessons that they have taught to me.

Finally, a special word of thanks is given to my wife Faye. Her patience, sacrifice, and encouragement have been unlimited in seeing me through graduate school and I will always be indebted to her.

I. INTRODUCTION

The requirement of detecting distorted or spatially nonuniform waves is a problem encountered in many physical situations where initially coherent signals are transmitted through an inhomogeneous or turbulent medium. This problem has placed limits on many physical measurements which are based upon the detection of a wave disturbance over a finite receiver aperture. For example, in optical and radio astronomy the determination of the angular size of many astronomical sources has been limited by wave distortion introduced by the earth's atmosphere and not by the diffraction limit imposed by the telescope's aperture.[1] To overcome these limitations, experimental techniques such as intensity correlation[2] (intensity interferometer), active phase correction[3] (rubber mirror) and intensity deconvolution[4,5] (speckle interferometry) have been proposed and tested. In the field of physical acoustics, researchers have long been aware of the problems associated with making quantitative measurements in the presence of wavefront distortion.[6-9] To minimize these problems, specimens were necessarily limited to materials which possess uniform elastic properties and which could be prepared flat and parallel. More recent efforts to apply ultrasound to the areas of quantitative imaging[10] and materials characterization[11] require a reevaluation of the problems associated with detecting and making quantitative measurements upon distorted wavefronts. Frequently, specimens of interest are by their very nature inhomogeneous or irregular in shape and thus wave distortion is inevitable. In this thesis, we describe a method of ultrasonic

detection which is insensitive to measurement errors caused by wavefront distortion. This detection technique allows quantitative ultrasonic determinations to be made on inhomogeneous and irregular materials using pulsed ultrasound. The technique also allows the limitations of conventional phase sensitive receivers to be assessed objectively.

The approach we investigate is based upon the nonlinear interaction of ultrasonic waves with the conduction electrons present within a single crystal piezoelectric semiconductor. This interaction, known as the acoustoelectric effect, makes it possible to produce large aperture, phase insensitive receiving transducers which have broad ultrasonic frequency response, good response time ($\sim 10^{-6}$ second), modest sensitivity ($\sim 10^{-6}$ watts/cm^2), and most importantly are insensitive to wavefront distortion.

In Chapter II we describe the physical principles underlying the acoustoelectric effect. Using the linear or small signal theory of the acoustoelectric effect we describe the effects of finite conductivity upon the propagation of ultrasonic waves within a piezoelectric semiconductor. We also investigate the nonlinear interaction of piezoelectrically induced carrier waves with piezoelectric fields.

In Chapter III we discuss the electrical properties of piezoelectric semiconductors. The time and frequency dependence of both the acoustoelectric and piezoelectric response of these materials to various forms of ultrasonic excitations is considered. Criteria are presented for the optimization of the acoustoelectric signal generated

by a piezoelectric semiconductor in response to transient and continuous wave ultrasonic radiation.

In Chapter IV we discuss the response of finite aperture piezoelectric and acoustoelectric receivers to non-uniform ultrasonic illumination. We focus primarily upon the fundamental differences in the detection properties associated with phase sensitive (piezoelectric) and phase insensitive (acoustoelectric) receivers. A number of experiments designed to illustrate these differences are proposed and discussed.

In Chapter V the experimental methods used to prepare single crystals of CdS as acoustoelectric receivers are presented. Various electrical circuits designed to facilitate the observation and utilization of the acoustoelectric effect are discussed. A number of ultrasonic calibration schemes are compared as a means of determining the absolute sensitivity (noise equivalent power) of a receiving transducer based on the acoustoelectric effect.

The results of electrical and ultrasonic measurements made upon CdS are presented in Chapter VI. Major emphasis is placed upon determination of the response time, ultrasonic bandwidth, and ultimate sensitivity associated with the acoustoelectric response of CdS. Application of the acoustoelectric effect as a phase insensitive receiver in attenuation and scattering measurements as well as tomographic imaging based on ultrasonic attenuation are demonstrated. A brief summary of the entire project is found in Chapter VII.

II. THEORY OF THE ACOUSTOELECTRIC EFFECT

A. Introduction

The acoustoelectric effect provides the physical basis for a phase insensitive ultrasonic transducer. In this chapter we present a treatment of the theory of the acoustoelectric effect. The acoustoelectric effect refers to the interaction of electrons and phonons in a material where there exists some mechanism which can couple the electrical properties to the mechanical properties.[12,13] Classically, the acoustoelectric effect can be described as a wave-particle drag phenomenon. The waves involved are stress waves associated with the propagation of ultrasonic energy and the particles are conduction electrons which are free to move under the influence of an applied force.

The acoustoelectric effect can be observed either as a change in the steady state current flowing through a material brought about by the presence of a propagating ultrasonic wave, or as a change in the propagation parameters of the ultrasonic wave brought about by some modifications in the electrical state of the material. Historically the later of these manifestations of the acoustoelectric effect has received the most attention because of the potential for attaining acoustic amplification (i.e., a negative ultrasonic attenuation coefficient).[14-18] The former manifestation of the acoustoelectric effect, has been receiving attention recently because it provides a sensitive tool for studying the details of electron phonon interactions[19-22] and because of the potential applicability in the area of phase insensitive ultrasonic detection.[23-29]

In this chapter we first present a plausibility argument, based upon the conservation of energy and momentum, by which we can derive the functional form of the acoustoelectric effect (i.e., the Weinreich relation).[30] This plausibility argument is completely general in that it is valid for any mechanism by which phonons and conduction electrons can interact. In the second part of this chapter we investigate the details of a particularly efficient coupling mechanism, the piezoelectric effect. We present a small signal (i.e., linearized) theory describing the acoustoelectric effect in piezoelectric semiconductors. Finally we discuss the nonlinear interaction of piezoelectrically induced carrier waves with piezoelectric fields.

B. Plausibility of the Acoustoelectric Effect

The acoustoelectric effect results in the production of an electric current by an acoustic wave. To be more specific, as an ultrasonic wave propagates through a material in which conduction electrons are present, a dc current can be generated along the direction of propagation of the acoustic wave.

The effect can be made plausible by considering a system of phonons (acoustic waves) incident upon and interacting with a system of electrons. As the electrons and the phonons interact, the electrons can either drain energy and momentum from the acoustic wave or supply energy and momentum to the acoustic wave. This interaction causes a change in the net momentum of the system of electrons in the direction of the wave propagation, thereby causing a detectable current.

Let us assume that the acoustic wave carries an energy density which may be expressed as $W = v_s p_s$, where v_s and p_s are the velocity and momentum density associated with the sound wave. Also assume that the spatial dependence of the energy density of the acoustic wave is describable in terms of an attenuation coefficient α_E so that $W(x) = W_o e^{-2\alpha_E x}$ where W_o is the original energy density. The spatial rate of change of the energy density is then

$$\frac{dW}{dx} = v_s \frac{dp_s}{dx} = \frac{dp_s}{dt} = -2\alpha_E W \qquad \text{(II.1)}$$

and can simply be interpreted as a net force exerted by the acoustic wave upon the conduction electrons. Conservation of momentum requires that

$$\frac{dp_s}{dt} + \frac{dp_e}{dt} = 0 \qquad \text{(II.2)}$$

where p_e is the momentum density of the electron system. Therefore the net force acting upon the system of conduction electrons is

$$\frac{dp_e}{dt} = 2\alpha_E W \qquad \text{(II.3)}$$

We can recast this force in terms of an effective electric field which we will call the acoustoelectric field E_{AE}. In terms of this effective field,

$$\frac{dp_e}{dt} = -nq\, E_{AE} = 2\alpha_E W \qquad \text{(II.4)}$$

where n is the number density of electrons and q is the electronic charge. The current caused by this effective field can be found using Ohm's Law $(J_{AE} = \sigma E_{AE})$,

$$J_{AE} = \frac{\sigma}{nq} 2\alpha_E W = -2\mu\alpha_E W \quad . \qquad \text{(II.5)}$$

where μ is the electron mobility. Let us further speficy that the acoustic wave can be described as a plane wave. In this case $W = \Phi/v_s$ where Φ is the intensity of the plane wave and

$$J_{AE} = -2\mu \frac{\alpha_E}{v_s} \Phi \quad . \qquad \text{(II.6)}$$

Here we see that the presence of an acoustic wave of intensity Φ in the material results in a net force on the conduction electrons present which in turn gives rise to an electrical current.

This model of the acoustoelectric effect is helpful for getting an overall view of the interaction of acoustic waves with conduction electrons but gives us no insight into the details of the interaction. The physics of the acoustoelectric effect is tied up with the wave propagation parameters v_s and α_E. To gain any further knowledge about the size or functional form of these parameters, a specific coupling mechanism must be proposed.

C. Acoustic Waves in Piezoelectric Semiconductors: Small Signal Theory

The piezoelectric effect has provided a strong coupling mechanism for studying the interaction of electron and phonons in semiconductors. A number of piezoelectric semiconductors are known. Some of these piezoelectric semiconductors are photosensitive and have made it

possible to easily study the conductivity dependence of the acousto-electric effect. Cadmium sulfide has been the most common of the piezoelectric photoconductors studied for three reasons: i) the piezoelectric effect is strong (CdS has a higher electromechanical coupling than quartz),[31-33] ii) the conductivity of CdS can be varied over many orders of magnitude by exposing it to light (CdS is an insulator in the dark), and iii) large single crystal samples of CdS can be grown conveniently.[34,35]

A general treatment of wave propagation in piezoelectric materials can be developed using a coupled wave theory. The fact that mechanical deformations produce electrical polarization within a piezoelectric material make it necessary to find simultaneous solutions of Newton's force law and Maxwell's field equations in order to describe wave propagation. A formal treatment of acoustic wave propagation in piezoelectrics of finite conductivity was first presented by Kyame[36] and his results are summarized in Appendix A. Kyame showed that the effect of piezoelectric coupling and finite conductivity on the acoustic waves was small and could effectively be handled with a slight modification of the elastic constants. A further reduction in complexity of the acoustic problem can be gained because for certain modes of wave propagation the interaction between piezoelectricity and the charge carriers can be effectively discussed in terms of a one-dimensional model. (See Appendix A for details).

Assuming that a one dimensional model of acoustic wave propagation is adequate for discussing the essential features of the acousto-electric interaction in cadmium sulfide, let us consider the propagation

of a longitudinal acoustic plane wave parallel to the "c" crystalline axis. The z components of the mechanical variables of interest, stress T_3, strain S_3, and particle displacement ξ_3, are defined as follows

$$S_3 = \frac{\partial \xi_3}{\partial z} \quad \text{and} \quad \frac{\partial T_3}{\partial z} = \rho \frac{\partial^2 \xi_3}{\partial t^2} \quad , \tag{II.7}$$

where ρ is the mass density. All of these mechanical variables are implicitly functions of time and position within the crystal. In our one dimensional plane wave model we assume a harmonic space and time dependence $\exp[i(kz-\omega t)]$ for these variables. The equations of state needed to derive a wave equation, are the piezoelectric constitutive relations. These relations provide the coupling between the mechanical fields (stress T and strain S) and the electrical field electric field E, and displacement D). The particular form of these relations we use is

$$\begin{aligned} T_3 &= c_{33}^E S_3 - e_{33} E_3 \\ D_3 &= \varepsilon_{33}^S E_3 + e_{33} S_3 \end{aligned} \tag{II.8}$$

where c_{33}^E is the mechanical stiffness measured at constant field, ε_{33}^S is the dielectric constant of the material measured at constant strain, e_{33} is the piezoelectric coupling constant. Once again, we are assuming harmonic space and time dependence for all of the field variables.

The semiconducting properties of the material can be modeled with the following three electrical equations

i) Ohm's Law

$$J_3 = \sigma_{33} E_3' \tag{II.9}$$

ii) Gauss' Law

$$\frac{\partial D_3}{\partial z} = -qn \tag{II.10}$$

iii) Continuity of Charge

$$\frac{\partial}{\partial z} J_3 = q \frac{\partial n}{\partial t} \tag{II.11}$$

$J_3 \equiv \mu q n_T$

where J_3 is the current density. The crystal conductivity σ_{33} is defined to be the product of the carrier mobility μ, the electronic change q, and the total number of charge carriers per unit volume n_T. The electric field E_3' is the total electric field experienced by the crystal and may be composed of an external bias field E_0 and internally generated piezoelectric field E_3. In this small signal or linear theory of the acoustoelectric effect we will assume that the number density of charge carriers can be described as having a large dc component n_0 and a small ac component n caused by the influence of piezoelectrically induced electric fields. By ignoring terms which are of second order in small quantities, these three electrical constraints [Eqs. (II.9)-(II.11)] can be reduced to a single equation describing the electric field,

$$ikD_3 = \frac{\sigma}{\left(\frac{\omega}{k} + E_0\mu\right)} E_3 \tag{II.12}$$

Equations (II.7), (II.8), and (II.12) now provide us with four linear equations in the four unknown field parameters: D_3, E_3, S_3, and T_3. A solution to this system of equation exists if the determinant of the coefficients is equal to zero,

$$\begin{vmatrix} ik & -\dfrac{\sigma}{\left(\dfrac{\omega}{k} + E_0\mu\right)} & 0 & 0 \\ 1 & -\varepsilon & -e & 0 \\ 0 & e & -c & 1 \\ 0 & 0 & -\rho\omega^2 & k^2 \end{vmatrix} = 0 \quad . \qquad (II.13)$$

This condition leads us to the following secular equation

$$\left\{\frac{k}{\omega}\right\}\left\{\left(1 + \frac{E_0\mu k}{\omega}\right)\left(\frac{k^2}{\omega^2}\left(1 + \frac{e^2}{c\varepsilon}\right) - \frac{\rho}{c}\right) + \frac{i\sigma}{\omega\varepsilon}\left(\frac{k^2}{\omega^2} - \frac{\rho}{c}\right)\right\} = 0 \quad . \qquad (II.14)$$

One trivial root to this secular equation is $(k/\omega) = 0$. This root corresponds to a mode of excitation of the system which does not propagate. The remaining equation is cubic in k/ω and describes three modes of excitation which do propagate but are not independent of one another. Some physical insight into the solution of the coupled wave problem can be gained by examining the secular equation in the absence of the piezoelectric effect. In that case the secular equation becomes

$$\left(1 + \frac{\varepsilon E_0 k}{\omega} + \frac{i\sigma}{\omega\varepsilon}\right)\left(\frac{k^2}{\omega^2} - \frac{\rho}{c}\right) = 0 \quad . \qquad (II.15)$$

In this limit, the secular determinant factors (i.e., the three modes of excitation uncouple) and is easily solved:

$$k_A^{\pm} = \pm\omega\sqrt{\frac{\rho}{c}} \longrightarrow v_s = \sqrt{\frac{c}{\rho}}$$

$$k_E = -\frac{\omega}{\mu E_o} - i\frac{\sigma}{\varepsilon\mu E_o} \quad . \tag{II.16}$$

Two modes of propagation, k_A^+ and k_A^-, correspond to acoustic waves propagating in the positive and negative direction with the velocity of sound v_s. The third mode of propagation corresponds to the propagation of the bunched electrons in a direction opposite that of the applied bias field E_o with a velocity equal to the drift velocity $v_D=-\mu E_o$. This wave of bunched electrons is damped out at a rate which is proportional to the conductivity relaxation frequency (σ/ε) of the material.

Some physical insight into behavior of the coupled wave system can be gained if we look at the cubic secular equation in the limit of weak piezoelectric coupling. We would like to investigate the effect of piezoelectric coupling upon the acoustic propagation modes. In order to do this, we can expand the acoustic root k_A^+/ω about its uncoupled value $1/v_s$,

$$\frac{k_A^+}{\omega} = \frac{1}{v_s} + A + iB \quad . \tag{II.17}$$

Here A and B represent small correction terms to our original uncoupled solution. By substituting this equation into the original cubic secular equation and ignoring terms which are quadratic in correction terms A and B we are able to reduce the problem to a simultaneous set of two

equations in the two correction terms. We find that the weakly coupled wavevector k_A^+ has the following components

$$v = v_s \left\{ 1 + \frac{e^2}{2c\varepsilon} \frac{1}{\left(1 + \frac{\omega_c/\omega}{(1 - (v_D/v_s))} \right)^2} \right\}$$

$$\alpha_E = \frac{\omega}{v_s} \frac{e^2}{2c\varepsilon} \left\{ \frac{\frac{\omega_c}{\omega}\left(1 - \frac{v_D}{v_s}\right)}{\left(1 - \frac{v_D}{v_s}\right)^2 + \left(\frac{\omega_c}{\omega}\right)^2} \right\} \qquad \text{(II.18)}$$

where ω_c is the conductivity relaxation frequency. The imaginary part of the wavevector α_E is the electronic attenuation coefficient and describes the rate at which electrons and phonons exchange energy. These results are essentially those first derived by Hutson and White.[37] We have made the simplifying assumption that the electromechanical coupling coefficient k_T^2 is small compared to unity. This coupling coefficient is an index of the strength of the piezoelectric effect in a particular material. The dielectric constants measured under free and clamped conditions (ε^T and ε^S, respectively) are related to the mechanical stiffness constants measured under open and short circuit conditions (c^E and c^D, respectively) in the following way: $(c^D - c^E)/c^D = (\varepsilon^T - \varepsilon^S)/\varepsilon^T = k_T^2$. For weakly coupled materials such as cadmium sulfide, we are justified in assuming that

$$\frac{e^2}{c\varepsilon} = k_T^2/(1-k_T^2) \approx k_T^2 \quad .$$

In Figure II.1 the velocity of sound and the electronic attenuation coefficient are plotted as a function of the drift velocity v_D for a fixed crystal conductivity σ. For no bias field applied ($v_D = 0$) we see

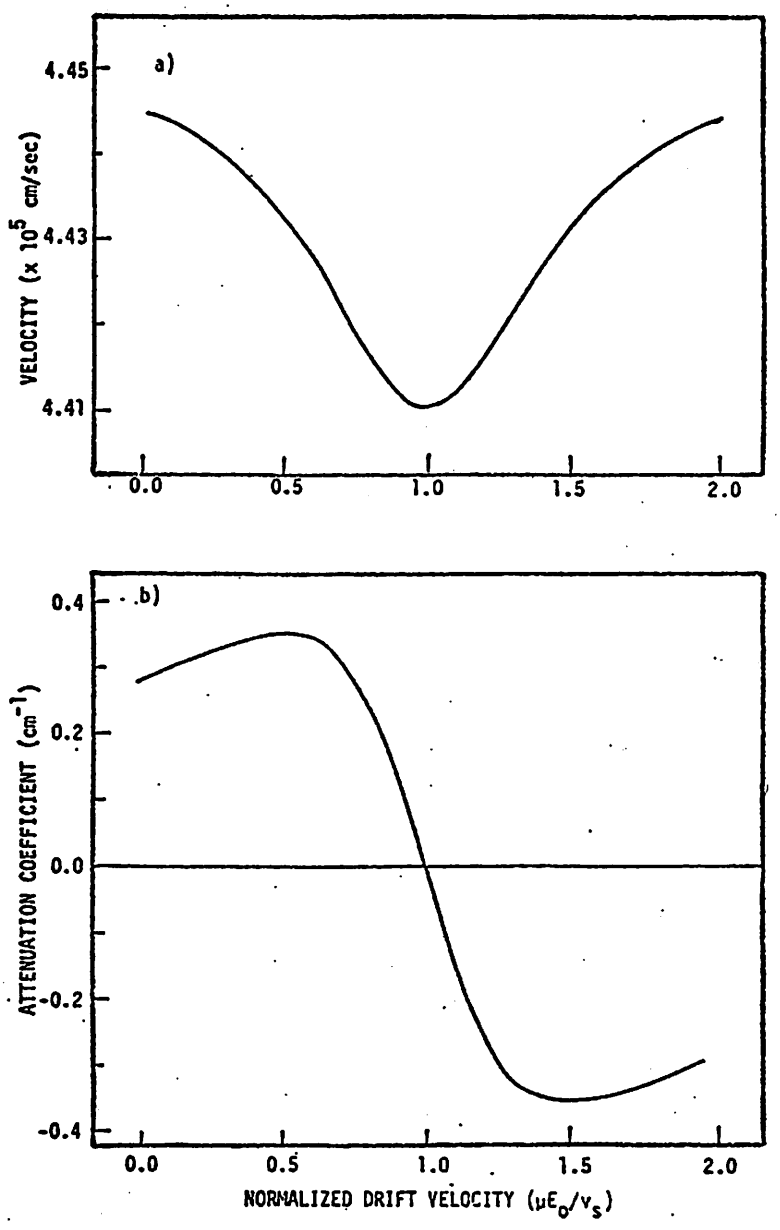

Figure II.1. Velocity and attenuation coefficient versus drift velocity in a weakly coupled piezoelectric semiconductor. The drift velocity has been normalized by the velocity of sound in the material. The small signal theory of the acoustoelectric effect [Eq. (II.18)] was evaluated using the electrical and mechanical properties of cadmium sulfide found in Table I; ω_c/ω was assumed to be 0.5.

that there is a finite amount of energy lost by the acoustic wave to the system of conduction electrons and that the velocity of the acoustic wave approaches the piezoelectrically stiffened limit. As the drift velocity of conduction electrons goes to the velocity of sound we see that the velocity of the acoustic wave approaches its unstiffened limit and that the attenuation coefficient goes to zero. This behavior is plausible because from the frame of reference of the conduction electrons the doppler shifted acoustic frequency has gone to zero. As the drift field is increased even further (drift velocity greater than the velocity of sound) we see that the velocity of sound returns to the piezoelectrically stiffened limit and that the electronic attenuation coefficient goes negative. In this limit, the conduction electrons are pumping energy coherently into the acoustic waves. This behavior of the attenuation coefficient with drift field provides the basis for acoustic amplification.[14-19]

In Figure II.2 we show the conductivity dependence of α_E and v with no drift field applied ($v_D = 0$). In the low conductivity (insulator) limit, we see that the velocity of sound approaches the piezoelectrically stiffened limit and that very little attenuation of the sound by conduction electrons takes place. There are very few conduction electrons available to participate in any interaction. In the high conductivity (metal) limit we find that the velocity of sound approaches the unstiffened limit and that the electronic attenuation coefficient approaches zero. In this limit, the conductions electrons are able to move rapidly enough within the crystal to effectively "short out" the electric fields which accompany the acoustic disturbance. For some intermediate range of crystal

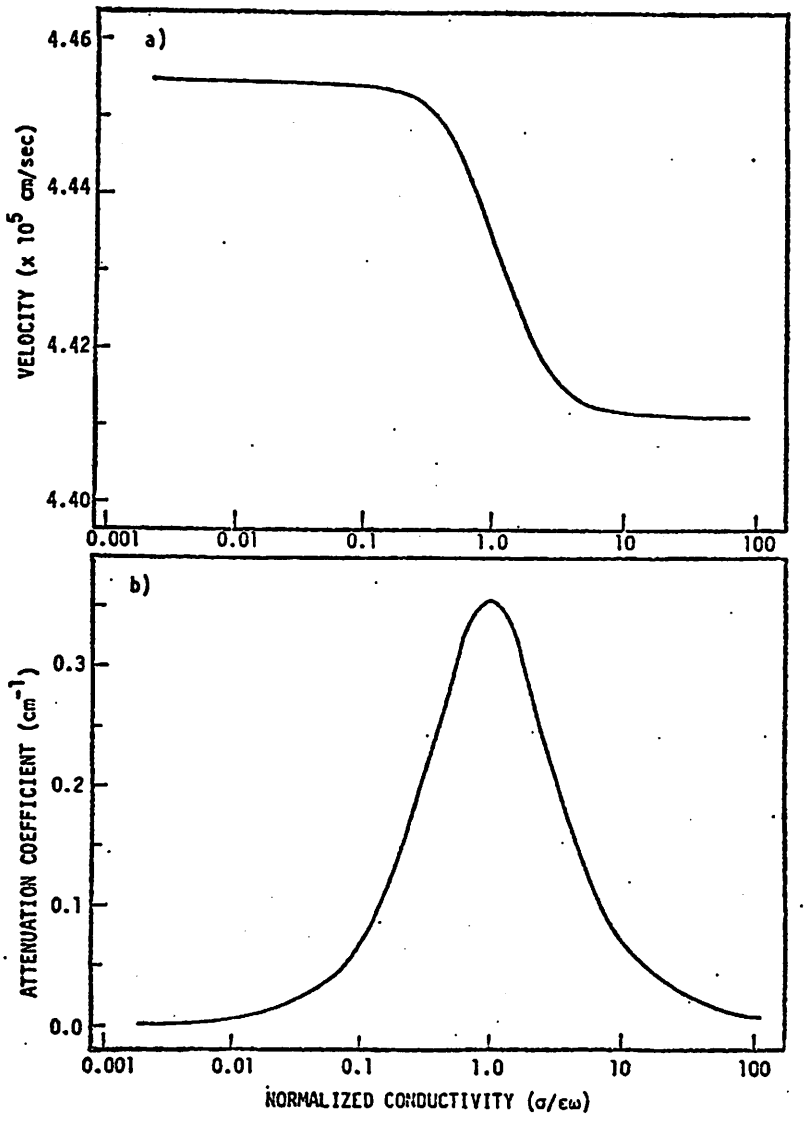

Figure II.2. Velocity and attenuation coefficient versus conductivity in a weakly coupled piezoelectric semiconductor. The crystal conductivity relaxation frequency has been normalized by the ultrasonic frequency. The small signal theory of the acoustoelectric effect [Eq. (II.18)] was evaluated using the electrical and mechanical properties of cadmium sulfide found in Table I; the drift velocity, $v_D = -\mu E_0$, was chosen to be zero.

$\sigma = \mu q \cdot n_7$

conductivities we find that there is a peak in the electronic attenuation coefficient. The physical basis of the attenuation maximum is that the piezoelectric fields are trying to "bunch" conduction electrons on about the same time scale as the electrons are trying to "unbunch" due to Coulomb repulsion. This process for transfer of energy between the electrical system and the mechanical system is a classical relaxation process. (Another relaxation process based upon diffusion also exists in piezoelectric semiconductors. Diffusion effects have been omitted for the development as presented here because they are only effective at coupling energy out of the ultrasonic system at frequencies in the 10^9 Hz range.) The "sinusoidal" electric fields accompanying the acoustic wave cause a "sinusoidal" electron bunching. Because of the finite conductivity of CdS, the spatial distribution of electric fields and bunched electrons is phase shifted relative to the elastic deformations. This phase lag results in the irreversible transfer of energy between the acoustic and electronic systems.

Explanation of 2nd order effect

The exact phase relationship between the bunched carrier wave n, the piezoelectric field E_3, and the elastic strains S_3, can be obtained by going back to the original set of Eqs. (II.7), (II.8), and (II.12) and solving for the field parameters explicitly. After some algebra we find that

$$n = \frac{e\omega_c}{qv_s} \frac{S_3}{\left(1 - \frac{v_D}{v_s}\right) + i\,\frac{\omega_c}{\omega}} = -\frac{\sigma}{qv_s} \frac{E_3}{\left(1 - \frac{v_D}{v_s}\right)} \quad . \qquad \text{(II.19)}$$

We are now in a position to evaluate the validity of this small signal theory. The major assumption made so far has been that the effects of the ac conductivity, or bunched electrons n, upon the propagation of an acoustic wave is small compared to the effects of the dc conductivity or static electron distribution. In other words

$$\left|\frac{n}{n_o}\right| \ll 1 \quad . \tag{II.20}$$

Evaluating this ratio at maximum attenuation ($\omega_c/\omega = 1$) and zero drift field ($v_D = 0$) leads us to the condition

$$S_3 \ll \frac{\sqrt{2}\, v_s \varepsilon}{\mu e} \quad . \tag{II.21}$$

Plugging in physical parameters typical of CdS we find that the strain amplitude must be much less than 3×10^{-5} for the small signal theory to be valid. This corresponds to acoustic intensities present within the crystal less than approximately 16 watts/cm^2. A limit of approximately 1 watt/cm^2 was not exceeded for the measurements reported later in this thesis.

D. Acoustic Waves in Piezoelectric Semiconductors: Higher Order Effects

In the previous section we found that for low acoustic energy densities, we are justified in ignoring the effect of the ac conductivity (i.e., bunched electrons) upon the wave propagation parameters ($k = \omega/v_s + i\alpha_E$) within a piezoelectric semiconductor. This is not to say, however, that effect of the bunched electrons is negligible. The interaction of the bunched electrons with the piezoelectric fields

associated with the traveling acoustic waves is the origin of the acoustoelectric signal.

1. Acoustoelectric Current

The nonlinear term in the current density E_3 can be calculated to lowest order using the results of the linear theory of the previous section. In general, n and E_3 represent quantities which vary harmonically in space and time. Let us call the average of the nonlinear current density the acoustoelectric current J_{AE},

$$J_{AE} = \langle q\mu n E_3 \rangle = q\mu \frac{1}{2} \mathrm{Re}(n \cdot E_3^*) \quad . \tag{II.22}$$

From Eq. (II.19) we see the J_{AE} is proportional to the square of the strain associated with the acoustic wave. Upon substitution of Eqs. (II.19) into (II.22) and by making use of Eq. (II.18) we find that

$$J_{AE} = -2\mu\alpha_E W = -2\mu\alpha_E \frac{\Phi}{v_s} \quad . \tag{II.23}$$

The current generated by the nonlinear interaction of the piezoelectric field with the bunched electrons distribution gives rise to a current which is directly proportional to the rate of energy exchange from the acoustic wave to the electron distribution, α_E, and the instantaneous acoustic intensity Φ. This result is identical with that first obtained by Weinreich.[30]

The theoretical value for the wave propagation parameters α_E and v now allow us to estimate the order of magnitude of the acoustoelectric current. Using values for the material properties of CdS found in

Table I and assuming an incident ultrasonic intensity of 1 watt/cm^2 and a cross sectional area of 1 cm^2 we estimate I_{AE} at five megahertz to be on the order of 500 microamps. This current is sufficiently large to be observable and provides the basis for the application of the acousto-electric effect as an ultrasonic receiving transducer.

2. Strongly Coupled Piezoelectric Semiconductors

So far we have limited our discussion to the interaction of free charges and acoustic waves in weakly coupled piezoelectric semiconductors, i.e., materials such as cadmium sulfide in which $e^2/c\varepsilon \ll 1$. In this limit, the effect of piezoelectricity upon the wavenumber k_A is small and we are able to determine the magnitude of the effect upon wave propagation by using the simple approximation discussed in Section C. It is conceivable however, that more strongly coupled piezoelectric materials might become available in which this approximation is no longer valid. At present no single material with both semiconducting and strong piezoelectric coupling is available. However, based on the work of Fischler[38] and others,[39-41] it does seem possible to develop a composite device, consisting of a layered structure of separate piezoelectric material and semiconducting material, which would exhibit the desired piezoelectric and semiconducting properties.

Let us examine a hypothetical material which is strongly coupled and semiconducting and investigate its ultrasonic properties in the small signal limit. The secular equation [Eq. (II.14)] is still valid. However, we are now forced to solved exactly the cubic dispersion relation

Table I

Properties of CdS

Physical Parameter	Value
velocity of sound, v_s	4.4×10^5 cm/sec
electrochemical coupling coefficient $k_T^2 = e^2/c\varepsilon$	0.02
electron mobility, μ	300 cm^2/volt-sec

$$-\left(\frac{k}{\omega}\right)^3\left(1+\frac{e^2}{c\varepsilon}\right)v_D+\left(\frac{k}{\omega}\right)^2\left\{\left(1+\frac{e^2}{c\varepsilon}\right)+\frac{i\omega_c}{\omega}\right\}\left(\frac{k}{\omega}\right)\left(\frac{v_D}{v_s^2\omega}\right)-\frac{1}{v_s^2}\left(1+\frac{i\omega_c}{\omega}\right)=0 \tag{II.24}$$

in order to evaluate the effects of conductivity and drift velocity v_D on the acoustic modes. Although an analytical solution to the above equation may be possible, for purpose of illustration it was decided to evaluate this dispersion relation numerically. A numerical method for finding the complex roots of a polynomial with complex coefficients was implemented.[42] For purposes of demonstration, the material and piezoelectric properties of a piezoelectric ceramic (PZT-5H) and the semiconducting properties of cadmium sulfide were used.

In Figure II.3a we show the velocity of sound versus drift velocity and in Figure II.3b the attenuation versus drift velocity as calculated numerically from the above dispersion relation. The predictions of the weakly coupled [Eq. (II.18)] theory are also shown (dashed curves). The complete solution for the strongly coupled material is similar to the weakly coupled solution. However a strong degree of asymmetry about the $v_D = v_s$ has been introduced. (It should be noted that we have not taken into account the static strain dependence of the material stiffness, c. For strongly coupled materials, the static strain caused by application of a large drift field could be large. To take these effects into account, the third order elastic constants of the material must be known.)

In Figure II.4 we show the velocity of sound and attenuation versus material conductivity at zero drift velocity for the strongly

coupled material. Once again the predictions of the weakly coupled material are plotted for comparison. Qualitative agreement between the two theories is apparent. However, the magnitude of the attenuation and velocity dispersion as predicted by the complete solution is somewhat smaller than expected from the weakly coupled solution.

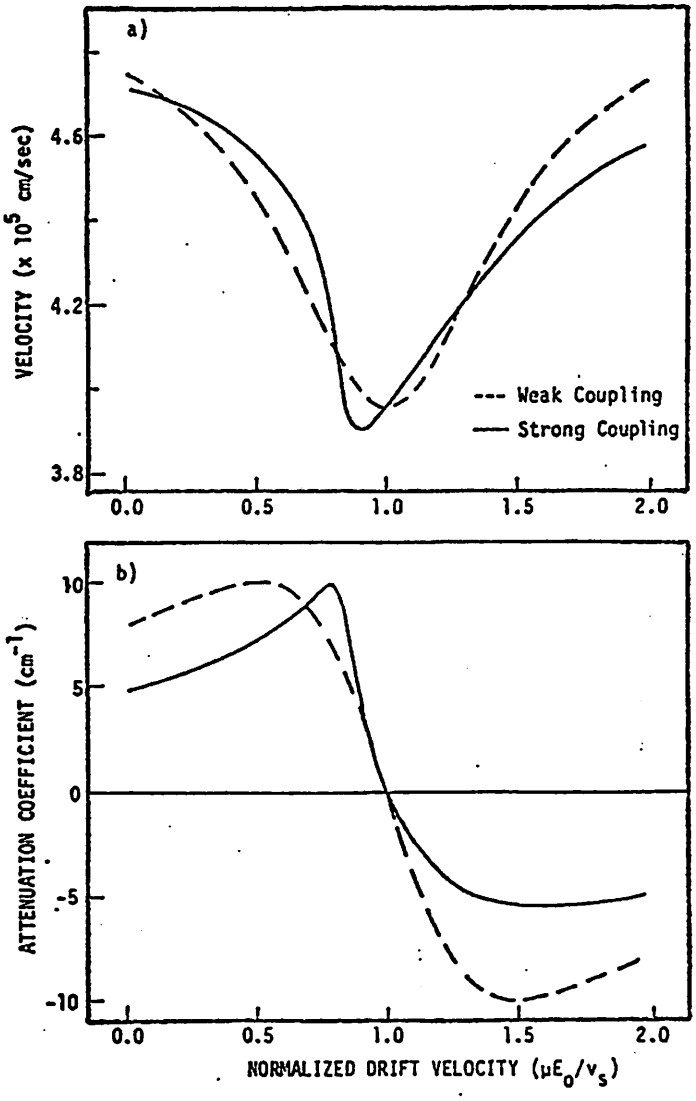

Figure II.3. Velocity and attenuation coefficient versus drift velocity in a strongly coupled piezoelectric semiconductor. The drift velocity has been normalized by the velocity of sound in the material. The cubic secular equation [Eq. (II.25)] was evaluated numerically for a material with the piezoelectric properties of PZT-5H ($e^2/c\varepsilon \approx 0.5$) and the semiconducting properties of CdS ($\mu \approx 300$ cm^2/V-sec); ω_c/ω was assumed to be 0.5. For comparison the predictions of the weak coupling theory [Eq. (II.18)] are shown by the dashed lines.

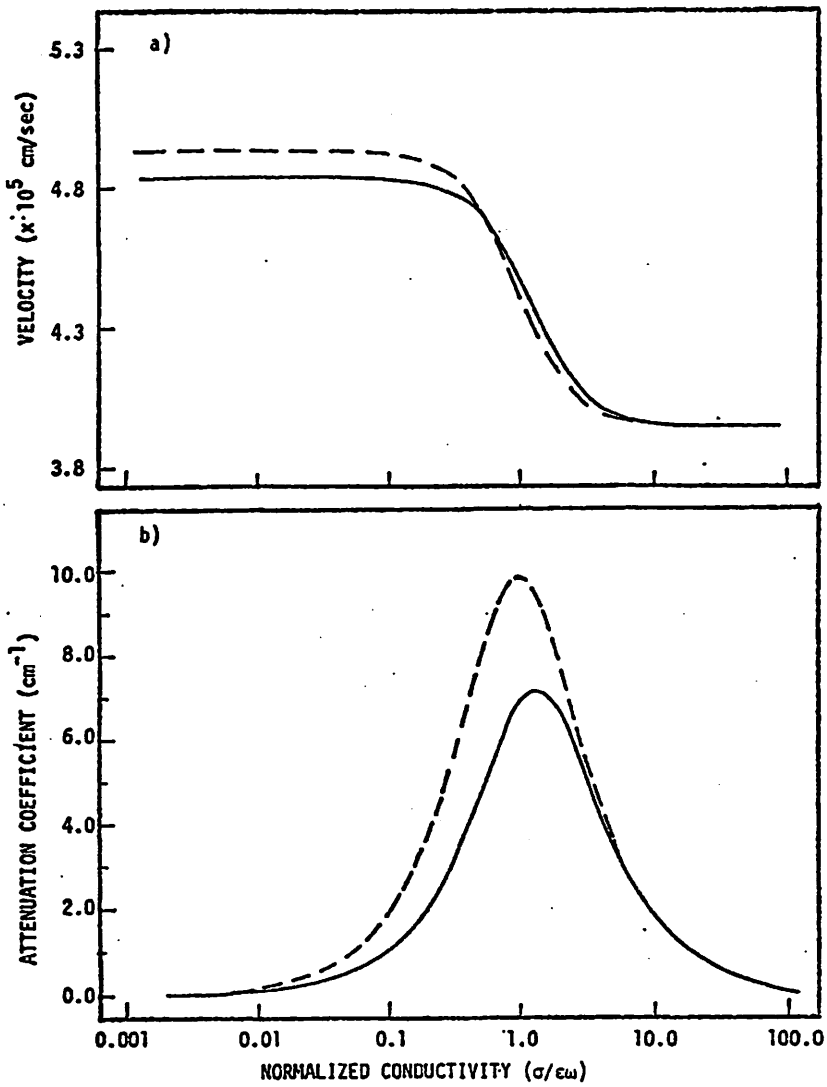

Figure V.4. Velocity and attenuation coefficient versus conductivity in a strongly coupled piezoelectric semiconductor. The crystal conductivity relaxation frequency has been normalized by the ultrasonic frequency. The cubic secular equation [Eq. (II.25)] was evaluated numerically for a material with the piezoelectric properties of PZT-5H ($e^2/c\varepsilon \approx 0.5$) and the semiconducting properties of CdS ($\mu \approx 300$ cm^2/V-sec); the drift velocity was chosen to be zero. For comparison the predictions of the weak coupling theory [Eq. (II.18)] are shown by dashed lines.

III. PIEZOELECTRIC SEMICONDUCTORS AS ELECTRICAL SIGNAL SOURCES

A. Introduction

We have seen how the interaction of elastic strains with bunched conduction electrons in a piezoelectric semiconductor resulted in the flow of a macroscopic current: the acoustoelectric current. This is not the only electrical signal, and indeed may not be the dominant electrical signal, generated when a piezoelectric semiconductor is exposed to ultrasound. A major component of the total electrical signal arises from the direct piezoelectric effect. In this chapter we examine the magnitude and frequency components associated with both the acoustoelectric and piezoelectric signals generated by piezoelectric semiconductors. The ultrasonic bandwidth of the piezoelectric and acoustoelectric responses of the crystal will be discussed both in terms of useful range of operating frequency and in terms of the various forms for pulsed ultrasonic energy which can be used. We conclude this chapter with a discussion of electrical noise, i.e., extraneous electrical signals which fall into the electrical bandwidth associated with the acoustoelectric effect.

B. Piezoelectric Response of CdS

In 1960, cadmium sulfide was demonstrated to be more strongly piezoelectric than quartz.[31,32] Theories developed previously to account for the electrical response of piezoelectric resonators and of thick piezoelectric plates were therefore available for describing the piezoelectric properties of CdS. Some features of these theories are presented here for two cases of pulsed ultrasonic excitation: i) short

pulses and ii) long ultrasonic pulses. By short ultrasonic pulses we mean pulses with temporal extent comparable to or less than the transit time through the piezoelectric plate. By long pulses we mean pulses with temporal extent much greater than the acoustic transit time, i.e., essentially continuous waves.

When describing the electrical properties of a piezoelectric material it is important to chose a formalism which allows such properties as finite propagation speed and reflection properties to be modeled. A transmission line formalism is suitable for this purpose.

1. Open Circuit Response of Piezoelectric Insulator

Let us consider the continuous wave response of a plate of cadmium sulfide as it is excited by a plane longitudinal wave of ultrasound. For the time being, we will consider the case of insulating CdS ($\omega\varepsilon >> \sigma$). Consider the situation illustrated in Figure III.1 where we can see an ultrasonic wave with displacement amplitude A impinging upon a piezoelectric plate of length ℓ and characteristic acoustic impedance Z which is bounded on each side by nonpiezoelectric material with characteristic acoustic impedances Z_1 and Z_2, respectively. A wave of (complex) amplitude $\tilde{B}$ is reflected from the piezoelectric material and a wave of amplitude $\tilde{E}$ is transmitted through the material. In addition, two waves of amplitude $\tilde{C}$ and $\tilde{D}$ propagate in opposite directions within the material. We assume that the incident wave A has been present for a sufficient long period of time so that steady state conditions have been achieved. The propagation constant $\tilde{\theta}$ is of the form $\alpha + i(\omega/v)$ in each of the three different media. Here α and v represent the attenuation and velocity of sound in each of these materials.

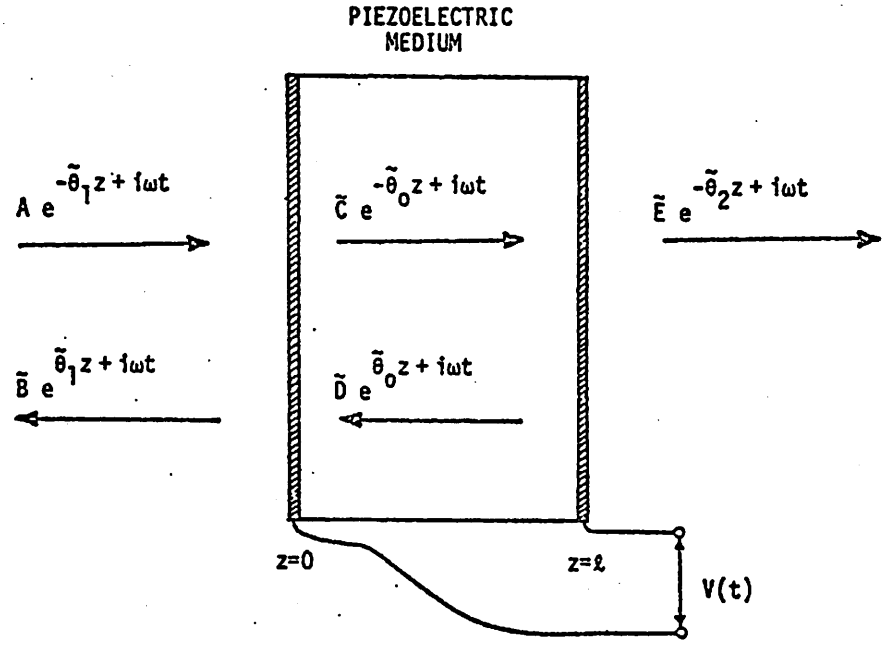

Figure III.1. Particle displacement waves associated with continuous wave illumination of a piezoelectric plate.

The characteristic acoustic impedance of each material is defined as the ratio of the acoustic pressure $\tilde{T}S$ to the particle velocity $\tilde{u} = d\xi/dt$ of a uniform plane wave within each material, i.e.,

$$Z = \frac{\tilde{T}S}{\tilde{u}} \approx \rho v S$$

where S is the cross sectional area and we have assumed $\alpha/k \ll 1$.

We would like to derive an expression for the voltage developed across the piezoelectric plate and show how this voltage is related to the behavior of the surfaces of the piezoelectric material and to the ultrasonic frequency. The following form of the piezoelectric constitutive relations are useful in this regard[43,44]

$$T = cS - hD = c\frac{\partial \xi}{\partial z} - hD \quad , \tag{III.1a}$$

$$E = -hS + D/\varepsilon = -h\frac{\partial \xi}{\partial z} + D/\varepsilon \ . \tag{III.1b}$$

In this case of a piezoelectric insulator, Gauss' law ($\nabla \cdot D = 0$) allows us to integrate Eq. (III.1b) directly

$$V = \int_0^{\ell} E dz = -h[\xi(\ell) - \xi(0)] + \frac{Q\ell}{\varepsilon S}$$

$$V = -h[\xi(\ell) - \xi(0)] + \frac{I}{i\omega C_0} \tag{III.2}$$

where we assumed an harmonic time dependence of the surface charge density Q/S and have identified $\varepsilon S/\ell$ as the static plate capacitance C_0

of the piezoelectric plate and I as the current. Under open circuit electrical conditions ($I = 0$) we find that the voltage developed across the plate is proportional to the difference in displacements of the surfaces of the piezoelectric plate,

$$V = -h\left\{\tilde{C}(e^{-\tilde{\theta}\ell} - 1) + \tilde{D}(e^{\tilde{\theta}\ell} - 1)\right\} \quad . \tag{III.3}$$

The frequency dependence of the voltage produced across the plate can be calculated by taking into account the mechanical boundary conditions imposed upon the plate at $z = 0$ and $z = \ell$. By demanding that the stress T and particle velocity $\partial\xi/\partial t$ be continuous at the boundaries we arrive at the following four equations in the unknown amplitudes $\tilde{B}$, $\tilde{C}$, $\tilde{D}$, and $\tilde{E}$.

$$\begin{aligned}
-Z_1(A - \tilde{B}) &= -Z(\tilde{C} - \tilde{D}) \\
-Z(\tilde{C}e^{-\tilde{\theta}\ell} - \tilde{D}e^{\tilde{\theta}\ell}) &= -Z_2\tilde{E}\,e^{-\tilde{\theta}_2\ell} \\
A + \tilde{B} &= \tilde{C} + \tilde{D} \\
\tilde{C}e^{-\tilde{\theta}\ell} + \tilde{D}e^{\tilde{\theta}\ell} &= \tilde{E}\,e^{-\tilde{\theta}\ell}
\end{aligned} \quad . \tag{III.4}$$

After some algebra we find that

$$\tilde{C} = \frac{(1 - r_o)A}{1 - r_o r_\ell\, e^{-2\tilde{\theta}\ell}}$$

and

$$\tilde{D} = \frac{r_\ell(1 - r_o)Ae^{-2\tilde{\theta}\ell}}{1 - r_o r_\ell\, e^{-2\tilde{\theta}\ell}} \tag{III.5}$$

where r_o and r_ℓ are the reflection coefficients,

$$r_o = \frac{Z - Z_1}{Z + Z_1} \quad , \qquad r_\ell = \frac{Z - Z_2}{Z + Z_2} \quad . \tag{III.6}$$

Substitution of the results into Eq. (III.3) for the voltage developed across the plate yields,

$$V = \frac{Ah(1 - r_o)\left\{1 - (1 + r_\ell)e^{-\tilde{\theta}\ell} + r_\ell\, e^{-2\tilde{\theta}\ell}\right\}}{1 - r_o r_\ell\, e^{-2\tilde{\theta}\ell}} \tag{III.7}$$

$\tilde{\theta}$ and hence V are implicitly functions of the ultrasonic frequency ω.

In order to gain some physical insight into the frequency dependence of piezoelectric plate alone, let us consider the case of the isolated piezoelectric plate, i.e., $r_o = r_\ell = 1$. If we assume a constant acoustic energy input at each frequency (ωA = constant) and ignore the $(1-r_o)$ factor in Eq. (III.7) then

$$V(\omega) \propto \frac{1}{\omega} \tanh \frac{\tilde{\theta}\ell}{2} = \frac{1}{\omega} \tanh \frac{\left(\alpha + i\frac{\omega}{v}\right)\ell}{2} \quad . \tag{III.8}$$

Expanding $V(\omega)$ and taking the magnitude we find

$$|V(\omega)| \propto \frac{1}{\omega}\left[\frac{\tanh^2 \alpha\ell/2 + \tan^2 \frac{k\ell}{2}}{1 + \tanh^2 \alpha\ell/2 \tan^2 \frac{k\ell}{2}}\right]^{1/2} \quad . \tag{III.9}$$

We see that the voltage produced by an isolated piezoelectric plate is strongly frequency dependent and has maxima whenever $k\ell/2$ is equal to some odd integer (harmonic number) times $\pi/2$. This condition is equivalent to saying that a maximum in the response occurs whenever the plate is equal in thickness to some odd number of half-wavelengths. Voltage resonances of the piezoelectric plate therefore occur half as often in frequency (at odd harmonics) as the mechanical resonances of the plate. The magnitude of each voltage resonance is also proportional to $(1/\omega)$ or to the inverse of the harmonic number.

Of course, piezoelectric plates are not always used as free resonators and are generally in contact with some other materials. It is true however that this overall characteristic of odd harmonic resonance persists as long as the materials in contact with the piezoelectric plate are of comparable or lower characteristic mechanical impedance. To illustrate this point, we evaluated Eq. (III.7) for the case of a piezoelectric resonator consisting of cadmium sulfide, loaded on one side by water and on the other side by air. The material properties of CdS shown in Table II were used to evaluate the reflection coefficients r_o and r_ℓ, and the theory of Hutson and White[37] [Eq. (II.14)] was used to evaluate the frequency dependence of the attenuation coefficient. The particular values in Table II were chosen to facilitate comparison with experimental results presented in Chapter VI. Figure III.2 shows the magnitude of the piezoelectric voltage generated as a function of $k\ell$. The loading of the piezoelectric material by a low impedance material such as water does not change the characteristic odd half wave resonant nature of the response.

Table II

Resonator Properties

Physical Parameter	Value
$v = \sqrt{c/\rho}$	4.411×10^{5} cm/sec
σ	8.4×10^{-7} $(\Omega\text{-cm})^{-1}$
$\varepsilon^{s}/\varepsilon_{o}$	9.53
$k_T^2 = e^2/c\varepsilon$	0.02

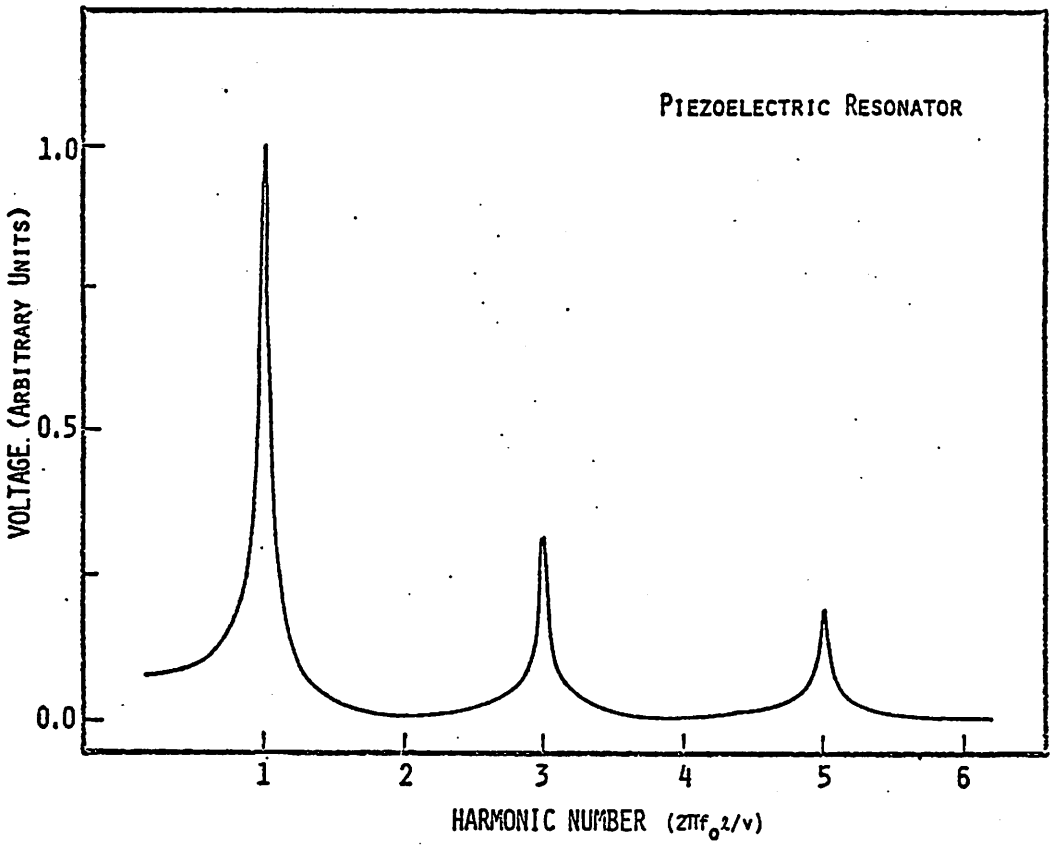

Figure III.2. Magnitude of piezoelectric voltage generated by resonant plate as a function of harmonic number ($k\ell$). The piezoelectric properties of CdS were used to evaluate Eq. (III.7) for a plate loaded on one side by water and on the other side by air [$r_0 = 0.87$ and $r_\ell = 1$].

Let us return to the case of a non-isolated piezoelectric plate described by Eq. (III.7). Although the continuous wave response of the mechanically loaded piezoelectric plate is completely described by this equation, in this form the equation does not give us adequate insight into how that response is built up at the onset of acoustic wave. Redwood [45] showed that this equation could be put into a physically enlightening form by expanding the denominator with the binomial theorem to yield

$$V = Ah(1 - r_o)\{1 - (1 + r_\ell)e^{-\tilde{\theta}\ell} + r_\ell\, e^{-2\tilde{\theta}\ell}\}\{1 + r_o r_\ell\, e^{-2\tilde{\theta}\ell} + r_o^2 r_\ell^2\, e^{-4\tilde{\theta}\ell} + r_o^3 r^3\, e^{-6\tilde{\theta}\ell} + \ldots\} \quad . \tag{III.10}$$

After collecting terms we find

$$V = Ah(1 - r_o)\left\{1 - (1 + r_\ell)e^{-\tilde{\theta}\ell} + r_\ell(1 + r_o)e^{-2\tilde{\theta}\ell} - r_o r_\ell(1 + r_\ell)e^{-3\tilde{\theta}\ell} + r_o r_\ell^2(1 + r_o)e^{-4\tilde{\theta}\ell} - \ldots\right\} \quad . \tag{III.11}$$

This form of the voltage response of a piezoelectric plate is reminiscent of the results predicted using a propagating wave model [46] of an acoustic resonator, and the result has a straightforward physical interpretation. We see that the continuous wave response can be thought of as the superposition of an infinite series of waves reverberating back and forth within the crystal. Expanding $e^{-N\tilde{\theta}\ell}$ as $e^{-N\alpha\ell}e^{-iN(\omega\ell/v)}$ allows us to show that each successive reflection within the plate is phase shifted by an amount commensurate with the acoustic transit time ℓ/v and decreased in amplitude by an amount $e^{-\alpha\ell}$. The reflection

coefficients also allow us to pick off the phase and relative magnitude of the reflection from each surface.

2. Open Circuit Response of Piezoelectric with Finite Conductivity

The result presented in the previous section can be modified to include the effects of finite conductivity upon the electrical response of a piezoelectric plate. In this section we outline that analysis for the conductivity and frequency region where the acoustoelectric effect is strong, i.e., $\sigma \approx \omega\varepsilon$.

The voltage developed across a piezoelectric plate of finite conductivity is obtained by integration of Eq. (III.1b) over the length of the crystal. In the case of finite conductivity, Gauss' law requires that

$$\nabla \cdot D = \frac{\partial D}{\partial z} = -qn$$

where q is the electronic charge and n is departure from equilibrium of the electron density within the crystal. The results of the analysis presented in Chapter II indicate that there is a direct relationship between the charge bunching described by n and the magnitude of the strain associated with the ultrasonic wave:

$$n = \frac{e\omega_c}{qv_o} \frac{1}{(1 + i\omega_c/\omega)} \left|\frac{\partial \xi}{\partial z}\right| = \tilde{K}\left|\frac{\partial \xi}{\partial z}\right| \quad . \qquad \text{(III.12)}$$

Here we have rewritten Eq. (II.19) for the case of zero drift field applied to the crystal. In other words, a charge carrier wave is associated with each of the elastic waves represented by $\tilde{C}$ and $\tilde{D}$ in Figure III.1. The magnitude of this charge carrier wave is related

to the magnitude of the strain amplitude by a complex proportionality constant $\tilde{K}$. Because we know the spatial dependence of the charge bunching in terms of the strain amplitudes, we can write the displacement field D in terms of the strain amplitude and can integrate Eq. (III.1b) directly to find the voltage developed across the plate,

$$V = \int_0^{\ell} E dz = -h \int_0^{\ell} \frac{\partial \xi}{\partial z} dz + \int_0^{\ell} \frac{D}{\varepsilon} dz$$

$$V = \tilde{C}(e^{-\tilde{\theta}\ell} - 1)\left(-h - \frac{q\tilde{K}}{\varepsilon\tilde{\theta}}\right) + \tilde{D}(e^{+\tilde{\theta}\ell} - 1)\left(-h - \frac{q\tilde{K}}{\varepsilon\tilde{\theta}}\right) + \frac{Q\ell}{\varepsilon S} \quad . \qquad \text{(III.13)}$$

Here the surface charge density Q/S is the constant of integration obtained from the integration of $\nabla \cdot D$. Once again we assume a harmonic time dependence associated with the ultrasonic wave in order to write $Q = I/i\omega$. Because the crystal has a finite conductivity and exhibits a resistance $R = \ell/\sigma S$ a current $I = +V/R$ will now flow through the crystal. Thus we can rewrite Eq. (III.13) as

$$V = -\left\{\frac{i\omega RC_o}{i\omega RC_o - 1}\right\}\left\{h + \frac{q\tilde{K}}{\varepsilon\tilde{\theta}}\right\}\left\{\tilde{C}(e^{-\tilde{\theta}\ell} - 1) + \tilde{D}(e^{+\tilde{\theta}\ell} - 1)\right\} \quad . \qquad \text{(III.14)}$$

A comparison of Eqs. (III.3) and (III.14) indicates that the net effect of finite conductivity upon the voltage developed by a piezoelectric plate is to modify the piezoelectric coupling constant somewhat

$$h \longrightarrow h + \frac{q\tilde{K}}{\varepsilon\tilde{\theta}} \qquad \text{(III.15)}$$

and to place a shunt resistor R across the plate.

The range of crystal conductivity in which we are most interested is the range which maximizes the exchange of energy from the ultrasonic wave to the conduction electrons. According to the Hutson and White theory[37] this maximum exchange occurs when

$$\frac{\sigma}{\varepsilon} = \omega_c = 2\pi f \quad , \tag{III.16}$$

i.e., when the conductivity relaxation frequency is equal to the ultrasonic frequency. It is useful to note that the conductivity relaxation frequency is identically equal to the inverse of the "time constant" associated with the shunted piezoelectric plate.

$$RC_o = \left(\frac{\ell}{\sigma S}\right)\left(\frac{\varepsilon S}{\ell}\right) = \frac{1}{\omega_c} \quad . \tag{III.17}$$

Evaluation of Eq. (III.14) at $\omega_c = \omega$ and comparison with Eq. (III.3) leads to the result that

$$\left|\frac{V(\sigma = \omega\varepsilon)}{V(\sigma = 0)}\right| \approx 1 \tag{III.18}$$

where we have made the assumption that $k/\alpha >> 1$ and that the wave amplitudes $\tilde{C}$ and $\tilde{D}$ are not altered appreciably by the presence of conduction electrons. The assumption that $k/\alpha >> 1$ is always true in CdS. The second of these assumptions however, is not strictly true because the addition of conduction electrons does alter the ultrasonic attenuation coefficient. Therefore the magnitude of $\tilde{C}$ and $\tilde{D}$ in Eq. (III.14) may be somewhat reduced over those in Eq. (III.3).

It is clear however that magnitude of the piezoelectric response of a resonator with finite conductivity will be appreciable and care must be taken to separate the piezoelectric and acoustoelectric response of the resonator.

3. Short Pulse Response

In this section we formalize some of the response characteristics of a piezoelectric plate exposed to a short pulse of ultrasound. In this context, the word short means that the pulse length is equal to or shorter than the acoustic transit time through the piezoelectric plate. The formalism presented here is a combination of a propagating wave model of resonator theory and the transmission line model of resonator theory. The particular factoring of Eq. (III.7) proposed by Redwood[45] makes the combination of these two resonator models quite natural.

The form of pulsed ultrasound we would like to consider is

$$A(t) = A\, e^{-i(kz-\omega t)}\, \Delta(t) \tag{III.19}$$

i.e., a gated continuous wave where $\Delta(t)$ represents an appropriate gating function. We take the following simple form for our gating function

$$\Delta(t) = \begin{cases} 0\,, & t \leq 0 \\ 1\,, & t < t < t_d \\ 0\,, & t \geq t_D \end{cases} \tag{III.20}$$

so as to produce a gated tone burst of ultrasound of duration t_d which begins at $t = 0$. Formally, Eq. (III.11) represents the time independent piezoelectric voltage generated by a plate as a function of frequency. However, from the "physical" way in which it is factored we are able to deduce the time dependence of the piezoelectric voltage

$$V(t) = Ah(1 - r_o)\left\{\Delta(t) - (1 + r_\ell)\Delta\left[t - \frac{\ell}{v}\right] e^{-\alpha\ell} e^{-ik\ell}\right.$$
$$+ r_\ell(1 + r_o)\Delta\left[t - \frac{2\ell}{v}\right] e^{-2\alpha\ell}\, e^{-i2k\ell}$$
$$\left. - r_o r_\ell(1 + r_\ell)\Delta\left(t - \frac{3\ell}{v}\right) e^{-3\alpha\ell}\, e^{-3k\ell} + \ldots\right\} \qquad \text{(III.21)}$$

where $\Delta(t-N\ell/v)$ represent the gating function delayed by N transit times through the plate. Because we have chosen t_d to be less than the acoustic transit time, only one of the terms in this infinite series is "on" at any particular time. In other words, we no longer observe any resonant plate response because interfering terms in the infinite series are no longer simultaneously present within the piezoelectric plate. Electrical signals are generated by the thick piezoelectric plate only when the ultrasonic pulse is in "contact" with one of the two surfaces of the plate, i.e., either when the pulse initially enters the plate or when it is subsequently reflected from one of the surfaces of the plate.[45,47-49] Therefore, the electrical signals generated by each surface of the plate are of a duration comparable to the ultrasonic pulse length.

It was pointed out by Redwood[45] that in the short pulse limit we are investigating, (i.e., $t_d < \ell/v$) the Mason equivalent circuit network[50] for a piezoelectric resonator can be reduced to a much simpler form. The short pulse equivalent circuit of a piezoelectric plate is shown in Figure III.3. In this limit the mechanical impedance of the transducer is purely resistive and the total equivalent circuit has the characteristics of a low pass filter. The magnitude of the load resistance R_L can be used to adjust the transfer characteristics of this filter. For many practical problems, R_L represents the input impedance of the amplifier used to measure the voltage across the plate. In situations where large values of R_L are required, the low pass nature of this network can be pronounced. The magnitude of the transfer function of this filter network for a strongly coupled piezoelectric material (PZT-4) is shown in Figure III.4 for three different values of load resistance, 50 Ω, 10^3 Ω and 10^6 Ω. These values were chosen because they are typical of the input impedance of practical amplifiers. For high values of the load resistance, low frequency components in the ultrasonic pulse are preferentially passed by the piezoelectric plate. In Figure III.5 we show the value of this transfer function for a piezoelectric material such as CdS when it is loaded by 10^6 Ω and 10^5 Ω. These values of the resistances were chosen because they are typical of the bulk resistance observed with photoconducting cadmium sulfide. Again we see the preferentially passage of low frequency components associated with the acoustic pulse.

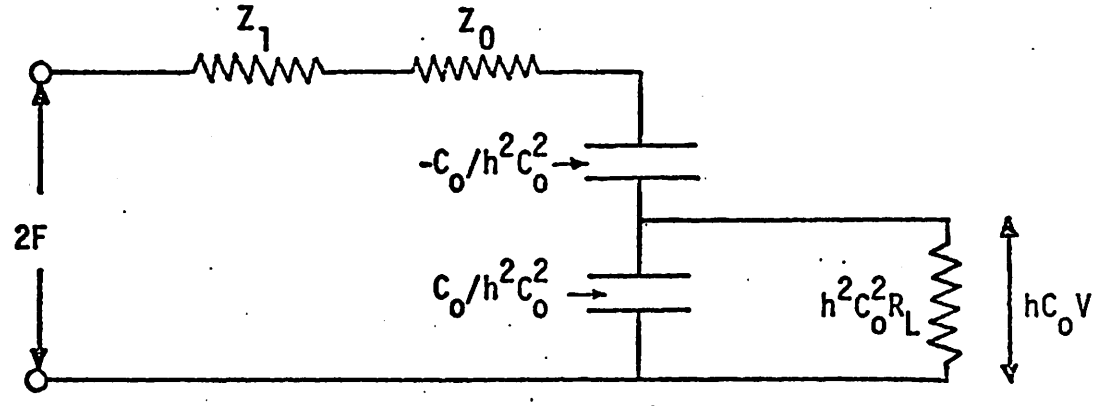

Figure III.3. Equivalent circuit describing the response of a thick piezoelectric plate to a short ultrasonic pulse. This circuit (after Redwood[45]) can be used to predict the voltage produced per unit force incident upon the plate when the ultrasonic pulse is shorter than the transit time through the plate.

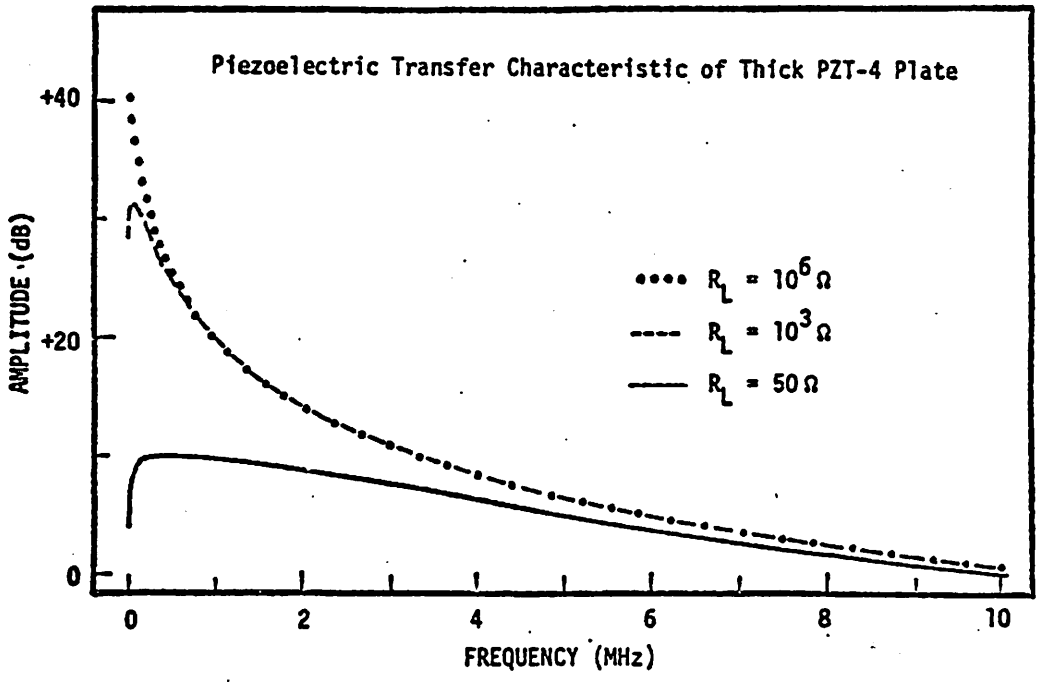

Figure III.4. Transfer characteristic of a thick PZT-4 plate for various resistive loads. A thick plate enhances the low frequency portion of the ultrasonic spectrum. The voltage response presented is relative to 4.7×10^{-2} volts per unit stress incident upon the plate. Assumed plate characteristics are $C_o = 1000$ pf, $h = 1.8 \times 10^9$ V/m and $Z_o = 2.9 \times 10^7$ Rayls, Z_1 was chosen to be representative of water.

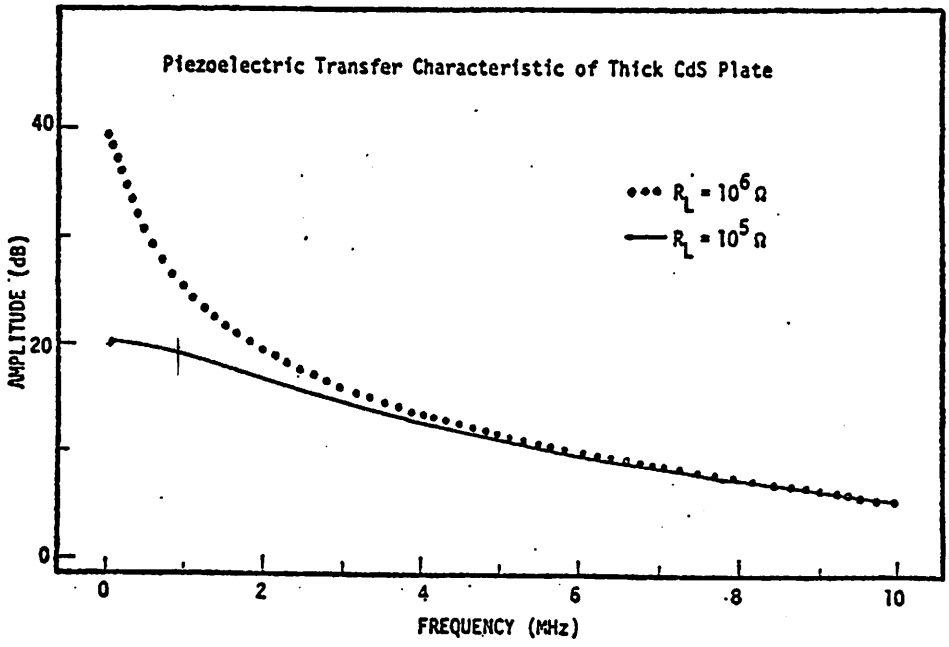

Figure III.5. Transfer characteristic of a thick CdS plate for various resistive loads. The low frequency portion of the ultrasonic spectrum is enhanced. The voltage response presented is relative to 3.7×10^{-2} volts per unit stress incident upon the plate. Assumed plate characteristics are, C_o = 0.8 pf, h = 5.2×10^9 V/m and Z_o = 2.1×10^7 Rayls, Z_1 was chosen to be representative of water.

In Figure III.6 we show the frequency domain response characteristic of a gated continuous wave pulse of ultrasound before and after it has been detected by the thick plate of PZT-4. The case illustrated is a 1.0 microsecond burst of 5 MHz center frequency ultrasound, and the value of R_L was chosen to be $10^5\ \Omega$. Even though the amplitude of the 500 KHz component of the acoustic pulse is 20 dB less than the amplitude of the center frequency component, we see that the amplitude of the 500 KHz component of the electrical signal produced by the thick piezoelectric plate can be comparable to that of the center frequency component.

These relatively large amplitude low frequency components associated with the propagation of short ultrasonic pulses in thick piezoelectric materials are of interest in the present work because they occur within the same electrical bandwidth as the acoustoelectric signals. We will return to this when we discuss signal to noise ratio considerations.

C. Acoustoelectric Signal—Open Circuit Voltage Produced by Long Pulses

From the results of Chapter II we saw that the nonlinear interaction of elastic strain and bunched electrons within a piezoelectric semiconductor could result in a net local current density or force upon the conduction electrons. This force was shown to be proportional to the local value of the acoustic intensity Φ. In this section we calculate the net acoustoelectric response of a piezoelectric plate under the conditions of long pulse or nearly continuous wave conditions illustrated in Figure III.1.

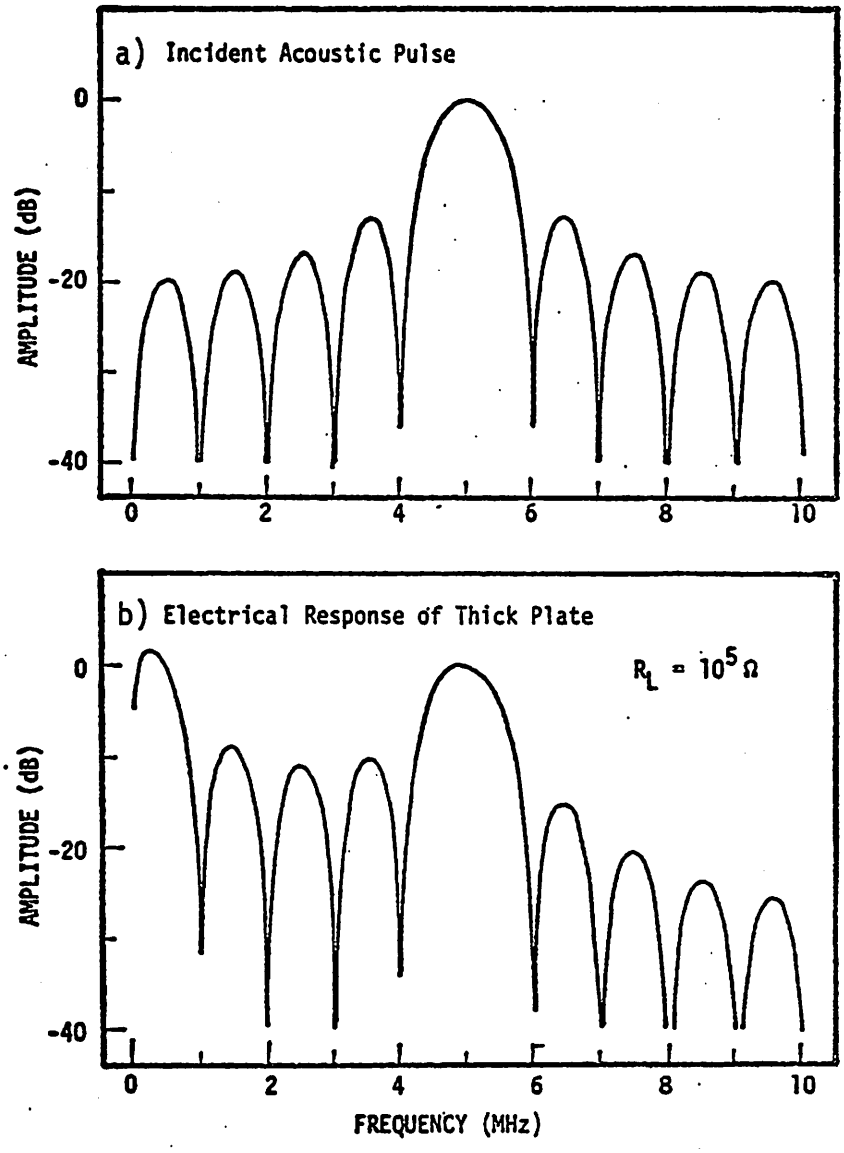

Figure III.6. Receiver properties of a thick plate of PZT-4. In panel a) we show the spectral amplitude of the stress associated with a one microsecond ultrasonic pulse with center frequency at 5 MHz. In panel b) the spectral amplitude of the voltage produced when stress pulse is incident upon a thick PZT-4 plate is shown.

In order to calculate the open circuit acoustoelectric voltage produced by a long pulse of ultrasound it is helpful to recast Eq. (II.23) in terms of an effective acoustoelectric field.

$$E_{AE} = \frac{J_{AE}}{\sigma} = \frac{-2\alpha_E}{ne}\frac{\Phi}{v} \quad , \tag{III.22}$$

where α_E is the attenuation coefficient describing the transfer of ultrasonic energy to the conduction electrons.

In the present context we have been using the term acoustic intensity Φ rather loosely to mean the average acoustic energy density times the ultrasonic phase velocity. In other words Φ is the time average of the power flow or the average acoustic Poynting vector, which is more properly defined as

$$\Phi = \frac{1}{2}\,\mathrm{Re}[u^* \cdot T] \tag{III.23}$$

where u is the particle velocity $[\partial\xi/\partial t]$ and T is the stress $[c(\partial\xi/\partial z)]$ associated with the acoustic wave. From this definition, the total power flow through the crystal can be broken into two components

$$\Phi_T = \frac{1}{2}\omega^2 Z\ \mathrm{Re}[(C+D)(C^*+D^*)] = \frac{1}{2}\omega^2 Z(C^*C + D^*D) \ . \tag{III.24}$$

No net power flow is carried by the cross terms. We can find the total acoustoelectric voltage generated across the crystal by integration of E_{AE} and using the above expression for the total acoustic power flow within the crystal

$$V_{AE} = \int_0^{\ell} E_{AE}\, dz = \frac{-\alpha_E \omega^2 z}{nev}\left\{|C|^2 \int_0^{\ell} e^{-2\alpha_T z}\, dz + |D|^2 \int_0^{\ell} e^{+2\alpha_T z}\, dz\right\}$$

$$\frac{\omega^2 Z}{2nev}\left(\frac{\alpha_E}{\alpha_T}\right)\left\{|C|^2\left(e^{-2\alpha_T \ell} - 1\right) - |D|^2\left(e^{+2\alpha_T \ell} - 1\right)\right\} \tag{III.25}$$

where α_T is the total attenuation experienced by the ultrasonic wave and is equal to the sum of the electronic attenuation coefficient α_E plus the background or lattice attenuation coefficient α_L. The quantities $|\tilde{C}|^2$ and $|\tilde{D}|^2$ which describe the magnitude squared of the two components of the standing wave present within the plate can be evaluated approximately using Eq. (III.5) and so

$$V_{AE} = \frac{\omega^2 Z}{2nev}(1 - r_o)^2 \, |A|^2 \left(\frac{\alpha_E}{\alpha_T}\right)\left\{\frac{\left(e^{-2\alpha_T \ell} - 1\right) - r_\ell^2 \, e^{-4\alpha_T \ell}\left(e^{2\alpha_T \ell} - 1\right)}{1 + r_o^2 r_\ell^2 \, e^{-4\alpha_T \ell} - 2 r_o r_\ell \, e^{-2\alpha_T \ell} \cos 2k\ell}\right\} \qquad \text{(III.26)}$$

In Figure III.7 we show the predicted form of V_{AE} versus frequency for an acoustoelectric resonator which is loaded on one side by water and on the other side by air for a fixed ultrasonic intensity incident upon the crystal, i.e., for $\omega^2 A^2$ constant. The properties of this resonator are the same as those described in Table I. As you can see, a resonant behavior is exhibited by V_{AE}. This resonant behavior is unlike V_{PE}, however, in that a maximum in signal amplitude occurs whenever $k\ell = n\pi$ for all integer values of n. We note that since V_{AE} is proportional to the time averaged power flow (averaged over a few cycles of ultrasonic wave) it no longer contains an $e^{i\omega t}$ time dependence. The above expression represents a dc voltage whose amplitude varies with ultrasonic frequency.

In order to gain some insight into the dependence of V_{AE} upon the length of the crystal, let us examine the case of an isolated acousto-electric resonator, i.e., $r_o = r_\ell = 1$. If we assume that we are able to

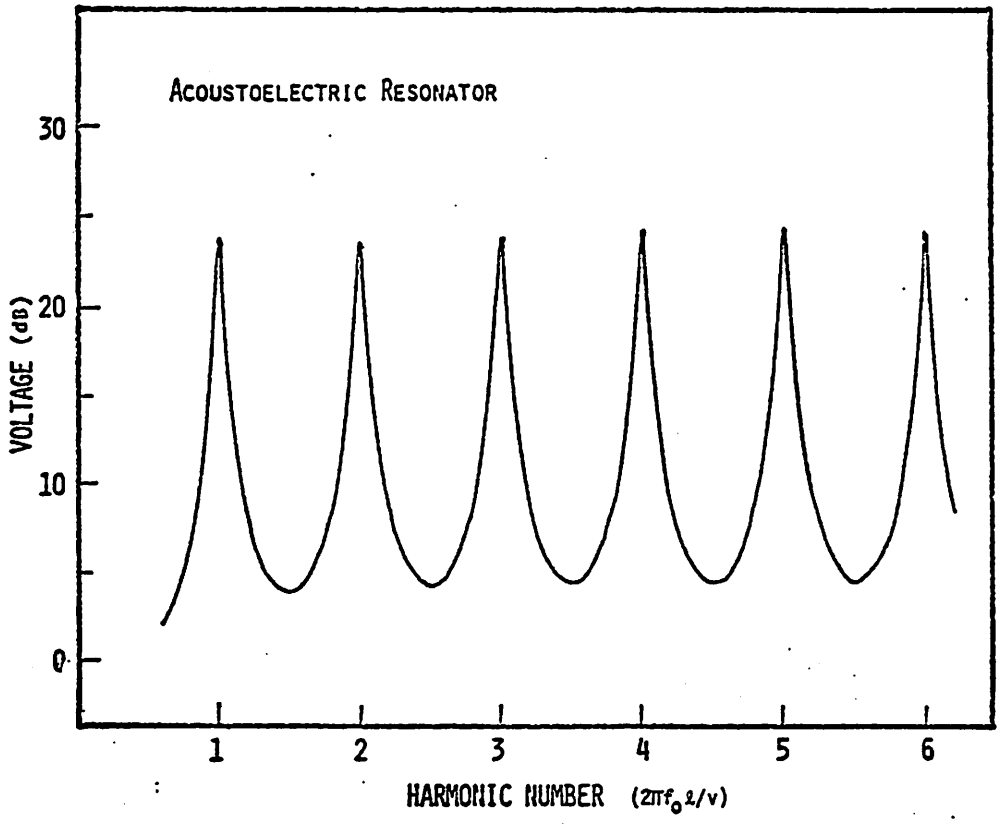

Figure III.7. Magnitude of the acoustoelectric response generated by a resonant piezoelectric semiconductor plate as a function of harmonic number ($k\ell$). The piezoelectric and semiconducting properties of CdS were used to evaluate Eq. (III.26) for a plate loaded on one side by water and on the other side by air ($r_0 = 0.87$ and $r_\ell = 1$).

get sound into such an isolated resonator (i.e., we ignore the fact that $(1-r_o)^2$ goes to zero) then we find that

$$V_{AE}^{R} \propto \left(\frac{\alpha_E}{\alpha_T}\right)\left\{\frac{e^{-4\alpha_T \ell} - 1}{1 - 2e^{-2\alpha_T \ell}\cos 2k\ell + e^{-4\alpha\ell}}\right\} \quad . \qquad \text{(III.27)}$$

Let us now suppose that we have adjusted the operating frequency of this resonator so that we are "on resonance", i.e., cos $2k\ell = 1$. At this frequency Eq. (III.27) becomes

$$V_{AE}^{R} \propto \left(\frac{\alpha_E}{\alpha_T}\right)\left(\frac{e^{-2\alpha_T \ell} + 1}{e^{-2\alpha_T \ell} - 1}\right) = -\left(\frac{\alpha_E}{\alpha_T}\right)\coth(\alpha_T \ell) \quad . \qquad \text{(III.28)}$$

The optimum crystal length is determined by maximizing the signal to noise ratio with respect to the crystal length. As we will discuss in Section III.H, the dominant source of electrical noise in a piezoelectric semiconductor is related to the Johnson noise associated with the electrical resistance of the crystal. The Johnson noise voltage is proportional to the square root of the crystal resistance, which is proportional to the length of the crystal. Thus we find the maximum signal to noise is obtained when

$$\frac{d}{d\ell}\left[-\frac{\alpha_E}{\alpha_T}\,\frac{\coth(\alpha_T \ell)}{\sqrt{\ell}}\right] = 0 \qquad \text{(III.29)}$$

This leads to the condition that

$$4\alpha_T \ell = -\sinh(2\alpha_T \ell) \quad . \qquad \text{(III.30)}$$

This requirement can be satisfied only in the limit of $\ell = 0$. Thus for resonant operation of an acoustoelectric resonator, the crystal should be made as thin as possible commensurate with satisfying the resonance condition. In other words, the best signal to noise is achieved if the crystal is operated at the fundamental resonance, $k\ell = \pi$.

Because we are at liberty to adjust the electronic attenuation coefficient α_E, we can also maximize Eq. (III.28) with respect to the electronic attenuation coefficient

$$\frac{d}{d\alpha_E}\left[\frac{\alpha_E}{(\alpha_E+\alpha_L)}\coth\left((\alpha_E+\alpha_L)\ell\right)\right] = 0 \quad . \tag{III.31}$$

This condition is satisfied when

$$\sinh\left(2(\alpha_E+\alpha_L)\ell\right) = \frac{2\alpha_E(\alpha_E+\alpha_L)}{\alpha_L}\ell \quad . \tag{III.32}$$

We find that the optimum condition for resonant signal generation is when the electronic attenuation coefficient is equal to the lattice attenuation coefficient

$$\alpha_E = \alpha_L \tag{III.33}$$

Typical values of α_L in CdS crystals are quite low and are generally hard to measure because they are masked by the electronic attenuation coefficient. A reasonable estimate for α_L is 0.05 cm^{-1}.

Let us now examine the condition for optimum crystal length for an isolated acoustoelectric resonator at antiresonance, i.e., when $\cos(2k\ell) = -1$. Under these conditions Eq. (III.26) becomes

$$V_{AE}^{A} \propto -\frac{\alpha_E}{\alpha_T}\tanh(\alpha_T\ell) \quad . \tag{III.34}$$

Once again, we would like to maximize the signal to noise ratio with respect to crystal length and so

$$\frac{d}{d\ell}\left[-\frac{\alpha_E}{\alpha_T}\frac{\tanh(\alpha_T\ell)}{\sqrt{\ell}}\right] = 0 \quad . \qquad \text{(III.35)}$$

This leads to the condition that

$$4\alpha_T\ell = \sinh(2\alpha_T\ell) \quad . \qquad \text{(III.36)}$$

This occurs when $\alpha_T\ell \approx 1.1$. For any reasonable length of crystal (1 to 2 cm) we find that the total attenuation coefficient α_T is essentially equal to α_E and so Eq. (III.36) also dictates the optimum value of α_E.

In the case of this relatively large value for $\alpha_T\ell$ (i.e., $\alpha_T\ell \approx 1.1$) it seems inappropriate to think of the acoustoelectric crystal as a resonator. The ratio of the resonant to nonresonant signal level predicted by Eq. (III.26) for $\alpha_T\ell = 1.1$ is only about 1.6. In this nonresonant mode we see that the maximum signal to noise is achieved if most of the acoustic energy can be dissipated on a single pass through the semiconducting crystal. The conclusion expressed by Eq. (III.36) is the same as arrived at by Southgate.[23] Southgate, however, was considering the response of a crystal to a burst of ultrasound which was shorter than the transit time through the crystal. From our result Eq. (III.36) we see that $\alpha_T\ell \sim 1.1$ is the optimum choice whenever the crystal is used in a nonresonant manner.

We are now in a position to compare the resonant and antiresonant signal to noise ratios. We will adjust the resonator parameters so that this comparison can be done at a single frequency. Physically

realizable values consistent with the previous optimization conditions are shown in Table II. The ratio of resonant to antiresonant signal to noise ratio under these conditions is

$$\frac{(S/N)_R}{(S/N)_A} = \frac{\left\{\left[\alpha_E/(\alpha_E+\alpha_L)\right]\coth\left((\alpha_E+\alpha_L)\ell\right)/\sqrt{\ell}\right\}_R}{\left\{\tanh\left((\alpha_E+\alpha_L)\ell\right)/\sqrt{\ell}\right\}_A} \qquad \text{(III.37)}$$

where the quantities in the numerator are taken from the resonant column of Table III and the quantities in the denominator are taken from the antiresonant column. We obtain

$$\frac{(S/N)_R}{(S/N)_A} \approx \frac{550}{0.57} \approx 950 \quad . \qquad \text{(III.38)}$$

Therefore, a resonant acoustoelectric detector designed to operate at 5 MHz is predicted to produce about 950 times better signal to noise than an antiresonant acoustoelectric detector operating at the same frequency. This improvement in signal to noise is achieved, however, only under steady state conditions. Resonator theory tell us that when an acoustic pulse is incident upon an element which has an $\alpha_T\ell = 0.004$, many reverberations are necessary (as on the order of the mechanical Q) before the steady state is achieved. For such a resonator the mechanical quality factor is on the order of 400. ($Q \sim \pi/2\alpha\ell \sim 400$). Thus, acoustic pulses on the order Q/f_0, or about 80 microseconds long are necessary to achieve this enhancement in sensitivity. In contrast, for a crystal with $\alpha_T\ell \sim 1.1$, only a single transit is necessary for steady state conditions to be achieved. Thus the response time for

Table III

Acoustoelectric Resonator Properties

	Resonant	Antiresonant
f	5 MHz	5 MHz
α_E	0.05 cm^{-1}	0.5 cm^{-1}
α_L	0.05 cm^{-1}	0.05 cm^{-1}
ℓ	0.044 cm	2 cm
v	4.4×10^5 cm/sec	4.4×10^5 cm/sec

our example is ℓ/v, or about 4 microseconds. This trade-off between sensitivity and response time usually dictates which type of acousto-electric detector is chosen for a particular application.

D. Acoustoelectric Response to Short Pulses

Let us now examine the acoustoelectric response of a piezoelectric semiconductor pulse of ultrasound whose length is less than or equal to the transit time through the semiconducting crystal. Equation (II.23) expresses the local acoustoelectric current density in terms of the local value of the acoustic power flow or intensity

$$J_{AE} = -\frac{\mu\alpha_E\omega^2}{v} Z\,\xi^*\xi \quad , \tag{III.39}$$

where we have rewritten Eq. (II.23) in terms of the ultrasonic frequency and particle displacement ξ. The macroscopic current flow per unit area through the semiconducting crystal is obtained by averaging the local current density over the crystal length.

The acoustoelectric signal is the result of energy transfer and is not limited to surfaces of the plate but is generated within the bulk of the semiconducting material. For this reason, an ultrasonic pulse of length t_d, propagating through a piezoelectric semiconductor with acoustic transit time ℓ/v will produce an electrical current of duration $\ell/v + t_d$. A formal expression for the time dependent acoustoelectric current can be obtained using a propagating wave model approach if we redefine our gating function $\Delta'(t)$,

$$\Delta'(t) = \begin{cases} 0 \ , & t < 0 \\ 1 \ , & 0 < t < t_d + \ell/v \\ 0 \ , & t > t_d + \ell/v \end{cases} \quad . \tag{III.40}$$

As before, we will understand $\Delta'(t - \ell/v)$ to be a similar gating function delayed by a time ℓ/v. Formally, the time dependent acoustoelectric current is of the form

$$\langle J_{AE} \rangle = \frac{I_{AE}}{Area} = - \frac{-Z\,\omega^2|A|^2\,\alpha_E \mu (1-r_o^2)}{v\ell} \left\{ \Delta'(t) I_1 - r_\ell^2\, \Delta'\left(t - \frac{\ell}{v}\right) I_2 + r_\ell^2 r_o^2\, \Delta'\left(t - \frac{2\ell}{v}\right) I_1 - r_\ell^4 r_o^2\, \Delta'\left(t - \frac{3\ell}{v}\right) I_2 + \ldots \right\} \qquad \text{(III.41)}$$

where r_o^2 and r_ℓ^2 are the intensity reflection coefficient at $z = 0$ and $z = \ell$ respectively and $\omega^2|A|^2$ is proportional to the intensity of the incident ultrasonic pulse. In the above expression I_1 represents the contribution of the pulses traveling from $z = 0$ to $z = \ell$ and is of the form

$$I_1'(t) = \begin{cases} \int_0^{vt} e^{-2\alpha z}\, dz & 0 < t < t_d \\ \int_{vt}^{\ell - vt_d + vt} e^{-2\alpha z}\, dz & t_d < t < \ell/v \\ \int_{\ell - vt_d + vt}^{\ell} e^{-2\alpha z}\, dz & \ell/v < t < \ell/v + t_d \\ 0 & \ell/v + t_d < t < 0 \end{cases} \qquad \text{(III.42)}$$

The three distinct portions represent the contributions made by the pulse to the signal as it enters into, propagates across and leaves the thick plate. A similar expression for I_2 can be written down which represents the contribution of "reflected" waves traveling from $z = \ell$ to $z = 0$.

As before, $\langle J_{AE} \rangle$ is proportional to the time average power flow within the crystal and as such contains no signal components at the ultrasonic frequency ω. However because of the finite pulse length, $\langle J_{AE} \rangle$ no longer strictly a dc signal. It contains frequency components determined by the ultrasonic pulse length t_D and by the transit time ℓ/v. In Figure III.8 we illustrate the predicted time and frequency domain response of $\langle J_{AE} \rangle$ for two specific cases of pulse length and mechanical loading. In case A we show the case where the ultrasonic pulse is 1/2 the length of the crystal ($t_d = \ell/2v$) which is unloaded at $z = \ell$ ($r_\ell = 1$) and loaded with water at $z = 0$ ($r_o = 0.87$). This set of mechanical loading conditions allows the ultrasonic pulse to reverberate within the crystal. Thus the maximum response in frequency is not located at dc but is shifted slightly upward.

In Figure III.9 we show the predicted acoustoelectric current response of a perfectly backed crystal ($r_\ell = 0$). Because no reverberations take place under these mechanical conditions, a single acoustoelectric current pulse should be observed with maximum frequency response at dc.

E. "Broadband" Acoustoelectric Response

The acoustoelectric effect refers to a net force exerted upon conduction electrons by an acoustic wave in a piezoelectric semiconductor. This force can be detected by measuring by either the current generated by the short circuited semiconductor or by measuring the open circuit voltage developed across the semiconductor. In this section we consider some aspects of measuring the acoustoelectric current or the acoustoelectric voltage with the goal of broad frequency response in mind.

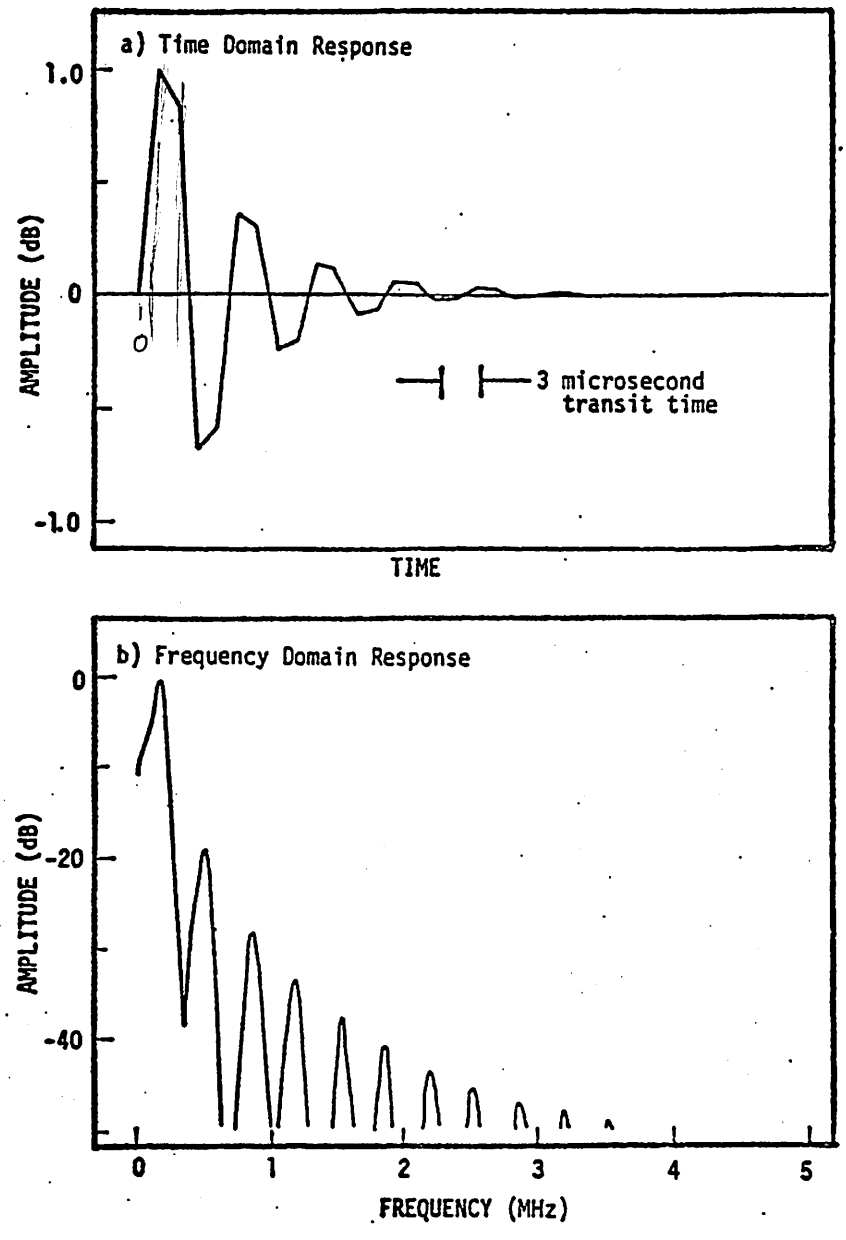

Figure III.8. Acoustoelectric response of CdS to short ($t_D = \ell/2v$) burst of ultrasound. In panel a) the time domain acoustoelectric current density predicted from Eq. (III.41) is shown. In panel b) the spectral amplitude of the acoustoelectric current density is shown. Transit time through crystal was assumed to be 3 microseconds, and r_o and r_ℓ were taken to be 0.87 and 1, respectively.

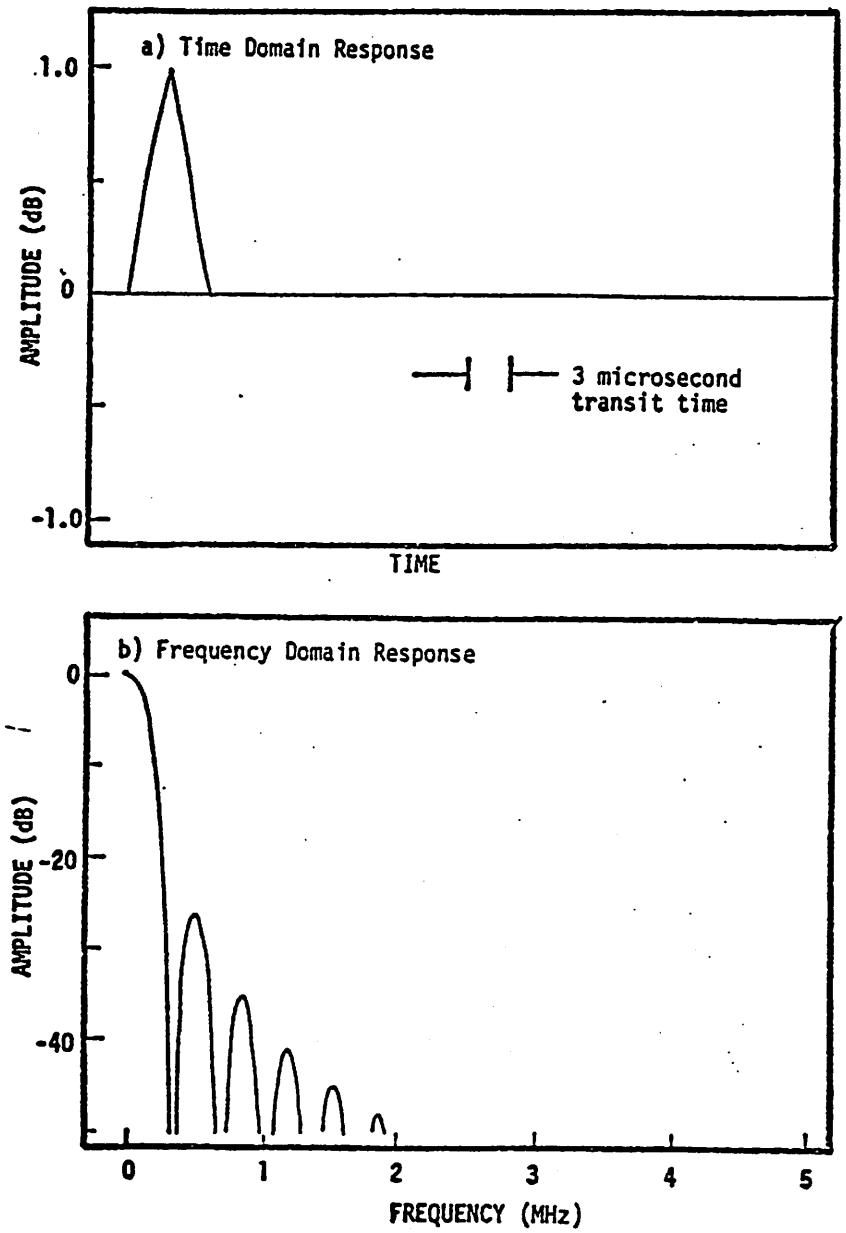

Figure III.9. Acoustoelectric response of CdS to a short ($t_D = \ell/v$) burst of ultrasound. In panel a) the time domain acoustoelectric current density predicted from Eq. (III.41) is shown. In panel b) spectral amplitude of the acoustoelectric current density is shown. Transit time through crystal was assumed to be 3 microseconds, and r_o and r_ℓ were taken to be 0.87 and 0, respectively.

Let us consider a single passage through a piezoelectric semiconductor of a gated burst of ultrasound with center frequency ω. Assuming that the acoustic burst is uniformly attenuated we can use the Weinreich relation[30] [Eq. (II.23)] to write the instantaneous current density

$$J_{AE}(\sigma,\omega) = -\mu \frac{\alpha(\sigma,\omega)}{v(\sigma,\omega)} \Phi \quad . \tag{III.43}$$

At a particular conductivity σ and ultrasonic frequency ω we see that the acoustoelectric current density is proportional to the ratio of the attenuation coefficient and the velocity of sound which are also functions of σ and ω. In Figure III.10 we plot the predictions of the Hutson and White theory[37] for α and v as a function of conductivity relaxation frequency σ/ε for three different ultrasonic frequencies. We see a set of relaxation curves and note that the position of these curves is determined by the ratio of the conductivity relaxation frequency to the ultrasonic frequency ω ($\omega_c/\omega = 1$). The amplitudes of the attenuation curves are proportional to the ultrasonic frequency. Over the range of conductivities illustrated the attenuation coefficient changes by a factor of 10 and the velocity of sound changes by a factor of approximately 0.01. Because $\Delta v/v_s$ varies by only about 0.01, the conductivity and frequency dependence of the acoustoelectric current is determined primarily by the attenuation coefficient $\alpha(\sigma,\omega)$.

The Weinreich relation can also be written in terms of an effective electric field E_{AE} which would produce this same current flow within the semiconducting crystal,

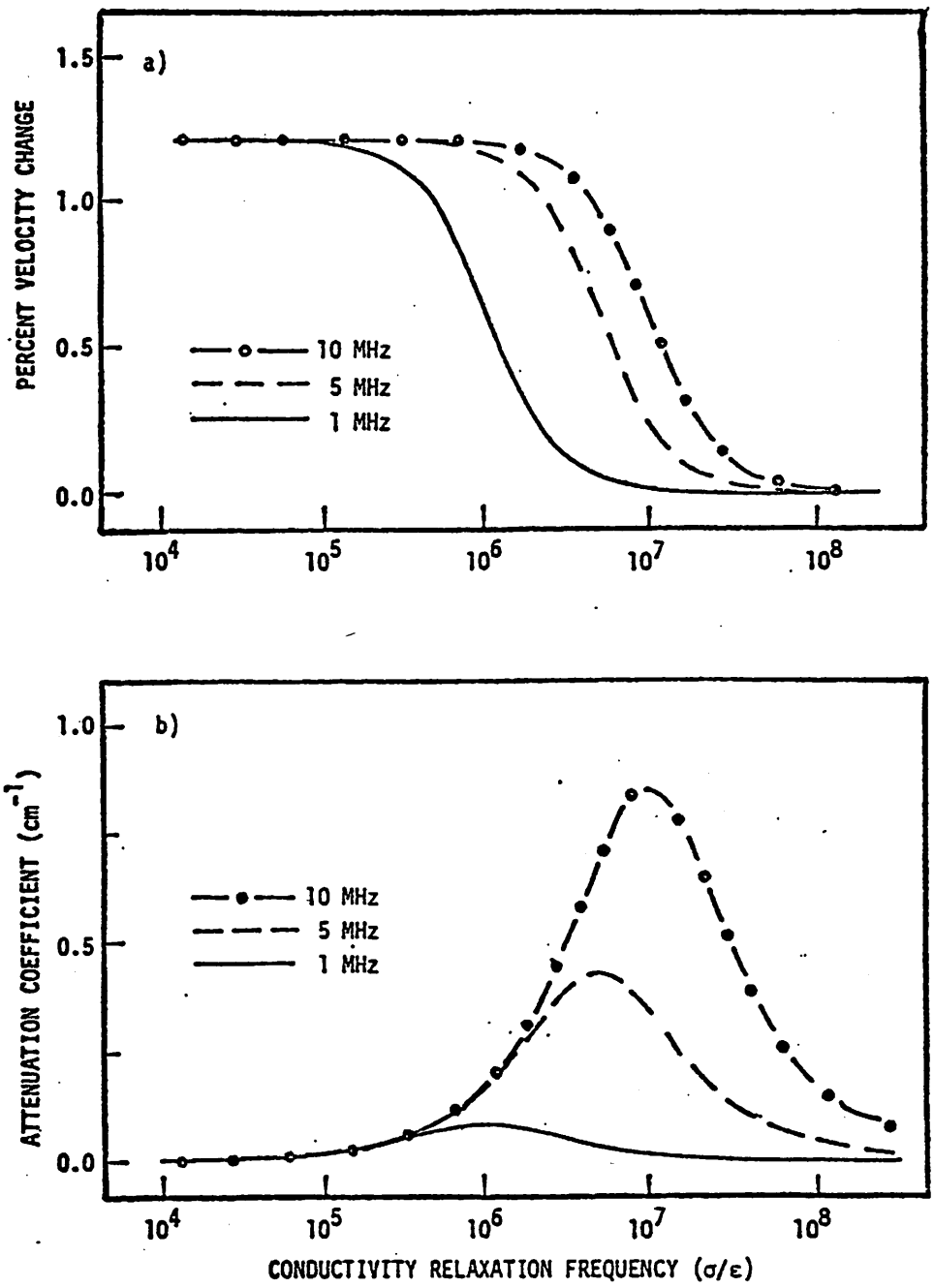

Figure III.10. Relative magnitude of dispersion and attenuation caused by acoustoelectric effect in CdS. In panel a) the percent velocity change predicted from Eq. (II.18) for three different ultrasonic frequencies is shown as a function of crystal conductivity. In panel b) the electronic attenuation coefficient is shown as a function of crystal conductivity for three different ultrasonic frequencies.

$$E_{AE} = \frac{J_{AE}}{\sigma} \approx \frac{2\mu}{v_s} \frac{\alpha(\sigma,\omega)}{\sigma} \Phi \quad . \tag{III.44}$$

This is the electric field strength which we used in Section III.E to predict the open circuit voltage response of a piezoelectric semiconducting plate. The conductivity and frequency dependence of Eq. (III.44) is determined by the ratio of the attenuation coefficient to the crystal conductivity. Using the expression for the attenuation coefficient from Eq. (II.18) (with no applied drift field) we find that

$$\frac{\alpha(\sigma,\omega)}{\sigma} = \frac{e^2}{2v_s c \varepsilon^2} \left\{ \frac{1}{1 + (\omega_c/\omega)^2} \right\} \quad . \tag{III.45}$$

When the conductivity relaxation frequency is less than the ultrasonic frequency, the effective field strength predicted is nearly independent of conductivity and ultrasonic frequency. Therefore, the open circuit voltage produced across a piezoelectric semiconductor in the low conductivity limit should be independent of ultrasonic frequency.

In Figure III.11 we plot the predicted forms of the acoustoelectric current density J_{AE} and the acoustoelectric field strength E_{AE} as a function of the conductivity relaxation frequency ω_c for three different values of the ultrasonic frequency. In panel a) we see that the optimum value of the conductivity relaxation frequency changes by a factor of 10 as the ultrasonic frequency changes by a factor of 10. From panel b) we see that a value of ω_c can be chosen ($\sim 2 \times 10^5$) which maximizes the acoustoelectric field strength for all of the ultrasonic frequencies chosen. The predictions of Figure III.11 indicate that a broadband

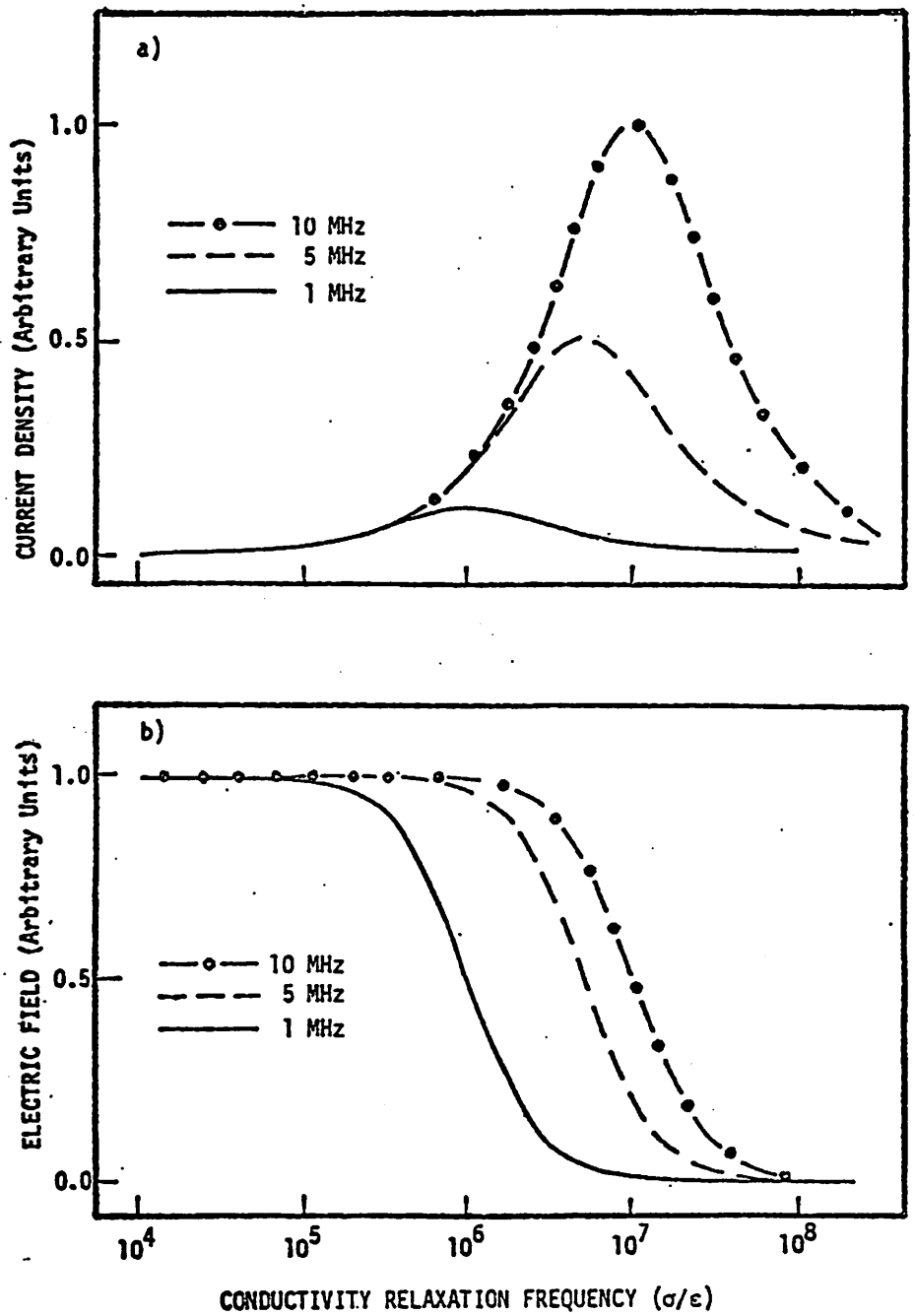

Figure III.11. Relative magnitude of acoustoelectric current density and acoustoelectric field strength in CdS. In panel a) the current density for three ultrasonic frequencies is shown as a function of the crystal conductivity. In panel b) the acoustoelectric field strength produced by three ultrasonic frequencies is shown as a function of crystal conductivity. At low values of crystal conductivity (i.e., $\sigma/\varepsilon \sim 10^5$) acoustoelectric field strength is large and constant for all frequencies considered.

ultrasonic detector, i.e., a detector with an efficiency which is frequency independent, can be achieved by measuring the open circuit acoustoelectric voltage.

In practice, it should be noted that the conductivity relaxation frequency cannot be decreased without limit. From an equivalent circuit point of view, the source impedance of the acoustoelectric voltage source goes to infinity as the conductivity relaxation frequency and hence conductivity go to zero. Any stray capacitance associated with the input of a signal amplifier will therefore make detection of short (1-2 μsec) ultrasonic pulses difficult. A typical operating point for the conductivity relaxation frequency might be 1×10^6 sec. At this conductivity the source impedance associated with a 1 cm long x 1 cm^2 single crystal of CdS is approximately $5 \times 10^5\ \Omega$. At this resistance level, care must be taken to minimize input capacitance if good pulse resolution (on the order of microseconds) is to be maintained. This point will be addressed later in Chapter V.

F. Noise and Sensitivity

In this section we consider sources of noise in the context of using CdS as a detector of ultrasound. We also discuss non-random electrical effects which arise from the direct piezoelectric effect in CdS. These non-random electrical signals are considered here as noise because they can potentially limit the sensitivity of an acoustoelectric detection scheme.

Much of the theory describing the noise generating properties of cadmium sulfide has been developed in the context of using CdS as a photodetector. A general survey of the sources of random noise observed in photoconductors has been given by Rose.[51] The sources of noise which he identified were: i) at low frequencies, contact noise associated with the way in which electrical contact is made to the surface of a semiconducting material, ii) at intermediate frequencies, generation-recombination noise associated with fluctuations in the number of thermally or optically excited current carriers and iii) at higher frequencies, Johnson or Nyquist noise which is present in any resistance element.

A series of experiments were performed by Shulman[52] to investigate the low frequency noise currents associated with the electrical contact to the surfaces of single crystals of CdS. He showed that the low frequency noise spectrum generated with metal contacts on CdS could be reduced if a low work function metal such as indium were used. This reduction in low frequency noise was attributed to the ohmic nature of the indium-CdS contact. It was further pointed out by Rose[51] that when ohmic contacts are provided to CdS crystal which exibit a negligible dark current (high resistivity crystals) the noise associated with the random fluctuations of thermally generated carriers can be neglected and thus only photocurrent noise and Johnson noise need to be considered. The noise current associated with the random fluctuations of photo excited charge carriers has been measured in CdS by Van Vleit et al.[53] They showed that the noise spectrum associated with photocurrent noise is slowly varying with

frequency at low frequencies to about 1000 Hz and then falls off rapidly ($1/f^2$) with increasing frequency.

We see that most of these sources of electrical noise can be eliminated from ultrasonic experiments by either careful sample preparation or by limitation of the electrical bandwidth. All of the ultrasonic measurements made upon CdS which are reported in this work were performed on single crystals which had been provided with ohmic electrical contacts, and most of the electrical measurements were band limited to the 10^3 to 10^6 Hz frequency range. For these reasons, the major source of electrical noise in our measurements can be attributed to the Johnson noise associated with bulk electrical resistance of the CdS crystal.

It is useful to compare the value of Johnson noise associated with bulk resistance of the CdS crystal to the acoustoelectric responsivity of CdS crystal. In this way, we can estimate the noise equivalent acoustic power, i.e., the acoustic power needed to generated an acoustoelectric voltage which is equal to the root mean square noise voltage produced by the crystal. For the acoustoelectric response of CdS as a broadband ultrasonic detector, the responsivity of interest is the "open circuit" voltage produced by the CdS crystal when it is exposed to a "short" burst of ultrasonic energy (vis., Section III.D). Equation (III.41) can be used to evaluate this responsivity,

$$V_{AE} = \langle J_{AE} \rangle SR = \frac{2\alpha_E \mu}{v\ell} SR\, \Phi_o \int_o^{\ell} e^{-2\alpha_T z}\, dz \qquad \text{(III.46)}$$

where Φ_o is the incident ultrasonic intensity R is the bulk crystal resistance and S is the cross sectional area. Here we have rewritten Eq. (III.41) in terms of the acoustoelectric voltage produced when the CdS crystal is perfectly matched to an acoustic load (i.e., $r_o = r_\ell = 0$). In other words, we consider only a single pass of the ultrasonic pulse through the crystal. Under these conditions we find that when the pulse length is equal to the crystal length, the acoustoelectric voltage is

$$V_{AE} = - \frac{\mu}{v\ell} SR \Phi_o \left(\frac{\alpha_E}{\alpha_T}\right)\left(1 - e^{-2\alpha_T \ell}\right) \quad . \tag{III.47}$$

From Section III.G, we saw that this signal was maximized with respect to thermal noise when the total ultrasonic attenuation coefficient α_T was equal to the electronic attenuation coefficient α_E and when $\alpha_T \ell$ was approximately equal to 1.1. Therefore the optimum voltage responsivity is

$$V_{AE}^{opt} \approx - \frac{\mu}{v\ell} SR_{opt} \Phi_o \quad . \tag{III.48}$$

We have written the crystal resistance as R_{opt} to emphasize the fact that for a specified geometry, the conductivity which optimizes $\alpha_E \ell$ also fixes the crystal resistance. The root mean square Johnson noise associated with this resistance is given by the well known expression

$$V_J = \sqrt{4kTR_{opt}\,\Delta f} \tag{III.49}$$

where k is the Boltzman's constant, T is the absolute temperature and Δf is the electrical bandwidth over which the measurement is to be made.

Equating the rms Johnson noise to the magnitude of the voltage responsitivity allows us to determine the noise equivalent acoustic power Φ_{min},

$$\Phi_{min} = \frac{v\ell}{\mu S}\sqrt{\frac{4kT\ \Delta f}{R_{opt}}} \quad . \tag{III.50}$$

Using the values specified in Table III we find the minimum detectable acoustic intensity in the presence of thermal noise is approximately 1.6×10^{-7} watts/cm^2.

The thermal noise generated by the bulk crystal resistance, however, is not the only source of extraneous electrical signal in the 10^3 to 10^6 Hz frequency range. For example when a high input impedance amplifier is used to measure the open circuit response of a piezoelectric plate to a short burst of ultrasonic energy, the low frequency components of the stress associated with the pulse can produce an appreciable electrical signal. Although we are attempting to measure the open circuit acoustoelectric response of a piezoelectric semiconductor to the high frequency stress components, we are forced to consider also the piezoelectric response of the plate to low frequency stress components because both resulting electrical signals fall in the same bandwidth.

The reduced Mason equivalent circuit (shown in Figure III.3) describing the response of the thick piezoelectric material to a short ultrasonic pulse allows us to estimate the magnitude of this effect. The magnitude of the transfer function of this equivalent circuit can be expressed in terms of volts produced per unit force incident upon the plate,

$$\left|\frac{V}{F}\right| = \frac{2}{h} \frac{\omega R}{\left\{\left(1 + \frac{\omega^2(Z_1 + Z_0)R}{h^2}\right)^2 + \left(\frac{\omega^2(Z_1 + Z_0)}{h^2 C_o}\right)^2\right\}^{\frac{1}{2}}} \qquad \text{(III.51)}$$

where R is the load resistance, C_o is the static plate capacitance, and h is the piezoelectric coupling constant. This transfer function can be used to calculate the low frequency electrical response $V_{PE}(\omega)$ to low frequency stress components $T(\omega)$

$$V_{PE}(\omega) = \left|\frac{V}{F}\right| T(\omega) S \quad , \qquad \text{(III.52)}$$

where S is the cross sectional area being considered. Because the acoustoelectric response of a piezoelectric semiconductor is proportionalto intensity or stress squared and the piezoelectric response of the material is proportional to stress, the acoustoelectric response of the material will always dominate at high stress levels. At low signal levels, however, the low frequency piezoelectric response of the plate will outweigh the acoustoelectric response of the plate. We are interested in estimating at what stress level the magnitude of these two responses are comparable, i.e.,

$$|V_{AE}| = |V_{PE}| \quad . \qquad \text{(III.53)}$$

In terms of the stress amplitude, Eq. (III.53) is satisfied if

$$\frac{\mu}{v\ell} SR \frac{|T(rf)|^2}{Z_1} = \left|\frac{V}{F}\right| T(\ell f) S \qquad \text{(III.54)}$$

where $T(rf)^2/Z_1$ is the incident ultrasonic intensity at the center

frequency of the pulse. Here we have noted a difference between T(rf) and T(ℓf) because the acoustoelectric response produces a low frequency voltage which is proportional to the stress at the higher radio frequency T(rf). In contrast, the piezoelectric plate does not perform this frequency transformation and so the low frequency voltage is proportional to the low frequency stress components T(ℓf).

In order to carry this analysis any further, we must assume a specific pulse shape so that the ratio of high and low frequency stress components can be determined. A typical ultrasonic pulse used in the present work consists of a 3 μsec tone burst of 5 MHz ultrasound. In the frequency domain, a sharp-edged pulse of this type produces a sin(x)/x spectrum with the result that some ultrasonic energy is present in the low frequency portion of the spectrum. For this case, the amplitude of the low frequency stress component centered at approximately 160 KHz is roughly a factor of 30 smaller than the center frequency stress component. Knowing this ratio we can now evaluate Eq. (III.54) using 160 KHz as the low frequency stress component and 5 MHz as the high frequency stress component to find the stress level at which the low frequency acoustoelectric and piezoelectric plate responses are comparable.

Using the typical values for CdS found in Table IV and using Figure III.5 to estimate the transfer function at 160 KHz of CdS loaded in a 500 KΩ resistor, we find that V_{PE} and V_{AE} are comparable when T(rf) is approximately equal to 1.1×10^{2} N/cm^{2}. This stress level corresponds to an ultrasonic intensity in water of approximately 1×10^{-6} watts/cm^{2}. We find that for the case considered this lower

Table IV

Typical Electrical and Mechanical Properties of CdS

v =	4.4×10^5 cm/sec
ℓ =	2 cm
μ =	300 cm^2/volt sec
S =	1 cm^2
f =	160; KHz
σ_{opt} =	4.2×10^{-6} Ω-cm
R_{opt} =	5×10^5
h =	5.2×10^9 V/m
$\varepsilon/\varepsilon_o$ =	9.53
C_o =	4.2×10^{-13} farad
Z =	2.1×10^7 Rayls

limit on detectable acoustic intensity is about an order of magnitude higher than the limit imposed by the Johnson noise associated with the resistance R. The limit imposed by the direct piezoelectric effect, however, is not a fundamental one in the sense that we are at liberty to "shape" the ultrasonic pulse in such a way as to substantially reduce the low frequency stress components in the pulse. Thus the sharp-edged pulse considered represents a worst-case analysis. Furthermore, many ultrasonic transmitting transducers are not capable of transmitting these low frequency stress components. Thus this low frequency piezoelectric signal does not impose the limit upon the sensitivity of an acoustoelectric receiver. In practice, therefore, the thermal noise of the CdS crystal regarded as a resistive element determines the limit of sensitivity.

IV. THE DETECTION OF SPATIALLY NON-UNIFORM ULTRASONIC RADIATION

A. Introduction

In the previous chapter the piezoelectric and acoustoelectric responses of a piezoelectric semiconductor to an acoustic plane wave of infinite extent at normal incidence were discussed. This treatment allowed us to look at the details of ultrasonic detection i.e., surface generation versus bulk generation, frequency components of the detected signal, and related matters. This ideal type of ultrasonic radiation, however, is rarely encountered in practical ultrasonic systems. Propagation of waves through non-parallel[7] or inhomogeneous[8] specimens is known to lead to ultrasonic wavefront distortion. Similarly, the effects of diffraction are known to introduce variations in the ultrasonic field parameters (amplitude and phase) even in the most elementary of pulse-echo or transmission experiments.[6,9,54-60]

In this chapter we consider the complications encountered in the detection of such non-uniform ultrasonic radiation. By non-uniform ultrasonic radiation we mean radiation which varies in either the amplitude or phase of the ultrasonic pressure field over the area of the receiver aperture. In this chapter we divorce ourselves from the details of piezoelectric and acoustoelectric receivers and focus upon the single major difference in the way each receiver detects a distorted ultrasonic wave. In particular, we focus on the difference between phase sensitive (i.e., piezoelectric-like) and phase insensitive (i.e., acoustoelectric-like) detection of non-coherent ultrasonic waves. Some experiments designed to illustrate this fundamental difference between piezoelectric and acoustoelectric receivers are proposed and discussed.

B. General Aspects of Piezoelectric Receivers—Phase Sensitive Aperture

The feature of piezoelectric receivers we explore in this section is that the electrical signals produced by these devices are proportional to the instantaneous (complex) amplitude of the incident ultrasonic field. This fact was illustrated in Section III.A for continuous wave operation of piezoelectrics and in Section III.C for the transient operation of piezoelectrics.

Practical piezoelectric receivers are finite aperture devices and because of this finite size, sample the ultrasonic field incident upon them at many different locations. Therefore in order to be able to interpret the output of a piezoelectric receiver, it is necessary to have some knowledge of the spatial character of the field incident upon it. The ultrasonic field incident upon a spatially extended piezoelectric receiver can be written in terms of a complex pressure field

$$\tilde{P}(x,y,z,\omega) = P_R(x,y,z,\omega) + i\, P_I(x,y,z,\omega) \qquad \text{(IV.1)}$$

where P_R and P_I represent the real and imaginary parts of the field at the point (x,y,z) and at the frequency ω. The electrical response of a piezoelectric plate to this pressure distribution is proportional to the instantaneous average of the complex pressure over the area of the plate.[6] If this pressure distribution is known, the magnitude of the piezoelectric response at the frequency ω of a plate located at a point z is

$$|V_{PE}(z,\omega)| \propto \left\{ \left| \int_{\sigma_R} P_R(x,y,z,\omega)\,dx\,dy \right|^2 + \left| \int_{\sigma_R} P_I(x,y,z,\omega)\,dx\,dy \right|^2 \right\}^{1/2}. \qquad \text{(IV.2)}$$

Here σ_R represents the surface of the receiver.

The integrals of the real and imaginary parts of the incident pressure field over the receiver aperture can be thought of as an instrumental interference effect. The effect is instrumental because it is intimately involved with the size, placement and geometry of the receiver element. The effect represents an interference because it is possible for cancellation of local electrical signals to occur when regions of positive and negative pressures occur simultaneously at different locations on the receiver aperture. This interference effect has come to be known as phase cancellation.

C. General Aspects of Acoustoelectric Receiver—Phase Insensitive Apertures

As we saw in Chapter III, the electrical signal produced by the interaction of elastic waves and charge carriers in a piezoelectric semiconductor is proportional to the square of the magnitude of the amplitude of the incident ultrasonic field. This fact was illustrated both in the case of continuous ultrasonic illumination [Eq. (III.26)] and pulsed ultrasonic illumination [Eq. (III.41)]. The acoustoelectric signal produced by a finite aperture piezoelectric semiconductor when it is illuminated by a nonuniform acoustic wave should therefore be proportional to the average value of the square magnitude of the complex pressure averaged over the receiver aperture,

$$V_{AE}(z,\omega) \propto \int_{\sigma_R} |\tilde{P}(x,y,z,\omega)|^2 \, dx \, dy \quad . \tag{IV.3}$$

Because we are integrating a positive definite quantity ($|\tilde{P}|^2$) over our receiver aperture no cancellation of signals can take place, regardless of the degree of wavefront distortion. Thus we find that no interference takes place in the expression for V_{AE}, unlike the case for V_{PE}.

(Strictly speaking, the acoustoelectric voltage is not an instantaneous average of $|\tilde{P}(x,y,z,\ )|^2$. From the analysis presented in Section III.F, we expect to see some smearing out of V_{AE} in time because of the finite transit time of the acoustic pulse through the detector. However for the purpose of comparing the output of a phase sensitive and phase insensitive receiver aperture, this slight amount of temporal averaging will be ignored.)

D. Diffraction Model

In order to investigate theoretically the detection properties of finite aperture phase sensitive or phase insensitive receiver in the presence of nonuniform ultrasonic illumination it is necessary to have a physically realizable model for producing "distorted" ultrasonic radiation. Once a specific model has been formulated, the complex pressure at the receiver aperture can be calculated and the integrated response of either type of detector predicted.

We have chosen to model the effects of non-coherent ultrasonic radiation in the context of diffraction theory. Figure IV.1 illustrates the geometry associated with the diffraction integral[61]

$$\tilde{P}(x,y,z,\omega) = \frac{-i\omega\rho_o}{2\pi} \int_{\sigma_s} \frac{u(\vec{r}_1)e^{i(\phi(\vec{r}_1)+k|\vec{r}_2-\vec{r}_1|)}}{|\vec{r}_2 - \vec{r}_1|} d\sigma_s \qquad \text{(IV.4)}$$

where ρ_o and k are the material density and wavevector in the medium through which the wave propagates. The aperture weighting function $u(\vec{r}_1)\exp(i\phi(\vec{r}_1))$ has been included to describe the amplitude and phase of the normal component of particle velocity over the transmitter aperture. Using

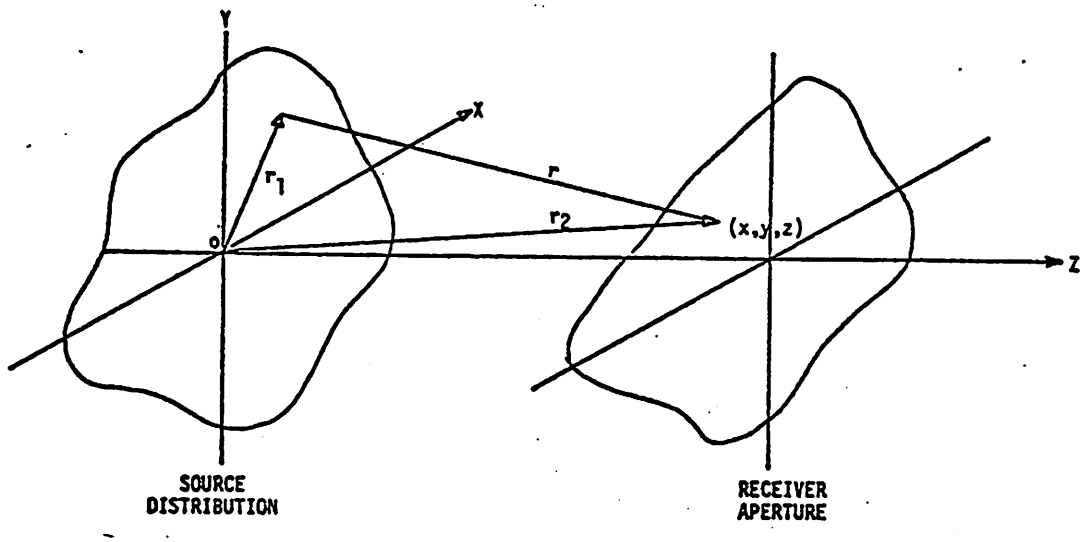

Figure IV.1. Geometry used to calculate the pressure distribution in the plane of the receiver. Diffraction theory can be used to calculate the complex pressure field for an arbitrary distribution of sources.

this diffraction integral we are able to calculate the complex pressure field produced by a source distribution located in the x-y plane at $z = 0$. The field at any specific point ($\vec{r}_2$) on the surface of the receiver aperture is proportional to an integral over the surface of the source distribution which corresponds to $\vec{r}_1$ taking on all possible values. The complete solution of the diffraction problem then involves letting $\vec{r}_2$ take on all possible values so that the complex pressure $\tilde{P}(x,y,z,\omega)$ can be determined at all points on the receiver aperture.

In order to model the production of non-uniform ultrasonic waves the arrangement illustrated in Figure IV.2 was chosen because it lends itself to an easily implemented, partially analytical, partially numerical solution. The distribution is seen to be invariant with respect to displacement in the y direction (i.e., extends from $-\infty$ to $+\infty$). This symmetry allows the source distribution to be considered as a sum of a series of strip sources located at points x_j, z_j. This configuration allows a variety of physically realizable source distributions to be "synthesized".

The diffraction integral can now be decomposed into a sum of strips (j) and each of width Δx_j and consisting of a line integral (dy),

$$\tilde{P}(x',y',z',\omega) = \frac{-i\omega\rho_o u}{2\pi} \sum_j \left\{ e^{i\phi_j} \Delta x_j \left[\int_{-\infty}^{\infty} \frac{e^{ikr_j}}{r_j} dy \right] \right\} \qquad \text{(IV.5)}$$

where

$$r_j = \left\{ (x'-x_j)^2 + (y'-y)^2 + (z'-z_j)^2 \right\}^{1/2}$$

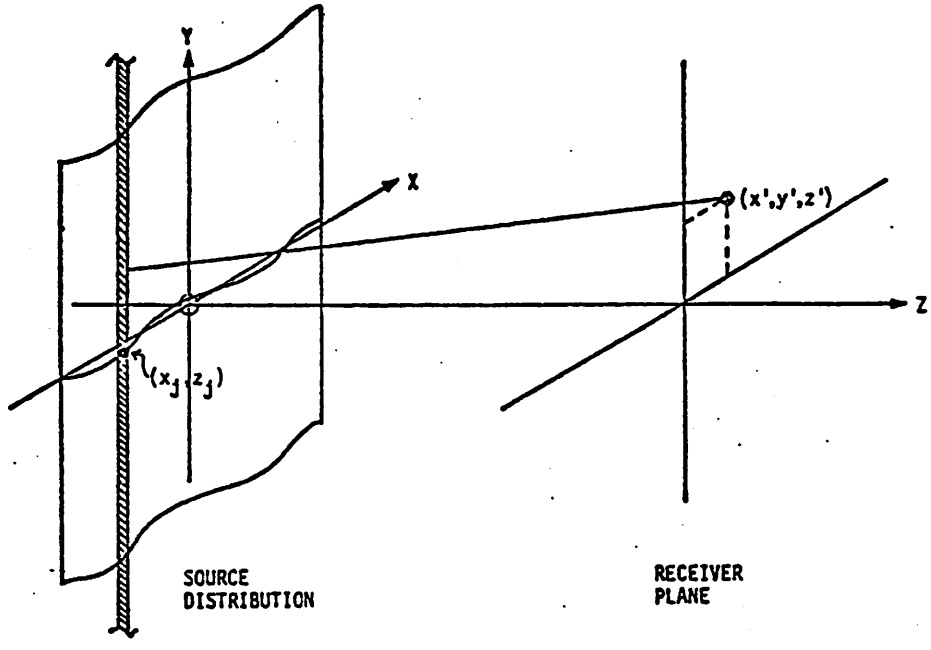

Figure IV.2. Geometry associated with the diffraction integral for a simplified distribution of sources. The source distribution is chosen to be invariant with respect to displacement in the y direction.

The integration over y determines the contribution of each strip to the pressure at the receiver aperture and the sum over j adds up the contributions of the strips. The magnitude of the particle velocity for each strip has been assumed constant and the phase factor ϕ_j allows each strip to radiate phase independent of the others.

Because the source distribution does not vary with translation in y direction, the complex pressure at the receiver aperture will also be invariant with respect to y displacements. It is sufficient therefore to calculate $\tilde{P}(x',y',z',\omega)$ along a line in the receiver aperture defined by y' = constant. For convenience we choose the line to be y' = 0 so that Eq. (IV.3)

$$\tilde{P}(x',o,y',\omega) = \frac{-i\omega\rho_o u}{2\pi} \sum_j \left\{ e^{i\phi_j} \Delta x_j \left[\int_{-\infty}^{\infty} \frac{e^{ik\sqrt{(x'-x_j)^2+(z'-z_j)+y^2}}}{\sqrt{(x'-x_j)^2+(z'-z_j)^2+y^2}} dy \right] \right\} \tag{IV.6}$$

This integral over y can be put into the form of the integral representation of the Hankel function[62]

$$\int_{-\infty}^{\infty} (\quad) dy = i\pi H_o^{(1)} [k(x'-x_j)^2 + (z'-z_j)^2)^{1/2}] \ . \tag{IV.7}$$

For the situations considered we will always place the receiver aperture at distances L such that kL >> 1, and so it is convenient to use the asymptotic form of the Hankel function,

$$H_o^{(1)}(kr) = \sqrt{\frac{2}{\pi kr}} e^{i(kr-\pi/4)} \ . \tag{IV.8}$$

In this approximation the expression for the complex pressure along the line $y' = 0$, in the receiver aperture becomes

$$P(x',o,z',\omega) = \omega\rho_o u \sum_j \frac{e^{i[k((x'-x_j)^2 + (z'-z_j)^2)^{1/2} + \phi_j]}}{(2\ k((x'-x_j)^2 + (y'-y_j)^2)^{1/2})^{1/2}} \Delta x_j \quad . \qquad (IV.9)$$

In order to evaluate this expression numerically, it is necessary to choose a specific distribution of strip sources.

1. Proposed Experiments: Transmission

The first source distribution analyzed is considered schematically in Figure IV.3. The physical situation being modeled is presented in panel a). We consider a bounded plane wave normally incident upon and transmitted through a plastic object which is flat and parallel except for a step discontinuity milled into one of its surfaces at $x = 0$. This physical situation is modeled by the distribution of sources presented in panel b). The difference $\Delta\phi$ in phase of the excitation for sources located at $x > 0$ and $x < 0$ corresponds simply to Δz the step thickness times the difference of the ultrasonic wave vector in the plastic material and water.

$$|\Delta\phi| = \Delta z(k_w - k_p) \quad . \qquad (IV.10)$$

The complex pressure produced by a distortion of 200 strip sources was evaluated numerically for 50 points on the receiver aperture over the frequency range of 3 to 8 MHz. The spatial extent of the source was chosen to be 1 cm and Eq. (IV.9) was evaluated for a receiver aperture of 1 cm placed a distance of 1 cm from the source. The ultrasonic wavevectors k_w and k_p were calculated assuming that the

a)

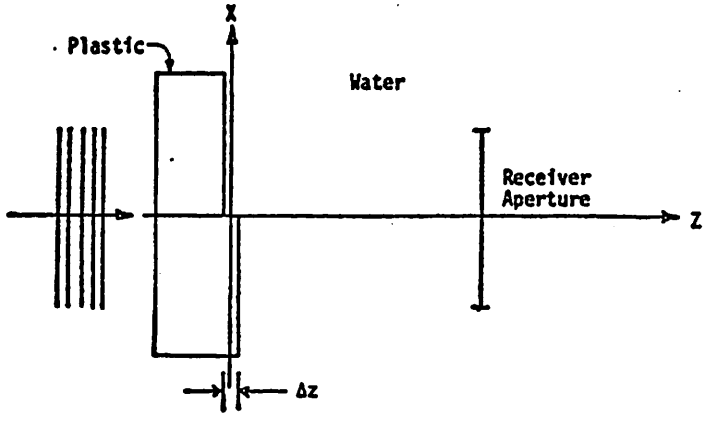

b)

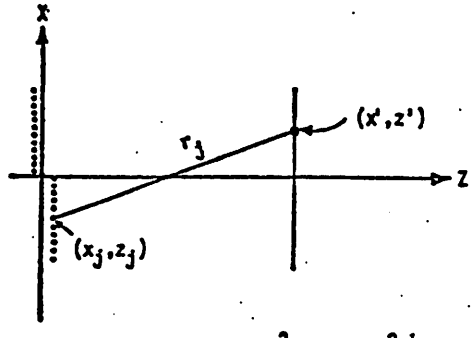

$$r_j = [(x'-x_j)^2 + (z'-z_j)^2]^{\frac{1}{2}}$$

$$|\Delta\phi| = \Delta z(k_w - k_p)$$

Figure IV.3. Geometry used to calculate the field distribution produced by a flat and parallel plate with step discontinuity. Experimental situation is schematically depicted in panel a). Complex pressure field is calculated in receiver aperture using 200 infinitesimally thin strip sources arranged as shown in panel b).

velocity of sound in water and plastic is 1.5×10^5 cm/sec and 2.5×10^5 cm/sec, respectively. The phase shift $\Delta\phi$ was evaluated assuming $\Delta z \sim 1$ mm. Although the numerical calculations were carried out at discrete frequencies over the range 3 to 8 MHz, for purposes of illustration results obtained at three "special" ultrasonic frequencies (3.8, 5.7, and 7.6 MHz) are singled out for comparison in Figures IV.4, IV.5, and IV.6. In each figure the real and imaginary parts of the complex pressure field are plotted in panel a) and the magnitude of the ultrasonic pressure field is shown in panel b). In Figure IV.4 and IV.6 (corresponding to ultrasonic frequencies of 3.8 and 7.6 MHz, respectively), we see that the real and imaginary part of the pressure fields are of a single sign over the receiver aperture. At these frequencies the phase shift $\Delta\phi$ introduced by the step discontinuity corresponds to 2 and 4 half wavelengths respectively. Therefore, the effects of the step discontinuity "disappear" and the field pattern is effectively that of a single flat distribution of sources. At the ultrasonic frequency of 5.7 MHz the step discontinuity introduces a phase shift of 3 half wavelengths in the field originating from the $x > 0$ portion of the source distribution relative to that originating from the $x < 0$ portion of the source distribution. This is manifested by the abrupt change in sign of the real and imaginary parts of the pressure distribution at the center of the receiver aperture.

Simulation of output of a phase sensitive or phase insensitive receiver over the full range 3 to 8 MHz can now be performed using the calculated pressure distributions. The output of a phase sensitive (piezoelectric) receiver can be predicted by integrating the complex pressure curves such as in panel a) of Figures IV.4, IV.5, and IV.6.

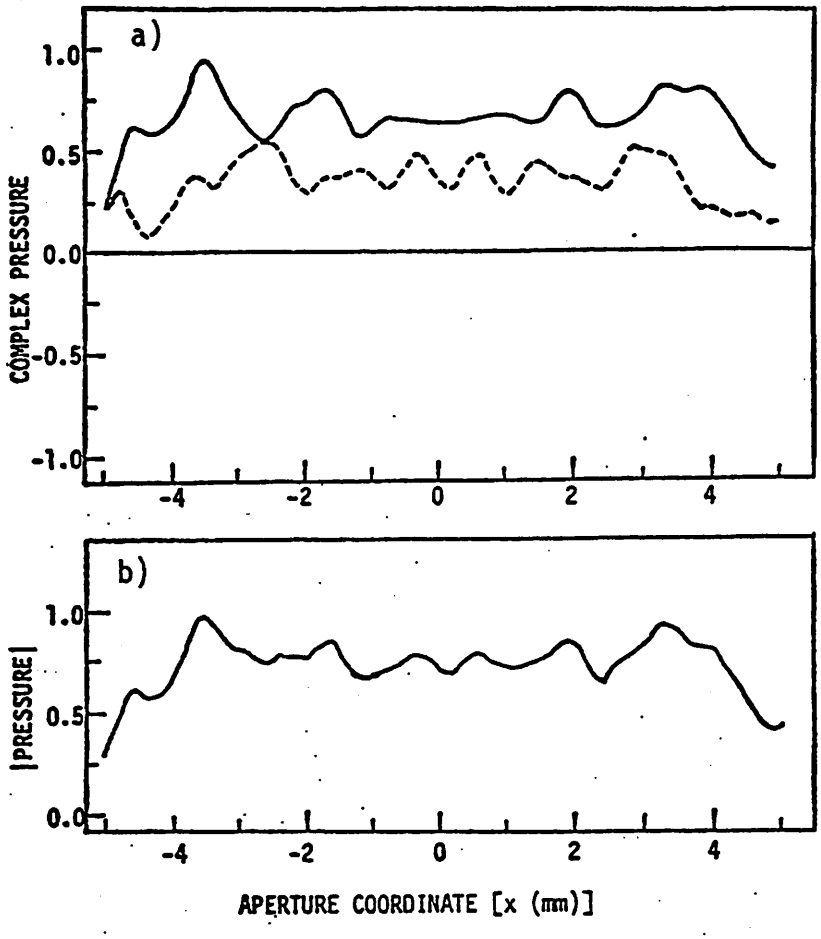

Figure IV.4. Complex pressure field at 3.8 MHz produced by step discontinuity. Real and imaginary parts of pressure field are shown in panel a) for a 1 cm receiver aperture located 1 cm from the stepped plate. The magnitude of the complex pressure over the receiver aperture is shown in panel b).

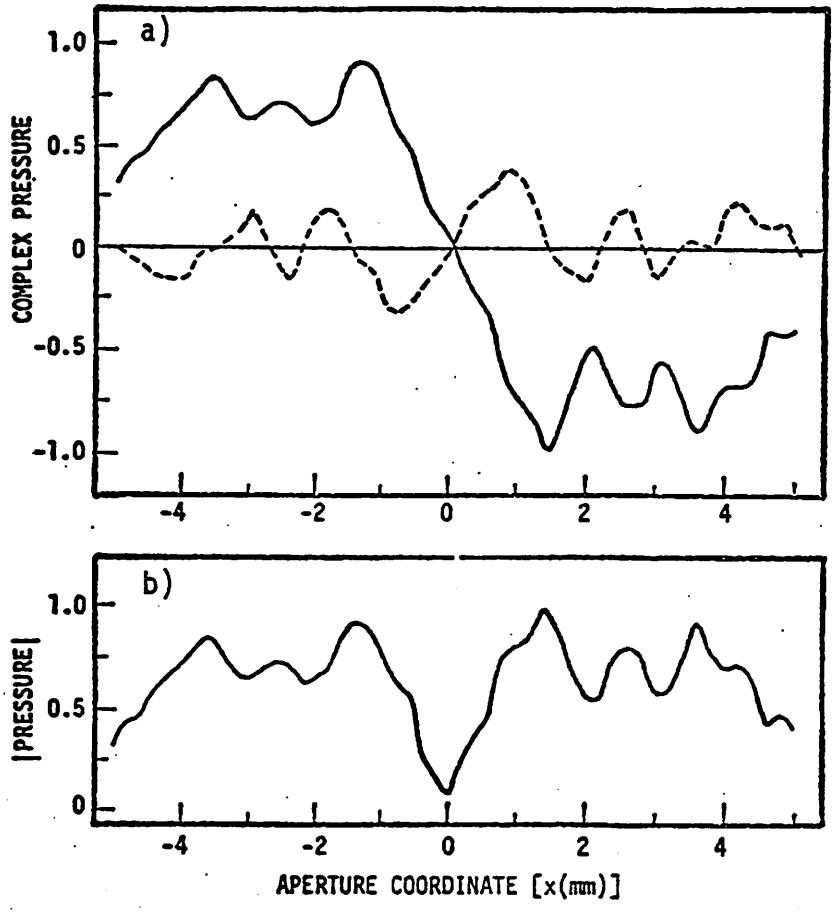

Figure IV.5. Complex pressure field at 5.7 MHz produced by step discontinuity. Real and imaginary parts of the pressure are shown in panel a) for a 1 cm receiver aperture located 1 cm from the stepped plate. The magnitude of the complex pressure over the receiver aperture is shown in panel b).

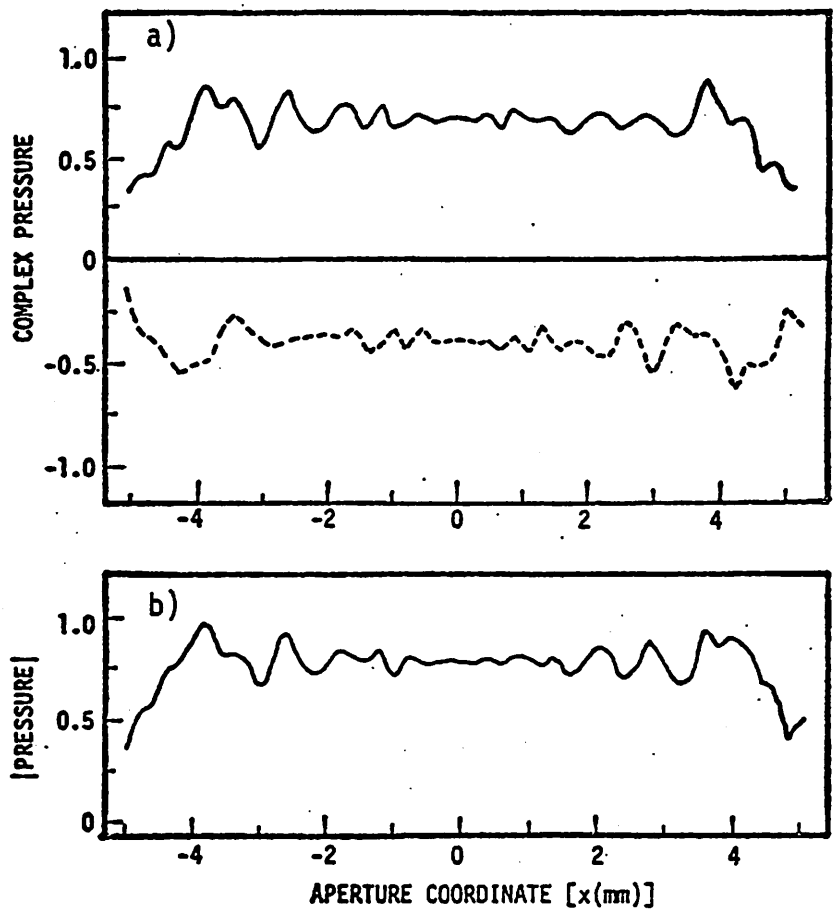

Figure IV.6. Complex pressure field at 7.6 MHz produced by step discontinuity. Real and imaginary parts of the pressure are shown in panel a) for a 1 cm receiver aperture located 1 cm from the stepped plate. The magnitude of the complex pressure over the receiver aperture is shown in panel b).

This integral can be done in one dimension because of the symmetry imposed,

$$|V_{PE}(z_1,\omega)| \propto \left\{\left(\int P_R(x_1,o,z_1,\omega)dx_1\right)^2 + \left(\int P_I(x_1,o,z_1,\omega)dx_1\right)^2\right\}^{\frac{1}{2}} . \quad (IV.11)$$

Likewise, the output of a phase insensitive (acoustoelectric) receiver can be predicted by integrating the magnitude of the pressure curves such as in panel b) of Figures IV.4, IV.5, and IV.6. In one dimensional form

$$V_{AE}(z_1,\omega) \propto \int |\tilde{P}(x_1,o,z_1,\omega)|^2 \, dx_1 \quad . \quad (IV.12)$$

In Figure IV.7 we present the results of these calculations in terms of the signal output as a function of frequency over the range of 3 to 8 MHz for a 1 cm receiver aperture. The square root of the output of the phase insensitive receiver is plotted in order to permit direct comparison with the output of the phase sensitive receiver. The output of the phase sensitive aperture (solid curve) goes to zero at certain ultrasonic frequencies (e.g., 5.7 MHz). At this frequency the waves emerging from one portion of the step are an odd number of half wavelengths out of phase with those emerging from the other portion. The fact that zero output should be expected at this frequency is illustrated by the antisymmetric nature of the components of the complex pressure field shown in Figure IV.5a. Partial or total cancellation of signal amplitude over a broad range of frequencies takes place with the phase sensitive receiver aperture. Any ultrasonic measurement which depends upon accurate knowledge of the signal amplitude will therefore be compromised by the use of this receiver. For example, the determination of the ultrasonic attenuation coefficient of the

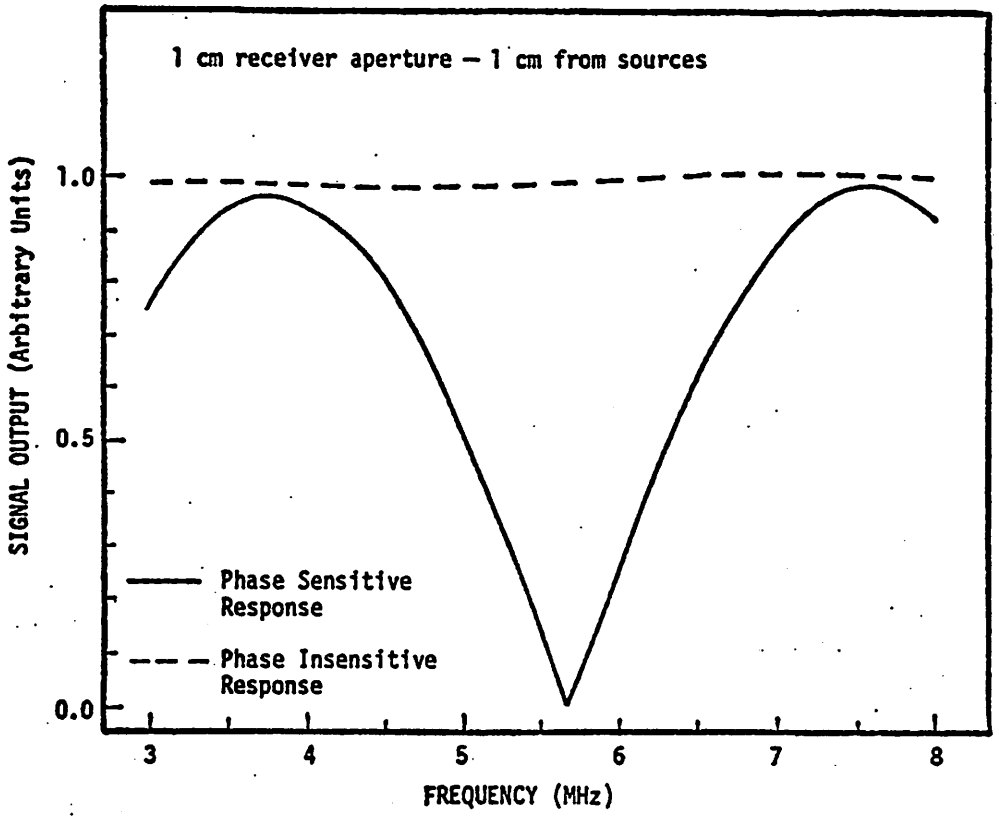

Figure IV.7. Signal amplitude versus frequency produced by phase sensitive and phase insensitive receiver aperture when placed in the pressure field produced by stepped plate. Output of phase sensitive receiver (solid line) is zero at 5.7 MHz; i.e., when the complex field distribution is antisymmetric over the receiver aperture. Output of phase insensitive receiver (dashed line) is nearly constant.

stepped plastic plate illustrated in Figure IV.3 would be severely compromised with the use of a phase sensitive receiver.

The predicted output of a phase insensitive receiver aperture is presented by the dashed curve in Figure IV.7. The output of this type of receiver is unaffected by the presence of the step in the distribution of sources. The frequency-independent nature of the output of the phase insensitive receiver is a consequence of the fact that no significant amount of ultrasonic energy has been lost from the field. Experimental results of measurement of the apparent attenuation coefficient of a stepped plastic plate using phase sensitive and phase insensitive receivers are presented in Chapter VI and compared with the predictions shown in Figure IV.7.

2. Scattering

A second class of source distributions designed to model a simple ultrasonic scattering measurement was considered. The scattering simulation is illustrated in Figure IV.8. Two cyclindrical sources are located in the x-z plane, a distance s apart. The plane containing the two scatterers is illuminated by a plane wave at an angle of incidence θ. Schematically, the distribution of sources can be modeled as two strip sources, located at $x = \pm s/2 \sin\theta$ and $z = \pm s/2 \cos\theta$, radiating with equal amplitude and with a phase difference determined by the separation $s \sin\theta$. The complex pressure in the plane of the receiver aperture consists of the coherent sum of the pressure produced by each of the strip sources independently:

$$\tilde{P}(x,z,\tilde{\theta}) \propto \frac{e^{-ik(s/2)\sin\theta}\, e^{i(kr_1-\pi/4)}}{\sqrt{kr_1}} + \frac{e^{ik(s/2)\sin\theta}\, e^{i(kr_2-\pi/4)}}{\sqrt{kr_2}} \qquad \text{(IV.13)}$$

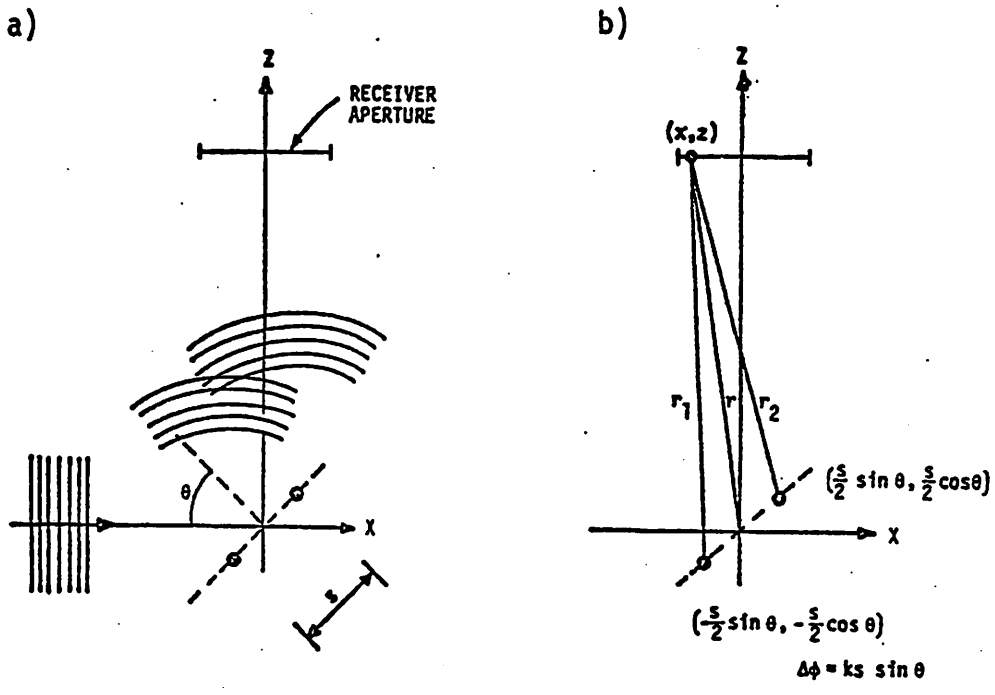

Figure IV.8. Geometry used to calculate field distribution produced by the scattering of a plane wave from two cylindrical scatterers. Experimental situation is depicted schematically in panel a). Complex pressure at a receiver aperture located at z = 20 cm and a scatterer separation s = 7.9 mm is calculated using the coordinate in panel b).

where

$$r_{\substack{1\\2}} = \sqrt{\left(x \pm \frac{s}{2}\sin\theta\right)^2 + \left(z \pm \frac{s}{2}\cos\theta\right)^2} \quad . \tag{IV.14}$$

After some algebraic manipulation and assuming that r_1 and r_2 can be approximated by r in the amplitude factors we find that

$$\tilde{P}(x,z,\theta) \propto \frac{e^{ik(r_1+r_2)/2}}{\sqrt{kr}} \cos[k(r_1 - r_2 - s\sin\theta)/2] \quad . \tag{IV.15}$$

The first term in Eq. (IV.15) suggests that the field pattern formed by the 2 strip sources is basically cylindrical in character. The second term, however, indicates that the amplitude of the wave is modulated by a cosine function which oscillates at a spatial frequency proportional to the difference between r_1 and r_2.

Although the pressure distribution in the receiver plane was computed at a large number of angles of incidence, for purposes of illustration results for three "special" angles [43.2°, 44.2°, and 45°] are presented in Figures IV.9, IV.10, and IV.11 In Figure IV.9 we show the complex pressure distribution at a frequency of 5 MHz produced in a receiver plane located at z = 20 cm by 2 cylindrical sources separated by a distance of 0.79 cm for an angle of incidence of 45°. In panel a) of Figure IV.9, the two rapidly oscillating curves represent the real and imaginary parts of the pressure field predicted by Eq. (IV.16). In panel b) of Figure IV.9 we show the magnitude of this pressure field. From the results shown in panel b) we see that a set of interference fringes analogous to a Young's interference pattern is formed in the plane of receiver aperture.

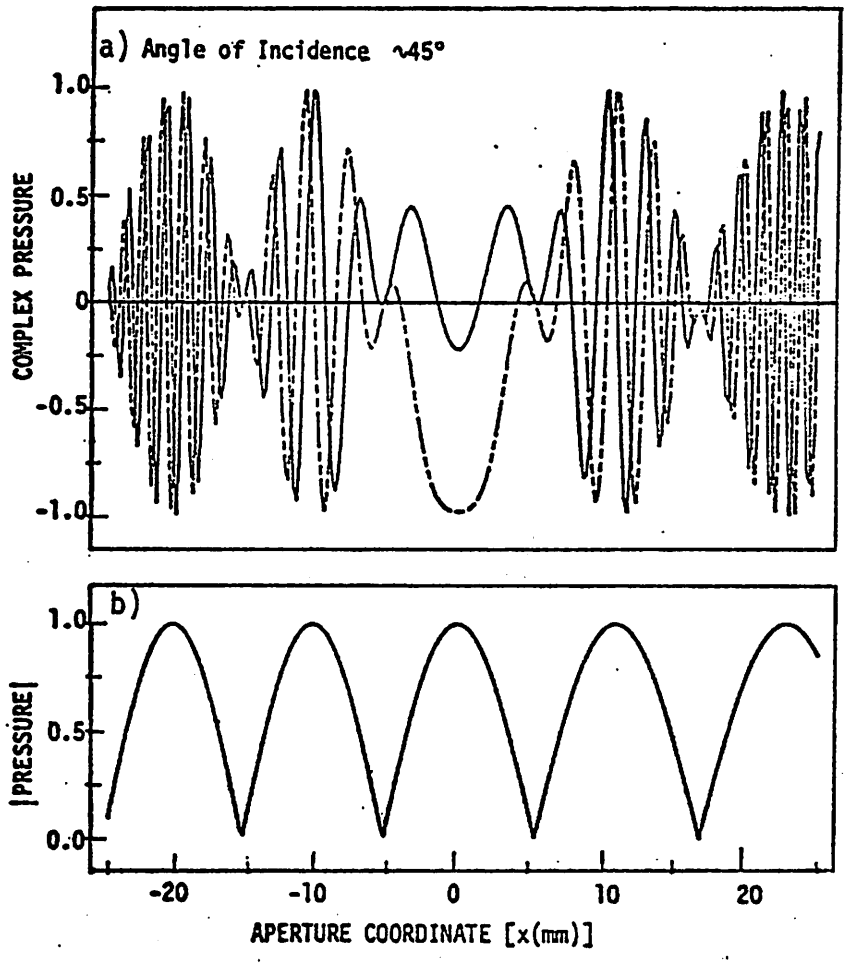

Figure IV.9. Complex pressure field produced by two cylindrical scatterers for $\theta = 45°$. Calculations were made assuming an ultrasonic frequency of 5 MHz. Real and imaginary parts of the pressure are shown in panel a) over a receiver plane located at $z = 20$ cm. Pressure distribution is nearly symmetric about $x = 0$ in the receiver plane. The magnitude of the complex pressure over the receiver plane is shown in panel b).

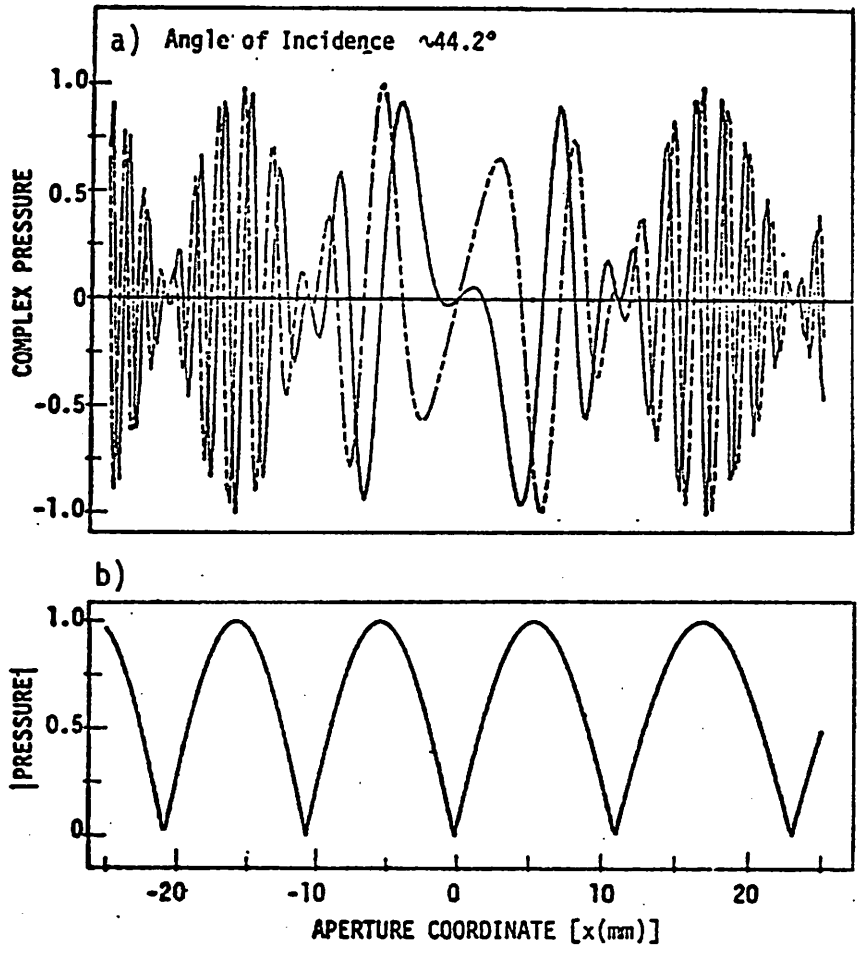

Figure IV.10. Complex pressure field produced by two cylindrical scatterers for $\theta = 44.2°$. Calculations were made assuming an ultrasonic frequency of 5 MHz. Real and imaginary parts of the pressure are shown in panel a) over a receiver plane located at $z = 20$ cm. Pressure distribution is nearly antisymmetric about $x = 0$ in the receiver plane. The magnitude of the complex pressure over the receiver plane is shown in panel b).

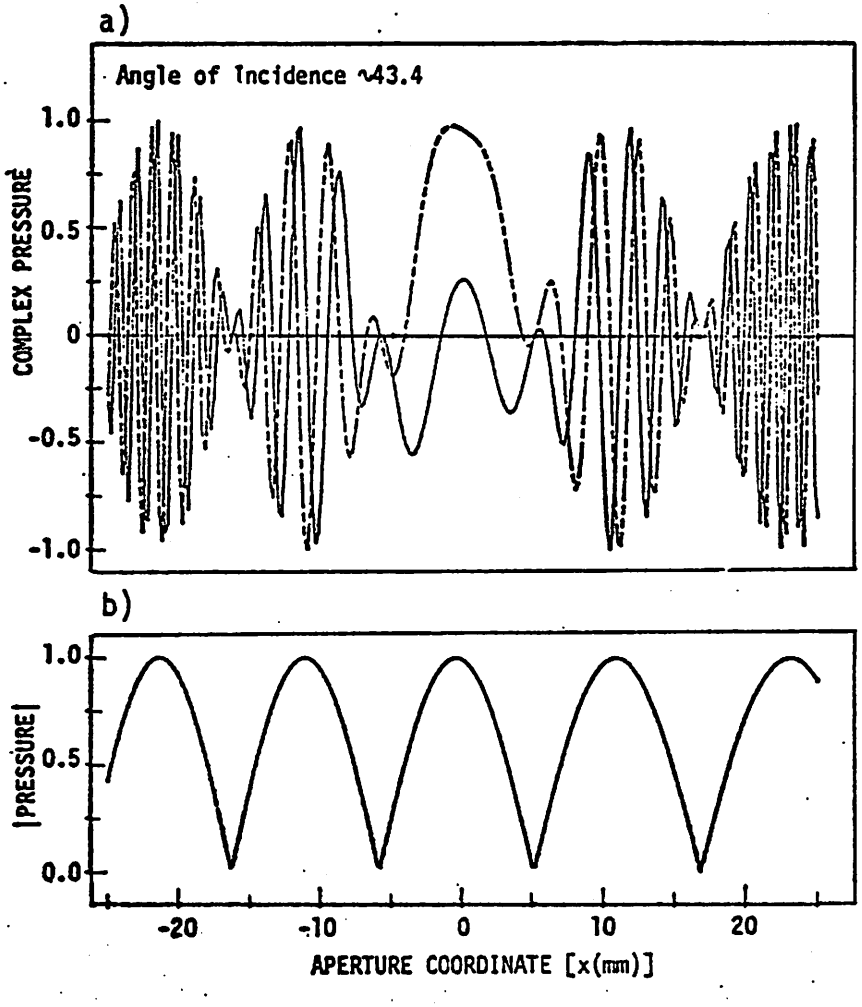

Figure IV.11. Complex pressure field produced by two cylindrical scatterers for $\theta = 43.4°$. Calculations were made assuming an ultrasonic frequency of 5 MHz. Real and imaginary parts of the pressure are shown in panel a) over a receiver plane located at $z = 20$ cm. Pressure distribution is nearly symmetric about $x = 0$ in the receiver plane. The magnitude of the complex pressure over the receiver plane is shown in panel b).

In Figures IV.10 and IV.11 we illustrate the field distributions at the angle of incidence of 44.2° and 43.4°, respectively. Once again, complex pressures are shown in panel a) and the magnitude of the pressure field are shown in panel b). As suggested by comparison of panel b) in Figures IV.9, IV.10, and IV.11, when the angle of incidence of the plane wave upon the rods is varied the set of interference fringes is swept across the plane of the receiver aperture.

Using field distribution plots such as those in Figures IV.9, IV.10, and IV.11 we can predict the output of finite sized phase sensitive and phase insensitive apertures. In order to facilitate the comparison of various sizes and types of receivers we have chosen to compare normalized receiver outputs. For the phase sensitive receiver this quantity is

$$\left|\int_{\sigma_R} \tilde{P}(x,y,\theta)dx\ dy\right| \Big/ \int_{\sigma_R} dx\ dy \qquad \text{(IV.16)}$$

where σ_R is the surface of the receiver element. For the phase insensitive receiver the normalized receiver output is

$$\int_{\sigma_R} |\tilde{P}(x,y,\theta)|dx\ dy \Big/ \int_{\sigma_R} dx\ dy \quad . \qquad \text{(IV.17)}$$

This normalization was chosen so that either type of receiver would yield outputs independent of size when illuminated by a uniform plane wave. Any departure from uniform illumination results in reduced receiver output.

Let us first consider the case of various sized receiver elements centered at $x = 0$ in the receiver plane, and calculate the output of these receivers as the angle of incidence of the incident plane wave upon the cylindrical rods is varied. For convenience we chose to consider rectangular receiver elements. Because the pressure distributions are

invariant with respect to translations in y, Eqs. (IV.16) and (IV.17) are reduce to one dimension. The receiver apertures became one dimensional apertures and the only relevant dimension, therefore, is the x extent of the receiver.

In Figure IV.12 we compare the output of three receiver apertures which are of different spatial extent. In panel a) we show the results predicted using a 0.5 mm phase sensitive and a 0.5 mm phase insensitive receiver. For the frequency chosen (5 MHz), this receiver is ∿60% larger than the acoustic wavelength. The spatial variations in the acoustic field produced at $x = 0$ in the receiver plane are much larger than 0.5 mm and so the outputs of the phase sensitive receiver and the phase insensitive receiver are nearly identical.

In panel b) of Figure IV.12 we show the results predicted when the size of the receiver aperture is increased to 3.2 mm (approximately 10 wavelengths). The phase insensitive (i.e., acoustoelectric-like) receiver produces an output which is similar to that of the 0.5 mm receiver. However some blurring of the interference pattern takes place. This blurring seems to be an accurate representation of the averaged acoustic field. The zeroes of the receiver output are smoothed out because there is always a finite amount of acoustic energy incident upon the receiver. In contrast, the phase sensitive (i.e., piezoelectric-like receiver produces zero output when the complex field distributions are antisymmetric over its surface. For example, the field distribution illustrated in Figure IV.10 for an angle of incidence of 44.2° shows such an antisymmetric field distribution. However, even at angles where the field distribution is antisymmetric a finite amount of acoustic energy is incident upon the receiver. The output of the phase insensitive

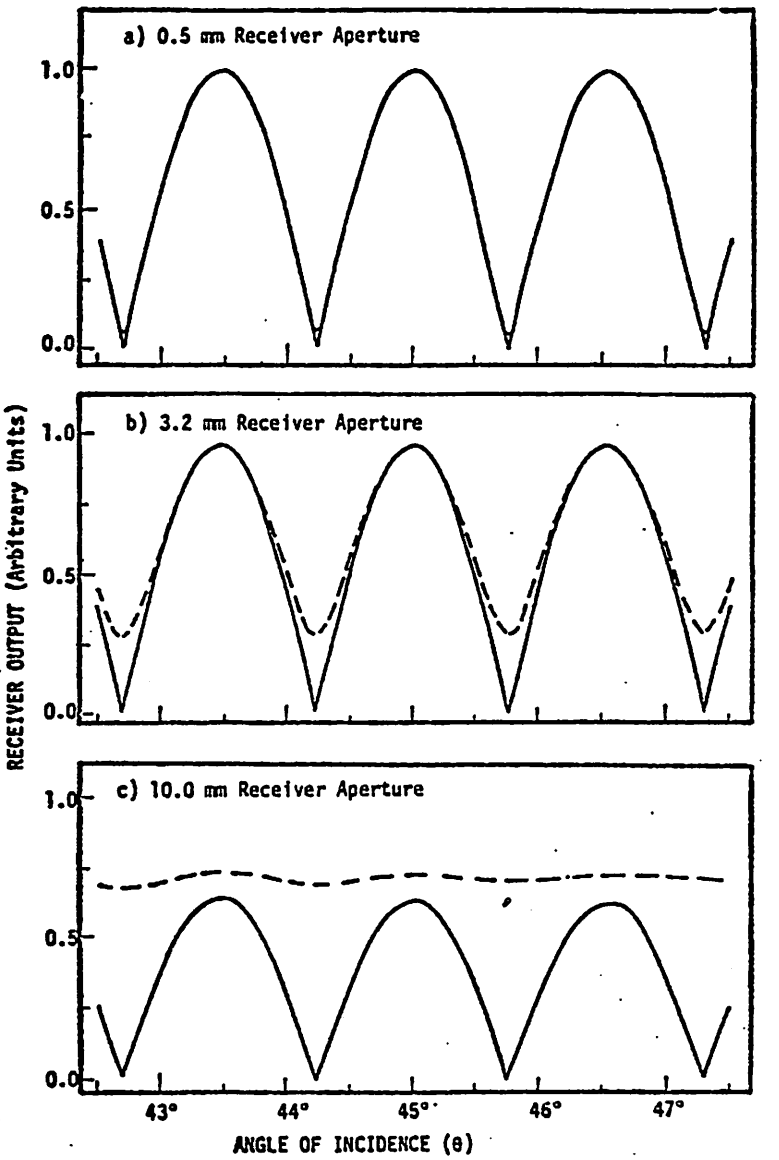

Figure IV.12. Comparison of predicted receiver outputs for various size phase sensitive and phase insensitive receiver apertures centered at $x = 0$ as a function of θ. Phase sensitive (piezoelectric-like) receiver outputs are shown with solid curves and phase insensitive (acoustoelectric-like) receiver outputs are shown with dashed curves. An output of 1.0 for each receiver size represents the output produced by uniform plane wave illumination.

receiver seems to reflect this fact more accurately. We note that the output of the phase sensitive receiver produces an output which looks deceptively like those produced by the point-like receiver of panel a).

In panel c) of Figure IV.12 we show the results predicted as the size of the receiver aperture is increased to 10 mm (approximately 33 wavelengths). The predicted output of the phase insensitive receiver only oscillates slightly as the angle of incidence is varied. This behavior can be attributed to the fact that the receiver is approximately equal in size to the fringe spacing and as one fringe moves out of the receiver aperture another moves in to keep the output nearly constant. In contrast, the output of the phase sensitive receiver still produces an output which looks deceptively like the output of the point-like receiver. It is interesting to note, that the output of the (1 cm) phase insensitive receiver is always greater than the comparable sized phase sensitive receiver. Even at angles where the phase sensitive receiver output is at a maximum, some "phase cancellation" still takes place. From Figure IV.9a it is evident that for a 1 cm receiver aperture, the real and imaginary parts of the complex pressure have both positive and negative values over the receiver aperture and so some phase cancellation takes place even at "favorable" angles such as 45°. The large (1 cm) phase insensitive receiver aperture will therefore give a better estimate of the total acoustic energy scattered into the solid angle defined by the receiver aperture than the large (1 cm) phase sensitive receiver for all angles of incidence considered.

Now let us consider fixing the angle of incidence θ at 45° and investigate the output of a small but finite size receiver element as it is scanned in the x direction in the receiver plane. The field pattern we are considering is shown in Figure IV.9. Under these circumstances the spatial variations in the acoustic field predicted by Eq. (IV.15) becomes quite rapid as the receiver is scanned away from $x = 0$ in the receiver plane.

In Figure IV.13 we again compared the normalized output [Eqs. (III.16) and (III.17)] of three different signal receiver apertures. The phase sensitive output of these apertures is shown by the solid line and the phase insensitive output is shown by the dashed line. In panel a) we compare these normalized outputs for a receiver aperture of 0.5 mm extent as it is scanned in the minus x direction of the receiver plane. The point-line nature of this small receiver aperture results in very similar phase sensitive and phase insensitive results. The interference fringes located at approximately $x = 0$, 10, and 20 mm are well resolved by either type of receiver. We note however, that even for this point-like phase sensitive receiver, some phase cancellation effects are still present as evidence by the fact that the amplitude of the interference maximum located at $x \sim 20$ mm is underestimated by $\sim$10%. We note that the phase insensitive receiver aperture allows one to measure the magnitude of the acoustic field present independent of rapid phase fluctuations.

In panel b) of Figure IV.13.we show the predicted results as the size of the receiver aperture is increased to 3.2 mm. As the receivers are displaced from $x = 0$ we note that the output of the phase sensitive

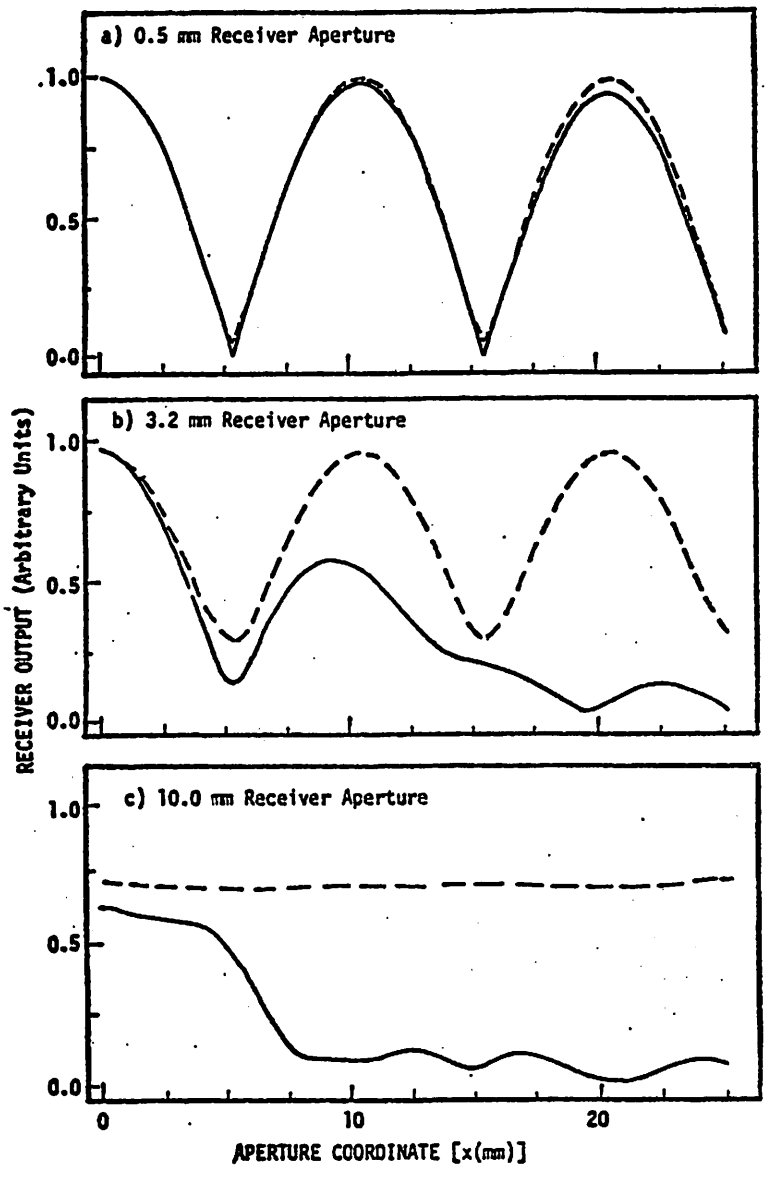

Figure IV.13. Comparison of predicted receiver outputs for various size phase sensitive and phase insensitive receiver apertures as a function of position (x) in the receiver plane. Phase sensitive (piezoelectric-like) receiver outputs are shown with solid curves and phase insensitive (acoustoelectric-like) receiver outputs are shown with dashed curves. An output of 1.0 for each receiver size represents the output produced by uniform plane wave illumination.

aperture is quickly reduced as compared with the phase insensitive aperture. The interference fringe centered at $\sim$10 mm is poorly represented, being both underestimated in amplitude and shifted in position. The predicted output of the phase insensitive aperture is able to accurately represent the amplitude and position of the interference fringe at $x \sim 10$ mm as well as the next fringe at $x \sim 20$ mm. As noted before, some blurring of the interference fringes takes place as a result of the use of the larger receiver. This blurring appears to accurately represent the averaging of a finite amount of acoustic energy present over the receiver aperture. Near $x = 0$ in the receiver aperture, where phase variations are slowest, we note that the phase sensitive and phase insensitive receiver aperture yield similar results.

In panel c) of Figure IV.13 we show the predicted results as the size of the receiver aperture is increased to 10 mm. The output of the 10 mm phase insensitive receiver aperture is nearly constant as it is scanned through the interference fringes. This nearly constant output is the result of the comparable size of the receiver and the interference fringe spacing. The fact that a finite amount of acoustic energy is incident upon the receiver aperture even when it is displaced by 25 mm from the center of the interference pattern is well represented by its output. In contrast, for the phase sensitive receiver we find that the representation of the interference fringe centered at $x = 0$ has been broadened and reduced as compared with the smaller receiver apertures. From the output of this receiver it is difficult to estimate the incident acoustic energy at positions beyond $x = 8$ mm.

In summary, the use of a phase insensitive receiver aperture permits a measurement of the magnitude of the average acoustic field across its face independent of rapid phase fluctuations. Thus a phase insensitive receiver should provide a quantitative estimate of such ultrasonic parameters as the total power scattered into a region defined by the receiver aperture. Measurements of the energy scattered by a pair of brass rods are compared with these predictions in Chapter VI.

V. EXPERIMENTAL METHODS

The experiments performed made use of single crystal of photosensitive cadmium sulfide obtained from the Eager Picher Corporation.[63] In this section we detail the methods which were used to prepare physically, evaluate electronically and calibrate ultrasonically these specimens. We also discuss the electronic circuits which were specially designed for the measurement and recording of the acoustoelectric signals.

A. Physical Preparation

The acoustoelectric interaction of longitudinal ultrasonic waves with conduction electrons in cadmium sulfide is strongest when full advantage is taken of the coupling provided by the piezoelectric effect. This condition dictates that the ultrasonic wavevector be parallel to the "c" crystalline axis in CdS. The crystalline structure of CdS is 6 mm (hexagonal), where the "c" crystalline axis is the six-fold symmetry axis.

A number of means are available for the identification of the six-fold axis in a crystalline material (e.g., light scattering, x-ray diffraction,[64] etc.). All of the samples prepared for this work were oriented using the Laue X-ray backscatter technique. The crystals studied were oriented to within 1° of the sixfold symmetry axis.

Once the six-fold symmetry axis was identified, crystals were roughly cut using a diamond impregnated cutoff wheel mounted on a modified surface grinding machine. The crystal faces perpendicular

tothe "c" axis were ground by hand to a 5 micron finish on cast iron laps using a kerosene carrier. These faces were subsequently polished using 1 micron grit and water on a felt lap. An additional optical window was prepared on thick single crystal specimens. This optical window parallel with the "c" crystalline axis was provided so that uniform illumination could be provided throughout the volume of thick crystal specimens. Finally, crystal surfaces were etched in a 50% solution of sulfuric acid for approximately 2 minutes, rinsed thoroughly in deionized water and degreased in alchohol vapors.

B. Electronic Evaluation

The acoustoelectric effect involves the bulk transport of electrons through the crystal specimen. Therefore, care must be taken to provide ohmic (i.e., nonrectifying) electrical contacts to the crystal surfaces. If non-ohmic contacts are provided to a semiconducting material the electrical behavior of the material can be dominated by the surface properties rather than the interactions taking place within the bulk of the specimen.

Non-ohmic behavior of metal-semiconductor contacts is a result of the presence of a potential barrier at the metal-semiconductor interfaces. Such a barrier can result from i) surface impurities i.e., oxide layers, ii) electronic surface states or iii) improper matching between the work functions of the metal and semiconductor. Over the years, the explanation for the observed non-ohmic behavior or certain metal contacts to CdS has shifted from the surface states argument[65,66] to the improper matching of work functions explanation.[67] Experimentally, it has been found that ohmic electrical contact to

CdS can be obtained by using a metal with a work function lower than that of CdS, such as indium or gallium.

For the crystals studied in this work, electrodes were formed using vacuum deposited indium. (Other techniques for making ohmic contact to CdS are also feasible but have not been evaluated in this work.[68] Specimens were evaluated electrically after plating in order to determine i) if the metal-semiconductor contacts were ohmic and ii) if the bulk crystal conductivity could be adjusted by photo-excitation into the proper region for observation of the acousto-electric effect. Electrical evaluation of plated CdS samples was done by making use of a series of current-voltage (I-V) curves. The ohmic nature of the crystal contacts is manifested by a linear I-V curve. The conductivity can be evaluated from the value of the slope of this curve. The photosensitivity of the crystal is determined by the extent to which the slope of the I-V curve changes in proportion to the light intensity incident upon the crystal.

A series of I-V curves as a function of light level were obtained and analyzed by making use of the HP-9825A calculator and the IEEE-488 interface bus system. The digital to analog converter (DAC) of the interface bus system applied a voltage ranging from -10 to +10 volts to the crystal. Current flowing through the crystal was measured and recorded by means of a transresistance amplifier in which the input impedance is equivalent to zero and the output voltage equals the input current times the feed-back resistance. The illumination for these measurements was provided by an incandescent lamp and was adjusted by the insertion of neutral density filters into the optical path. The crystal resistance as a

function of incident light intensity was determined by fitting the I-V curve for each light level with a straight line.

C. Electronic Circuits

Once it was determined on the basis of electrical measurements that a crystal was a good candidate for use as an acoustoelectric receiver, ultrasonic evaluations were carried out. In this section we describe methods devised for measuring and recording the acoustoelectric signal. The acoustoelectric effect results from a net force experienced by the conduction electrons as an acoustic wave propagates through a semiconductor and gives up energy to the conduction electrons. This force can be detected by either of two methods: 1) measuring the short circuit current which flows or 2) by measuring the open circuit voltage which is a result of charge displacement.

1. Preamplifier

Three different preamplifiers, one for measuring the short circuit current and two for measuring the open circuit voltage of the acoustoelectric signal, were built and tested. The current preamplifier consisted of a commercially available National Semiconductor LH0032 high input impedance operational amplifier in a transresistance or current-to-voltage configuration using a 10 MΩ feedback resistor. The input impedance of this device in this configuration is about 300 Ω over the desired bandwidth from dc to about 500 KHz. This is much lower than the typically observed bulk crystal resistances ($\sim 10^5\ \Omega$). Thus the preamp looks like a short circuit across the CdS crystal and the output of the preamp follows the acoustoelectric current.

With this preamp we were able to measure acoustoelectric signals down to 75 picoamps. The amplifier in this configuration did not have the bandwidth necessary to reproduce the piezoelectrically generated rf from surfaces of the CdS crystal.

Two high input impedance preamplifiers were used to measure the open circuit voltage generated by the crystal. The first of these preamplifiers consists of a National Semiconductor LH0033 high input impedance voltage follower. This preamplifier was capable of reproducing both the piezoelectric (radio frequency) and acoustoelectric (video) signals generated by the CdS crystal if care was taken to minimize stray input capacitance. The preamp was also capable of driving a moderate length of coax cable.

The second voltage preamplifier design considered is shown in Figure V.1. The advantage of this design was that only a single field effect transistor (FET) is mounted near the CdS crystal. Bias and signal voltages were carried on a single coaxial cable. The bandwidth of this preamplifier was quite good (>30 MHz) because of the low input impedance of the common base amplifier stage. The overall gain of the preamp was approximately 10. With this preamplifier design we were able to measure signals as small as 50 μ volts with a 1 MHz bandwidth. Total dynamic range of the preamp was approximately 80 dB, with useable signal outputs from about 500 μvolts to 5 volts.

2. Filters

In the experiments we performed, it was necessary to observe piezoelectric (rf) and acoustoelectric (video) responses of the CdS crystal. Thus a number of high and low pass filters were built.

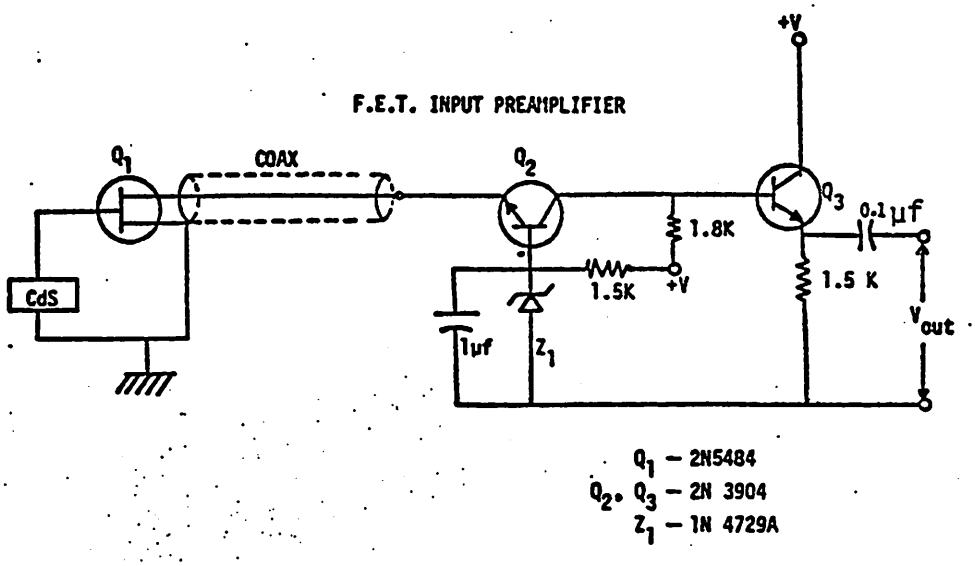

Figure V.1. High input impedance preamplifier used to measure the acoustoelectric voltage. The gain of this preamplifier is approximately 10.

Figures V.2 and V.3 are the schematic diagram for an active and passive low pass filter. Both filters were designed to isolate the acoustoelectric response of a CdS specimen and were designed to exhibit maximum flat amplitude response below the cutoff frequency of approximately 1 MHz. Figure V.4 is the schematic diagram of a high pass filter designed to isolate the piezoelectric response of the CdS specimen. This filter had a cutoff frequency of approximately 1 MHz. All of the filters were designed to exhibit approximately 20 dB/octave of signal suppression beyond their respective cutoff frequencies.

3. Amplifiers and Measurements System

Because the acoustoelectric signal varies in proportion to the acoustic intensity rather than the acoustic amplitude, it was necessary for any measuring system used to be capable of measuring a rather large range of signal amplitudes. We made use of two different variable gain amplifiers to provide the dynamic range needed: i) a variable gain amplifier in the receiving circuitry and ii) a variable gain preamplifier in the transmitting circuitry. For some of the experiments described later the gain of these devices was actively adjusted under computer control.

The variable gain receiver amplifier is shown in Figure V.5. It is a video amplifier exhibiting a maximum gain of 50 dB, with voltage controlled attenuator on the input. The amplifier ran at full gain when 0 volts were applied to $V_{control}$. The gain was reduced by 20 dB when -10 volts was applied to $V_{control}$.

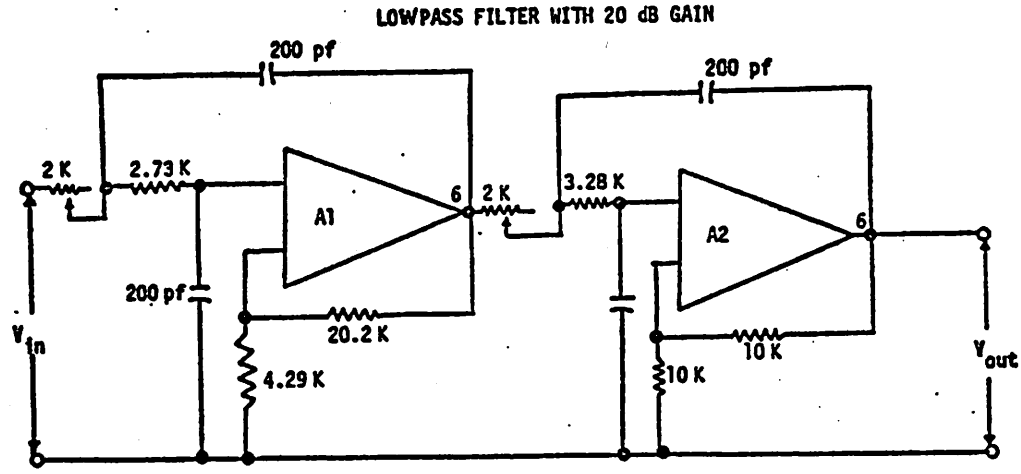

A1, A2 —Fairchild μA715HC

Figure V.2. Active low pass filter with 20 dB gain. This filter is used to separate the low frequency acoustoelectric response from the high frequency direct piezoelectric response of CdS specimens. Cutoff frequency is approximately 1 MHz.

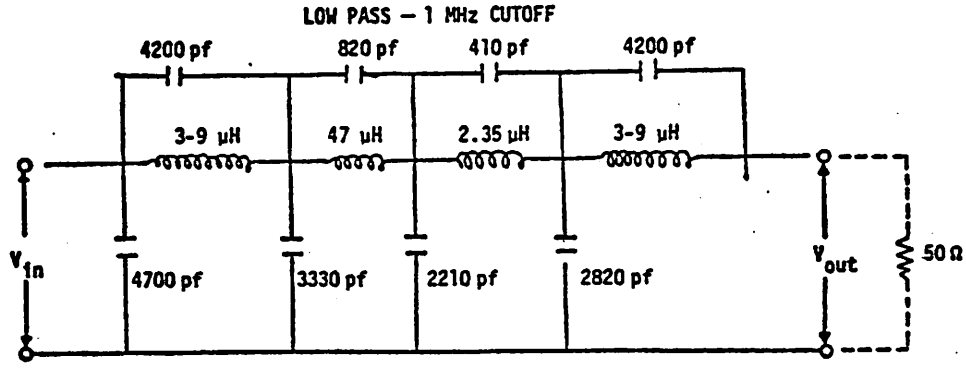

Figure V.3. Passive low pass filter. This filter is used to separate the low frequency acoustoelectric response from the high frequency direct piezoelectric response of CdS specimens. Cutoff frequency is approximately 1 MHz.

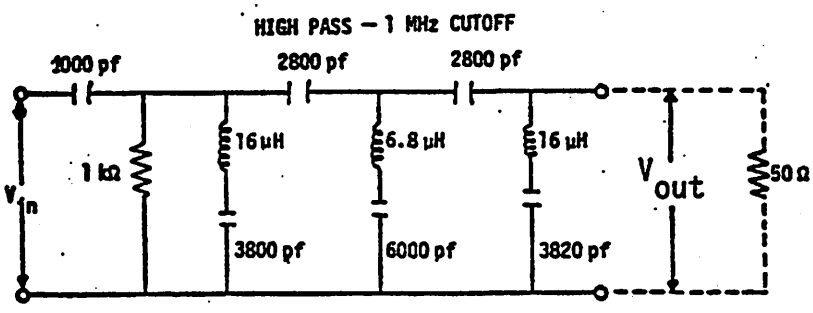

Figure V.4. Passive high pass filter. This filter is used to separate the high frequency piezoelectric response from the low frequency acoustoelectric response of CdS specimens. Cutoff frequency is approximately 1 MHz.

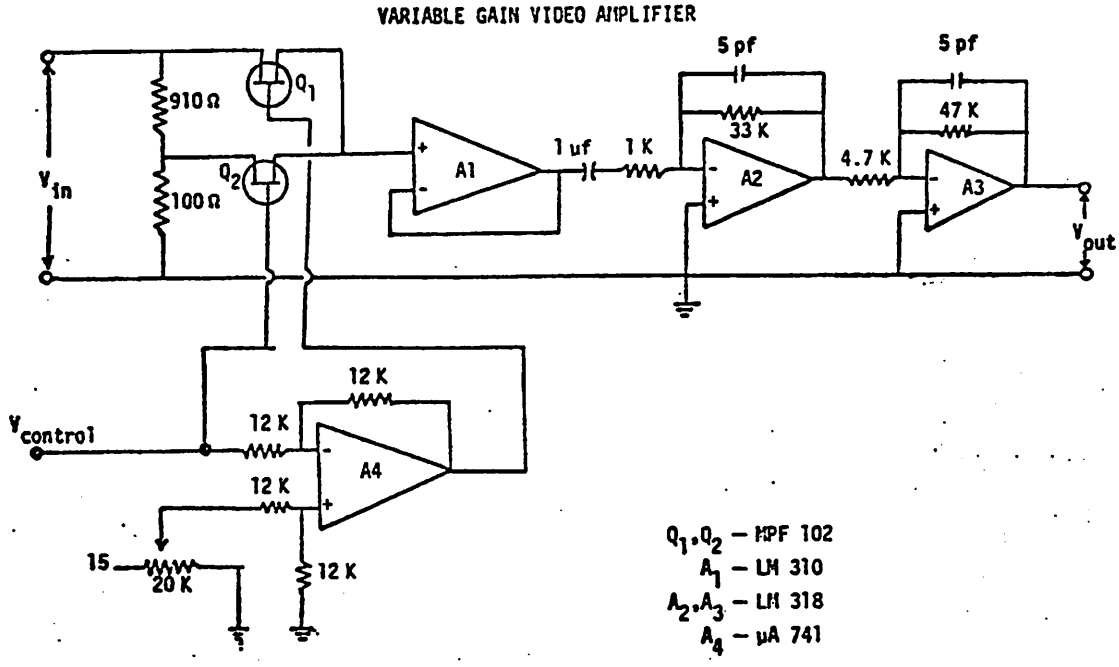

Figure V.5. Variable gain video amplifier. The maximum gain of this amplifier is approximately 50 dB. The amplifier has been provided with a voltage controlled attenuator at the input. Amplifier gain is reduced by 20 dB when -10 volts is applied to $V_{control}$.

The variable gain preamplifier on the transmitting transducer consisted of a Mororola MC1590G with automatic gain control. The rf pulse out of this amplifier stage could be varied over 60 dB when a 0-10 volt dc voltage was applied to the automatic gain control input of the amplifier. Output of this amplifier stage was applied directly to the input of an Electronic Navigation Industries radio frequency power amplifier (Model 240L or 300L) which was used to drive the transmitting transducer.

A logarithmic video amplifier and peak detector circuit was developed as another means for taking full advantage of the preamplifier dynamic range and to improve the data acquisition rate. The logarithmic amplifier and peak detector are shown in Figure V.6. The active element was an Optical Electronic Inc. (OEI 2910) bipolar logarithmic amplifier. The acoustoelectric signal is a video or unipolar signal, and we found that the best performance of this amplifier for unipolar signals was achieved by using the low impedance input mode of the device. Most of the ultrasonic experiments were performed with short ultrasonic pulses ($\sim$3 μsec) and moderate repetition rates (60 Hz to 1000 Hz). For this reason, a sample and hold circuit was generally used after this logarithmic amplifier circuit. A peak detector or pulse stretcher circuit was therefore added to the output of the logarithmic amplifier so that slight shifts in the sampling position would not be critical.

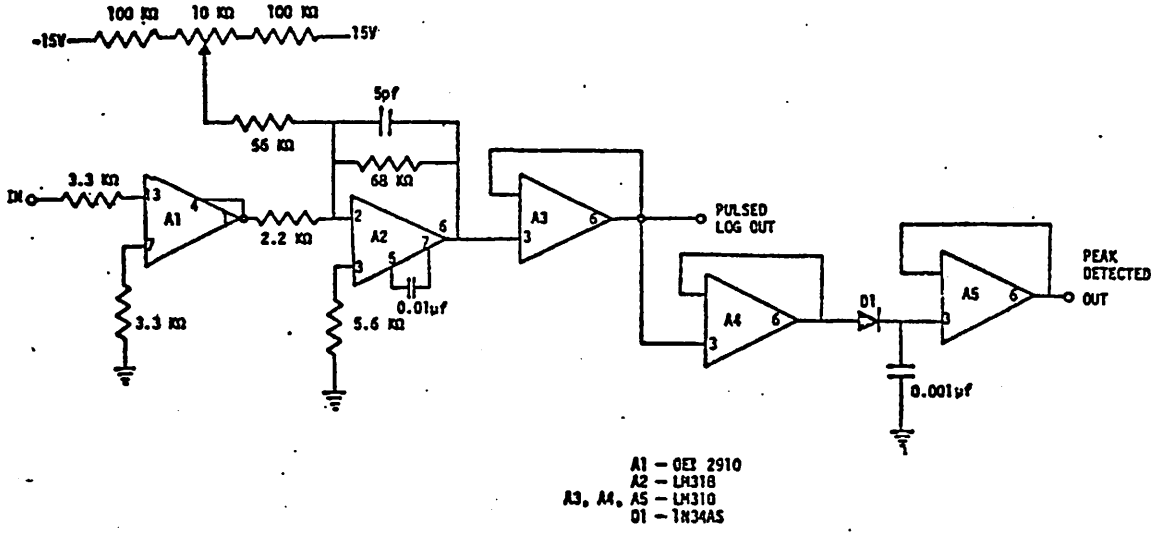

Figure V.6. Video amplifier with logarithmic gain characteristic. The active element is an Optical Electronics Inc., OEI 2901 bipolar logarithmic amplifier. A peak detector (pulse-stretcher circuit) has also been provided at the amplifier output.

The performance of the log amp and peak detector circuit are shown in Figure V.7. The voltage output of the peak detector is plotted as a function of voltage input to the log amp. The input signal consisted of a 3 microsecond pulse. Useable signal outputs are present for 4 decades of voltage input (80 dB dynamic range). This range was made to coincide with the range of electric signals provided by preamplifier circuit described previously (500 μvolts to 5 volts).

4. Transmitter Encoding

As a means for increasing the sensitivity of the acousto-electric receiver to pulsed ultrasound, a transmitter modulation scheme was implemented so that lock-in detection techniques could be used in the receiver circuitry. The heart of this system is the rf modulator circuit which is detailed in Figure V.8 The modulator was designed to provide carrier suppressed (200%) amplitude modulation of the transmitted ultrasonic pulse. This type of modulation was chosen so that all of the ultrasonic energy would be in a form which would contribute to the output of the lock-in amplifier. This modulation and the fact that the acoustoelectric receiver is not sensitive to the rf phase of the ultrasonic pulse combine to produce an amplitude modulated acoustoelectric receiver output which is at twice the frequency of the reference oscillator. A lock-in amplifier (Princeton Applied Research Model 126) capable of working at the second harmonic of the reference signal was therefore chosen. Although this system provided the expected improvement in sensitivity, most of the results presented in Chapter VI where achieved without the need for this additional instrumentation.

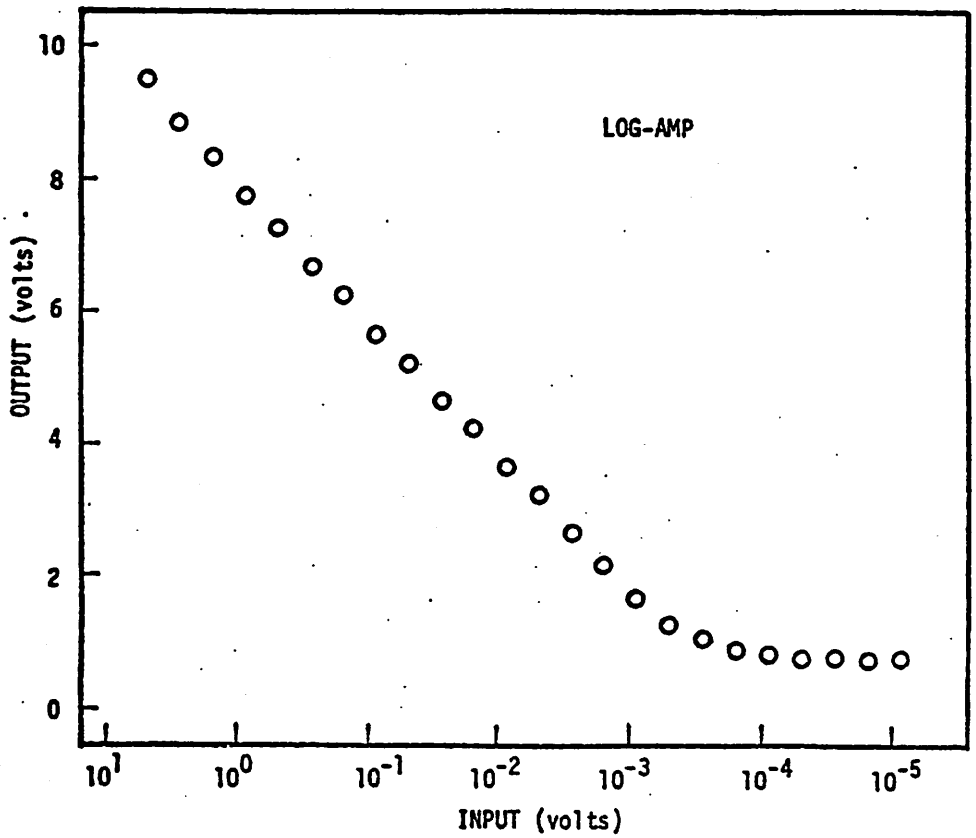

Figure V.7. Gain characteristics of logarithmic video amplifier. Gain and offset of amplifier A2 [see Figure V.6] have been adjusted to compress four decades of input voltage into one decade of output voltage. Measurements were made using 3 microsecond unipolar pulses.

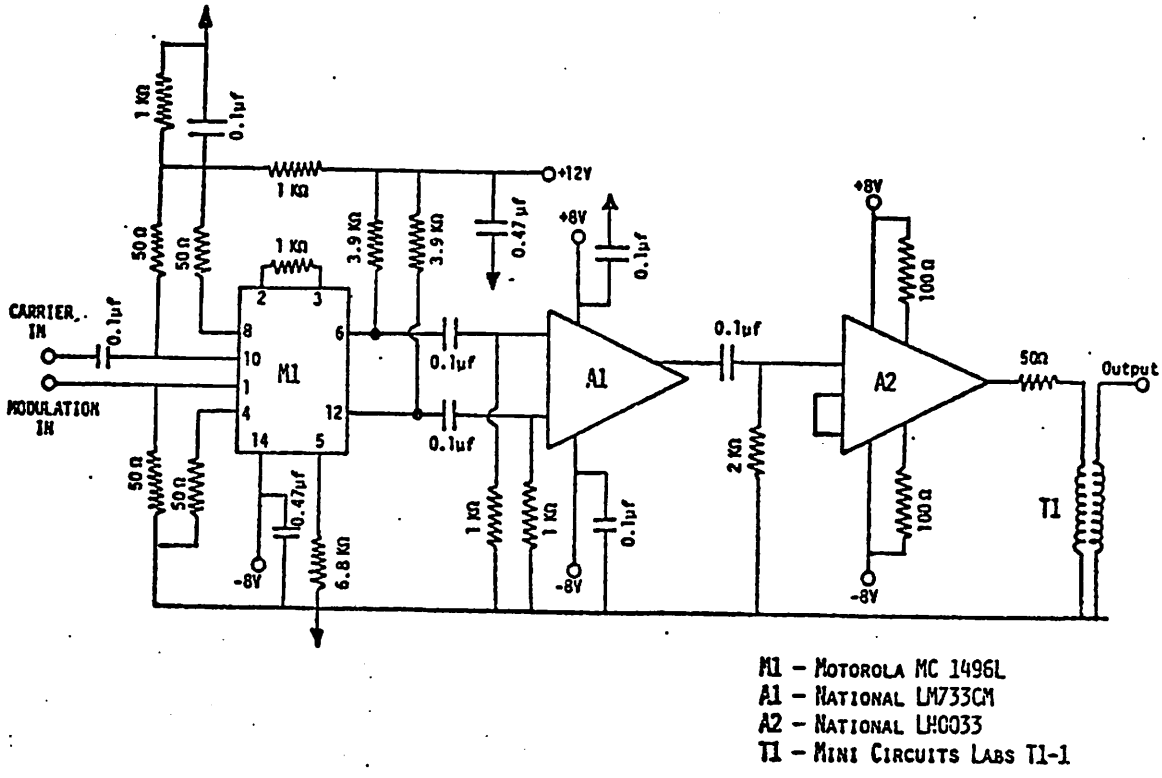

Figure V.8. RF modulator circuit used for encoding of transmitted ultrasonic pulse. Circuit consists of mixer-multiplier, gain, and buffer stages. The modulator was designed to provide carrier suppressed (200%) amplitude modulation of transmitted ultrasonic pulses.

D. Ultrasonic Calibration

The use of an ultrasonic receiving transducer based upon the acoustoelectric effect provides a new method for measuring ultrasonic intensity. Such a new method requires careful documentation and calibration so that its utility may be evaluated. One of the goals of this work was to determine the absolute sensitivity and ultrasonic bandwidth of an acoustoelectric transducer, and to compare its response to more conventional broadband receivers. Since an acoustoelectric transducer is strictly a receiving transducer, calibration consists of determining the electrical signal output as a function of acoustic intensity incident upon the transducer. The approach employed consisted of calibrating a piezoelectric transmitting transducer. A number of calibration techniques were considered for this purposes: i) electrical measurement of transmitter radiation resistance,[69] ii) "self reciprocity" calibration technique,[70-75] iii) radiation pressure measurements,[76,77] and iv) transient thermoelectric effect.[78-80] The following brief summary of each of these techniques is meant to illustrate the utility of each and to justify our choice of the transient thermoelectric effect.

i) The resonant radiation resistance technique for transducer calibration relies on the fact that the mechanical load into which a transducer is radiating can be thought of as an added resistive element in an equivalent circuit representation of the transducer. By assuming some form for the equivalent circuit of the unloaded transducer, (most often the Mason[50] equivalent circuit is assumed) the radiation resistance of a load such as water can be measured

and the power dissipated in this resistance calculated. This power represents the total acoustic power radiated by the transducer into the load. In order to quantify the ultrasonic intensity at a spot in radiated field, a sensitive means for determining changes in electrical impedance (such as an rf balanced bridge) and a detailed knowledge of the transducer's radiation field pattern are necessary.

ii) The "self reciprocity" calibration technique relies on the fact that for a single mode of excitation, the transmit and receive efficiency of a transducer should be identical. Transmit efficiency is defined as the ratio of total radiated acoustic power to the total electrical power delivered to the transducer. Receive efficiency is defined as the ratio of available electrical power generated by the transducer to the acoustic power incident upon the transducer. In order to implement this calibration scheme a knowledge of the complex impedance of the transducer is necessary so that available electrical power on receive can be calculated from voltage measurements and one must make all of the ultrasonic measurements in the far field (i.e., plane wave) limit so that the single mode of excitation assumption is not violated.

iii) The radiation pressure measurement technique relies on the physical interaction of the ultrasonic energy with either a nearly perfect absorber or reflector. The change in momentum of the ultrasonic wave is measured directly as a force or deflection on an absorber or reflector. Implementation of this calibration scheme requires a sensitive and fast responding mechanical system for the measurement of force.

iv) The transient thermoelectric effect allows one to determine the local ultrasonic energy density by measuring the time rate of increase of temperature within an absorbing medium. Measurements of ultrasonic intensity by this means are absolute and the method is broadband provided one has a knowledge of the frequency and temperature dependence of the absorption coefficient of the absorbing medium.

The transient thermoelectric effect was chosen for the absolute calibration of a transmitting transducer because of its inherently broadband character and because the method could be implemented using standard thermocouple measurement techniques.

E. The Transient Thermoelectric Effect

Let us consider a plane ultrasonic wave of energy density W_o incident upon an absorbing medium. At a position x_1 within the absorbing medium the measuring junction of a thermocouple probe is positioned. The rate of energy dissipation within the absorbing medium is related to the rate of rise of the total heat energy,

$$\left[\frac{dW}{dt}\right]_{t=0} + \left[\frac{dQ}{dt}\right]_{t=0} = 0 \qquad (V.1)$$

where Q, the total heat energy, is equal to the product of mass density ρ, the specific heat c and the temperature T. Measurement must be made as nearly as possible to the onset ($t = 0$) of the ultrasonic energy so that the effects of convection and conduction of heat away from the thermocouple probe can be ignored. This assumption also allows us to

ignore the temperature dependence of the density and the specific heat. If we assume that the ultrasonic energy density W(x) exhibits a simple exponential relation to depth in the absorber [$W(x) = W_o e^{-2\alpha x}$] we find that

$$2\alpha v_s W(x_1) = \rho c \left[\frac{dT}{dt}\right]_{t=0} . \qquad (V.2)$$

Rewriting in terms of the ultrasonic intensity we find

$$\Phi_o = \frac{\rho c}{2} e^{2\alpha x_1} \left[\frac{dT}{dt}\right]_{t=0} . \qquad (V.3)$$

Use of this equation therefore make it possible to measure absolutely the ultrasonic intensity incident upon our absorbing medium.

Equation (V.3) represents an accurate description of the rate of temperature rise in a homogeneous absorbing medium. However, when a thermocouple wire is placed in the absorbing medium, other sources of heat generation and dissipation must be considered. The major source of heat generation is viscous relative motion of the thermocouple wire within the absorbing medium. Two major sources of heat dissipation are due to i) the finite heat capacity of the thermocouple and ii) the finite heat conductivity of the thermocouple wires.

As shown by Fry and Fry[78] the effect of these sources of error are nonnegligible; however, the errors can be reduced by appropriately chosing the time after the onset of the acoustic pulse for the measurements of dT/dt. It has been shown both in theory and experiment that the magnitude of heating caused by viscous relative motion is of the same order of magnitude as the absorptive heating. The "time constant"

for viscous heating, however, is short, with the temperature rise associated with viscous heating reaching 50% of its ultimate value in 0.1 sec. Likewise, the time constant associated with the finite heat capacity of a copper-constantan thermocouple wire (12 μm) is short (on the order of 2 milliseconds). Typically, the rate of temperature rise (dT/dt) is made 0.5 sec after the onset of the acoustic pulse to minimize the effect of viscous heating and the finite heat capacity of the thermocouple. Goss et al[80] have also shown that for moderate beam widths ($\geq$ 4 mm, 1/2 power beam width) the magnitude of the errors associated with the heat conductivity of the thermocouple is approximately 0.5%.

Use of the transient thermoelectric effect to perform the calibration of a transmitting transducer required some knowledge of the spatial characteristics of the ultrasonic field so that sensitivity could be maximized and errors reduced. Beam profiles of a Panametric A309 were measured using a 1 mm diameter PZT probe as the receiver. Measurements were made along 7 different lines through the ultrasonic beam and at 3 different ultrasonic frequencies. From these measurements we were able to locate a region of the radiated ultrasonic field which was sufficiently large for accurate thermoelectric measurements and yet sufficiently small to produce measurable heating. These conditions had to be satisfied over a large ultrasonic bandwidth.

All measurements were done using a copper-constantan thermocouple in an 1/8 inch thick castor oil absorbing medium. The castor oil absorber was maintained at 10°C to increase its ultrasonic absorption coefficient. The ultrasonic attenuation coefficient of castor oil is

frequency dependent and at 10°C can be approximated as

$$\alpha(f) = 0.16\ f^{5/3}$$

where f is the ultrasonic frequency in MHz.[81]

A block diagram of the system used for the series of transient thermoelectric measurements is shown in Figure V.9. System control and data acquisition was performed using an HP-9825A calculator and IEEE-488 interface bus system. Separate timing of the transmitter pulse length was provided for accuracy. Low pass filtering of the thermocouple voltage was used to protect the high gain "dc" amplifier from rf pick up. This system was used to generated calibration data for a particular piezoelectric transmitter. A "universal" calibration curve of instantaneous acoustic intensity per volt squared of voltage drive over a range of ultrasonic frequency was generated. These data were used to measure the sensitivity and bandwidth of several acousto-electric devices.

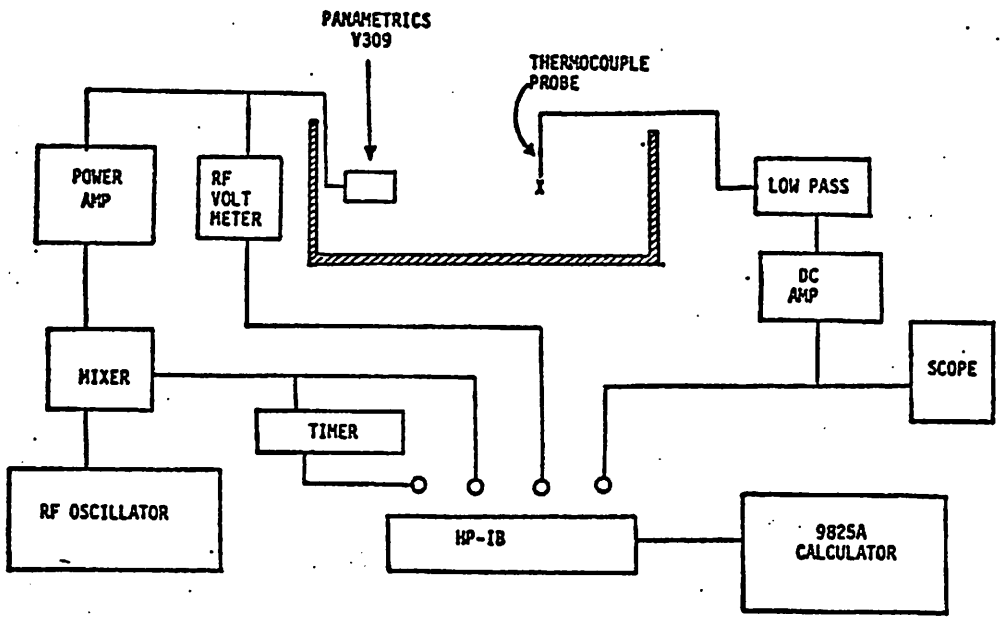

Figure V.9. Block diagram of system used for calibration of Panametrics transducer. Transient temperature changes in castor oil absorber caused by the transmitted ultrasonic pulse were recorded using a copper-constantan thermocouple. System control and data acquisition was performed using an HP-9825A desktop calculator and an HP interface bus system.

VI. EXPERIMENTAL RESULTS AND DISCUSSION

A. Introduction

In this chapter we present the results of a series of experiments which were designed to measure the acoustical and electrical properties of the piezoelectric semiconductor cadmium sulfide. The results of these experiments divide naturally into three areas: i) electrical properties of piezoelectric semiconductors, ii) physical acoustic properties of piezoelectric semiconductors, and iii) applications of piezoelectric semiconductors as phase insensitive ultrasonic receivers. Using this organization, we present the results of a series of experiments and discuss the significance of each experiment as it is presented.

B. Electrical Properties of Cadmium Sulfide

As we have seen in a previous chapter, the direct observation of electron-phonon interactions in a piezoelectric semiconductor depends upon our ability to adjust the conductivity of the semiconducting material into a region which facilitates the irreversible exchange of energy between the electron and phonon systems. In cadmium sulfide, this adjustment is usually accomplished by way of photoexcitation of electrons from the valence to conduction bands. In the dark, CdS is an insulator. Therefore the degree of photosensitivity for a particular single crystal of CdS determines the feasibility of observing the acoustoelectric effect.

Another electrical property associated with the observation of the acoustoelectric effect in CdS is related to the type of junctions which are formed at the surfaces of the crystal when it is provided with electrodes. As we discussed in Chapter III, ohmic (i.e., non-rectifying) electrical contacts to CdS are desirable for the reduction of electrical noise. Ohmic contacts to a piezoelectric semiconducting material are also necessary so that complications brought about by rectification of the piezoelectric signals generated at the surfaces of the crystal can be avoided. Non-ohmic electrical contacts also manifest themselves as an undesired photo-voltaic response as the illumination upon the crystal is changed. Electrical evaluation of the bulk photosensitivity of any CdS single crystal specimen and of the ohmicity of the electrical contacts with which it has been provided can be obtained from a series of current-voltage (I-V) measurements.

In Figure VI.1 we present a set of three I-V curves made upon a single crystal CdS specimen labeled LJB. This specimen was obtained from the Eagle Picher Electronics Division and is 1.32 cm thick and has a surface area of approximately 1.1 cm^2. The crystal surfaces were plated with indium using a vacuum deposition technique. From the nearly linear character of these I-V curves we see that ohmic electrical contacts have been provided to the crystal surfaces. The fact that the slope of the I-V curves change in proportion to the intensity of the illumination allows us to characterize the photo-sensitivity of this specimen. In Figures VI.2 and VI.3 we show a similar set of I-V curves for crystals labeled JRK and 452-2. These crystals were plated also with indium using a vacuum deposition technique.

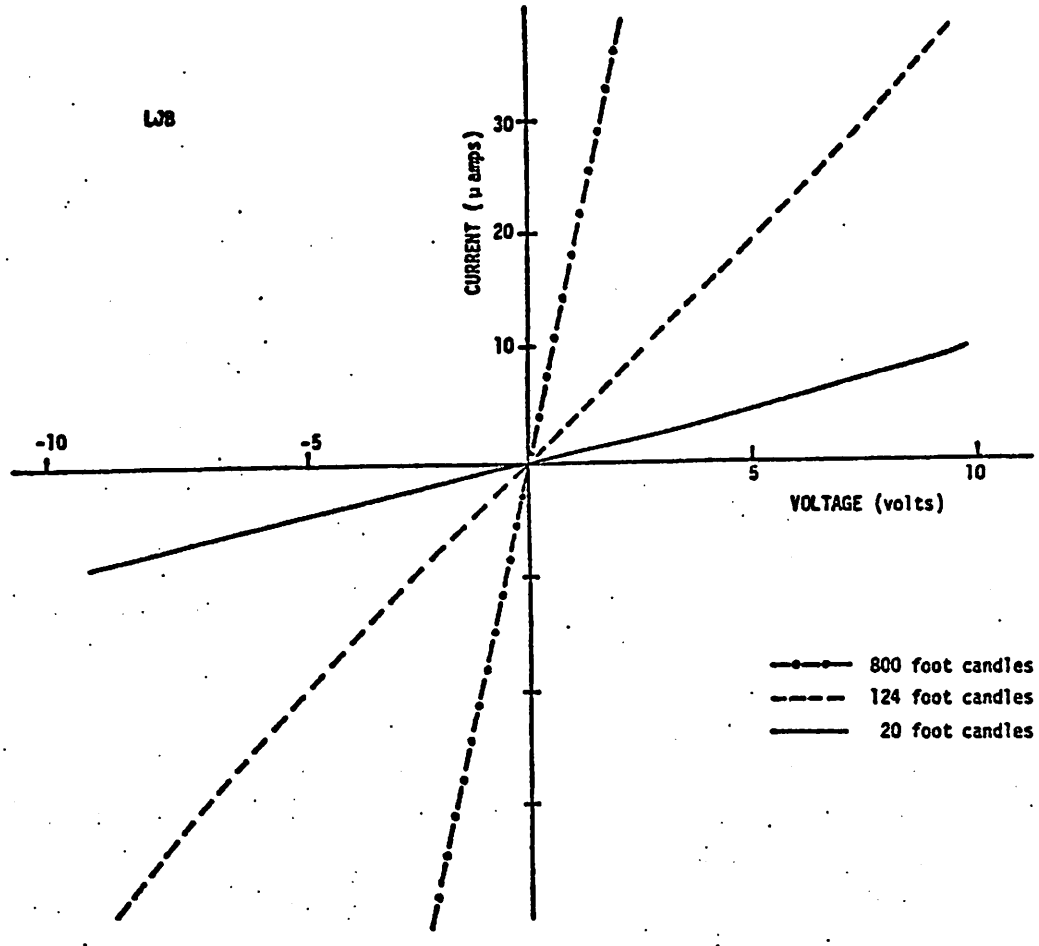

Figure VI.1. Current-voltage curves at three levels of light intensity for CdS crystal LJB with indium electrodes. Crystal dimensions are 1.3 cm thickness with approximately 1.1 cm^2 of active surface area. The linear I-V curves show that ohmic electrical contacts have been made to the crystal surface. The slope of the I-V curves changes with level of light intensity showing that the bulk of the CdS crystal is photosensitive.

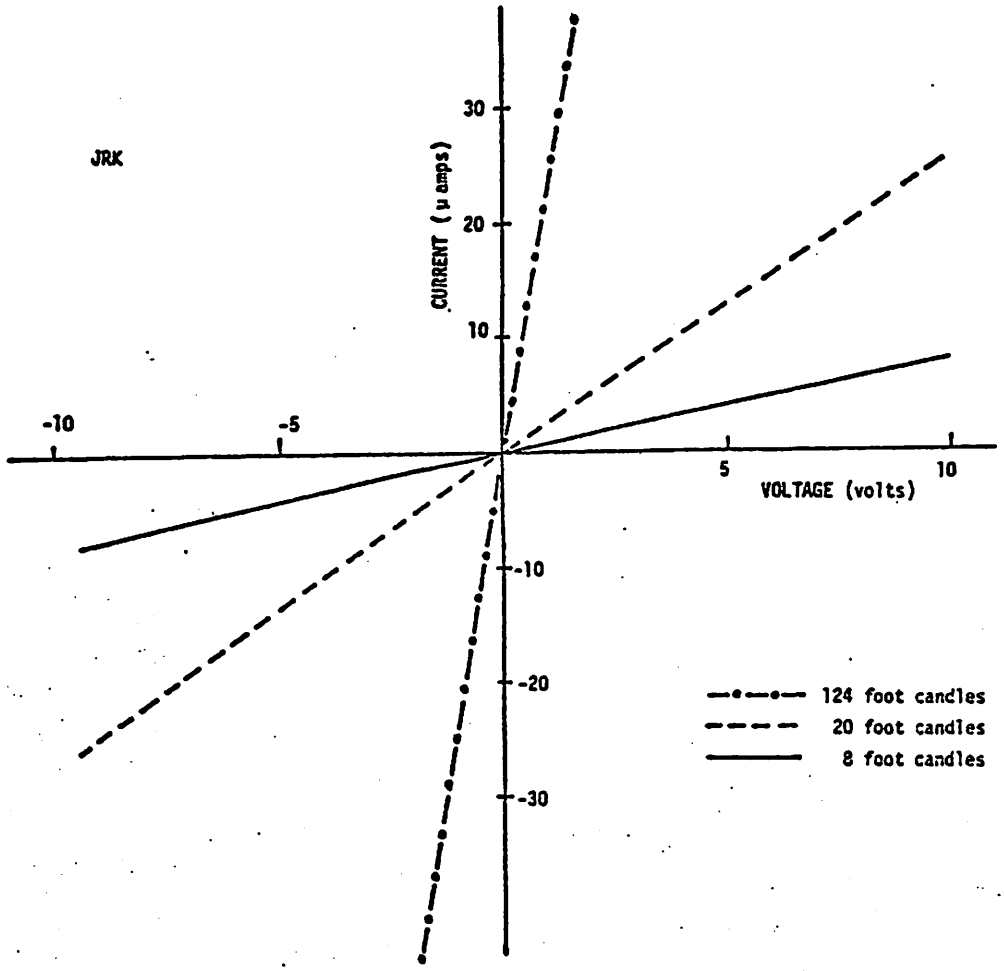

Figure VI.2. Current-voltage curves at three levels of light intensity for CdS crystal JRK-1 with indium electrodes. Crystal dimensions are 2 mm thickness with approximately 1.1 cm^2 of active surface area. The linear I-V curves show that ohmic electrical contacts have been made to the crystal surface. The slope of the I-V curves changes with level of light intensity showing that the bulk of the CdS crystal is photosensitive.

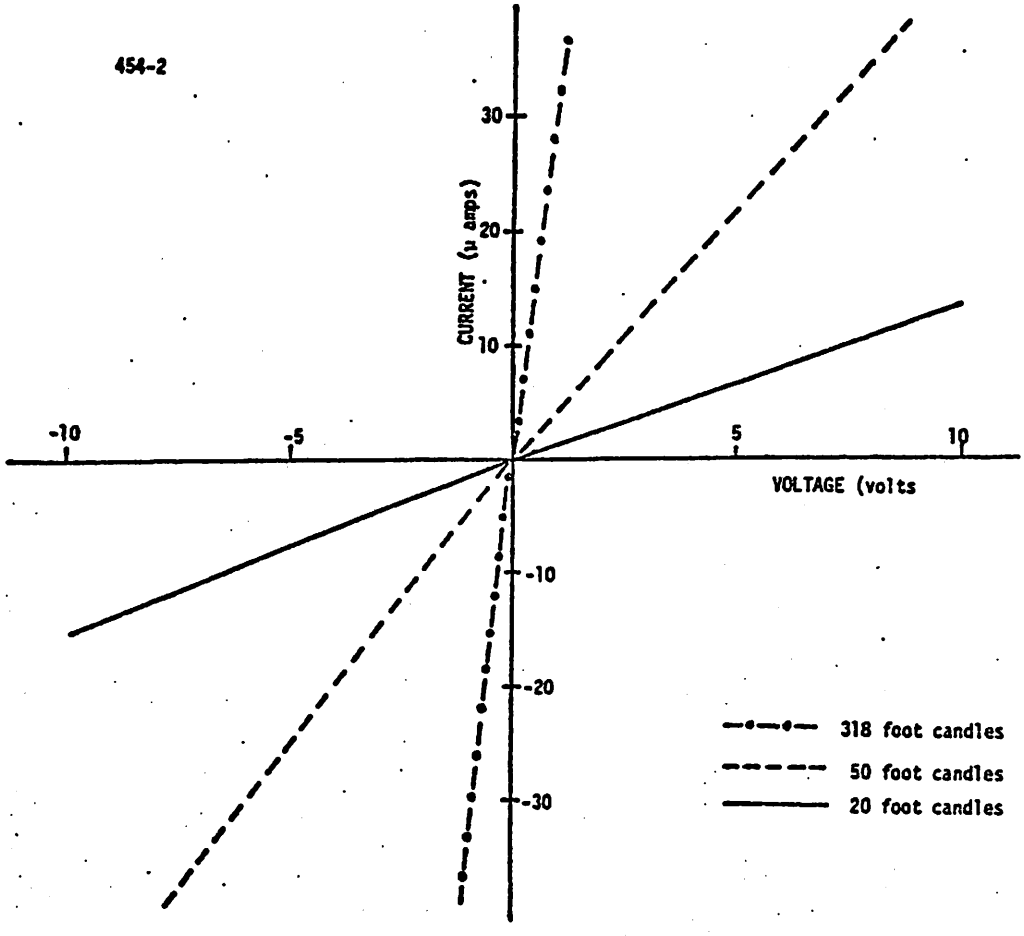

Figure VI.3. Current-voltage curves at three levels of light intensity for CdS crystal 454-2 with indium electrodes. Crystal dimensions are 1.5 mm thickness with approximately 1 cm^2 of active surface area. The linear I-V curves show that ohmic electrical contacts have been made to the crystal surface. The slope of the I-V curves changes with level of light intensity showing that the bulk of the CdS crystal is photosensitive.

The intensity of the illumination for all of these measurements was determined using a Gossen Pan-Lux light meter and the intensity was adjusted using Kodak Neutral Density Filters.

In Figure VI.4 we show the bulk resistance of these three crystal specimens as a function of light intensity. All three crystal exhibit photosensitivity such that the crystal conductivity is roughly proportional to the intensity of the incident light. The fact that the crystal resistance is not strictly proportional to the inverse of the incident light intensity is a phenomenon which has been discussed by Rose[51] and Bube.[82] The presence of sub-linear or super-linear conductivity versus light level curves is thought to indicate the presence and character of impurity electron levels within the band gap of CdS. For our purposes, however, it is sufficient to note that the crystal conductivity of these specimens is adjustable over three decades. This means that a range of crystal conductivities are at our disposal for optimization of the acoustoelectric effect.

Not every indium film which is vacuum deposited to CdS yields a linear I-V curve. In Figure VI.5 we present a series of I-V curves which were made on a high conductivity CdS crystal identified as JGM-1. This crystal was prepared in essentially the same manner as the previous three crystals. The I-V curves, however, exhibit a high degree of non-linearity and look similar to the I-V curve of a diode. We note that this crystal is photosensitive. A photovoltaic response was also observed with this crystal which is consistent with the observation of non-ohmic electrical contacts.

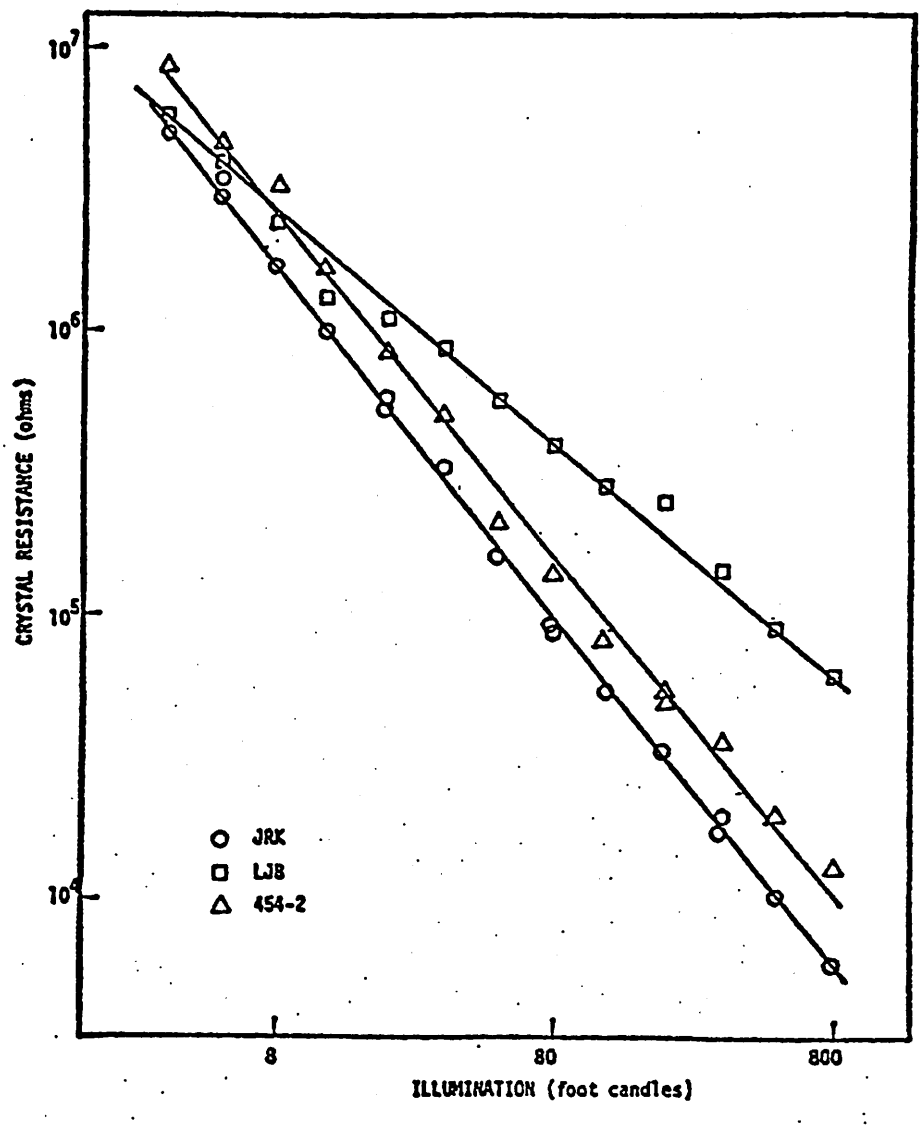

Figure VI.4. Bulk crystal resistance as a function of incident light intensity. The crystal resistance was determined from the slope of previous I-V curves. All three crystals are photosensitive with crystal conductivity approximately proportional to incident light intensity.

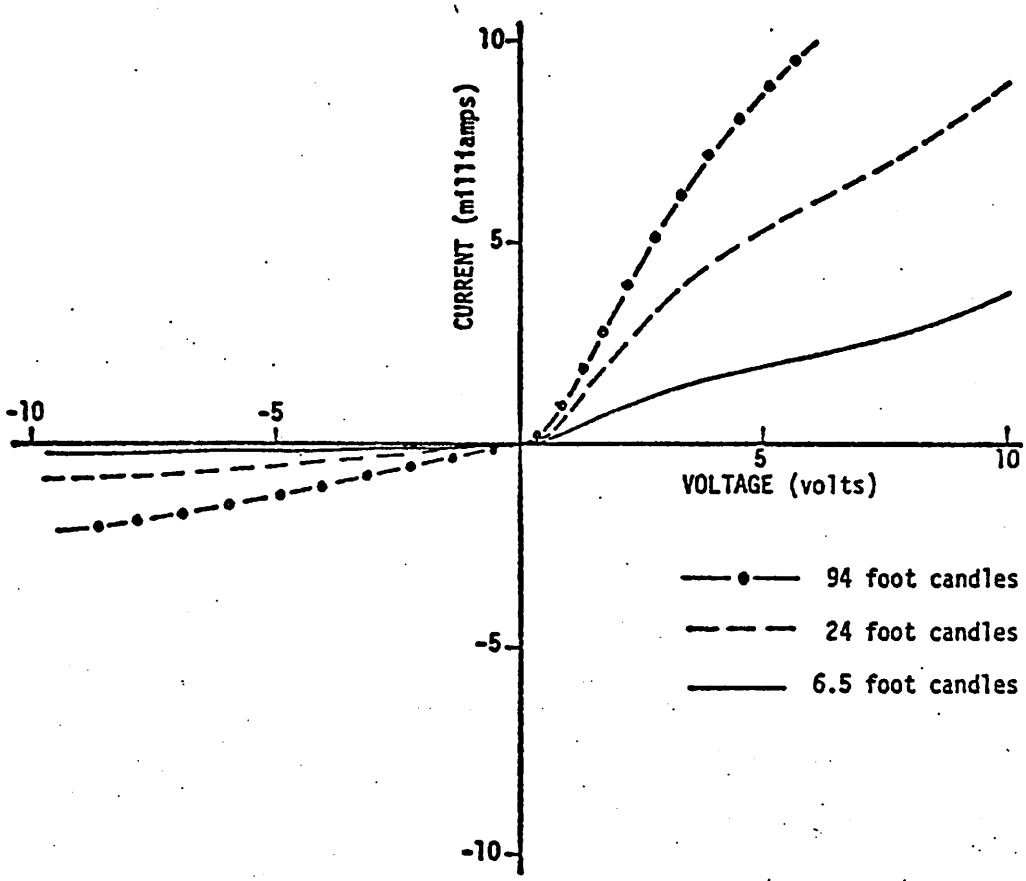

Figure VI.5. Current-voltage curves at three levels of light intensity for CdS crystal JGM with indium electrodes. Crystal dimensions are 6 mm thickness with approximately 0.24 cm^2 of surface area. The nonlinear I-V curves demonstrate that rectifying (non-ohmic) electrical contacts have been made to this crystal.

We found that indium contacts to CdS, deteriorate (corrode) over a period of approximately 12 months. In order to make electrodes with better long term stability, the properties of composite electrodes (i.e., multiple layer metal films) were also investigated. Indium-aluminum composite electrodes were vacuum deposited onto a single crystal CdS specimen identified as MOD-1. The I-V curves obtained with this plating are presented in Figure VI.6. The presence of an aluminum film over the indium layer appears to have no effect upon the observed ohmicity of the I-V curves. The photosensitivity of crystal MOD-1 is evident from Figure VI.6. The long term stability of these electrodes has not yet been evaluated.

C. Physical Properties of CdS

Electron-phonon interactions via the acoustoelectric effect can be observed in CdS by noting changes in the propagation parameters of an ultrasonic wave (attenuation coefficient and velocity of sound) brought about by a modification of the electrical properties of the CdS. The acoustoelectric effect can also be observed by the generation of an electrical signal which results from the exchange of energy between the acoustic wave and conduction electrons. In this section we present results related to both of these means of observing the acoustoelectric effect. Emphasis is placed upon the generation of an electrical signal by the acoustoelectric effect. Properties of this signal such as its frequency dependence, absolute sensitivity and noise limitations have been measured and are reported.

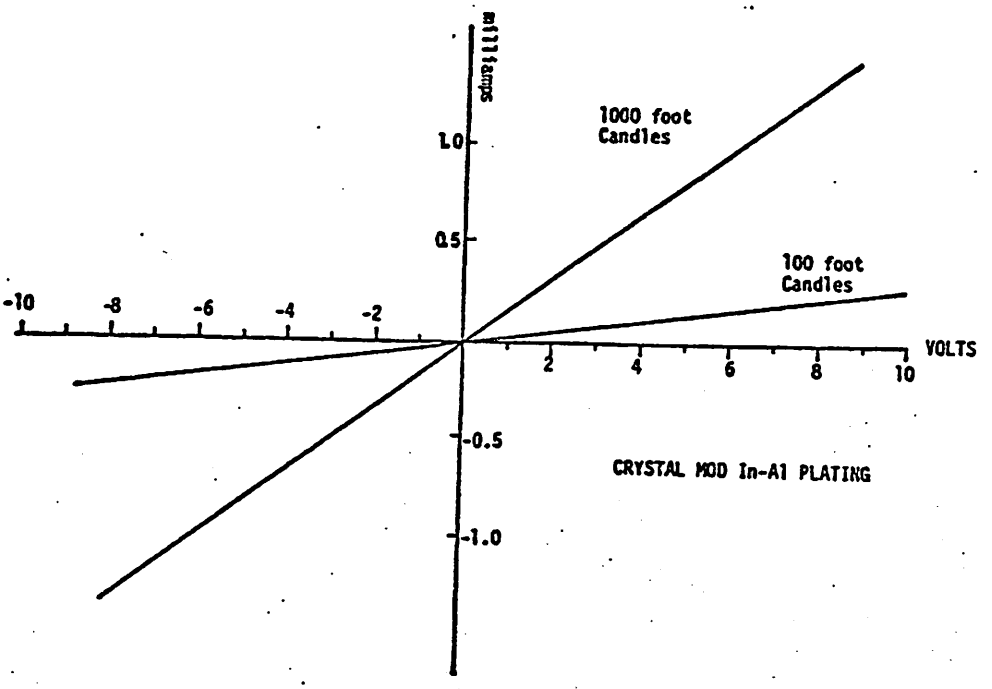

Figure VI.6. Current-voltage curves at two levels of light intensity for CdS crystal MOD with indium-aluminum electrodes. Crystal dimensions are 1.5 cm thick with approximately 0.82 cm^2 of surface area. Composite metal film electrodes do not adversely affect the ohmicity of the electrical contacts.

1. Attenuation Coefficient

In this section we present the results of a series of measurements designed to determine the electronic attenuation coefficient in CdS at a frequency 5 MHz. A conventional pulse echo experiment was performed using a two microsecond burst of 5 MHz ultrasound as the transmitted ultrasonic pulse. The CdS crystal, LJB-1, was coupled to the transmit/receive transducer by a water path. The specimen was air backed. The time delay associated with the water "buffer" path was approximately 60 microseconds. For each ultrasonic pulse transmitted, a series of ultrasonic pulses were received. The received ultrasonic pulses were the result of reflections from the water-CdS interface and of subsequent reverberations of the ultrasonic pulse within the CdS sample. The amplitudes of these subsequent reverberations were exponentially decreasing with time and were related to the ultrasonic attenuation suffered by the pulse on each successive round trip through the specimen.

To determine the attenuation coefficient of the CdS specimen, the output of the transmit/receive transducer was amplified and sent to an rf amplifier with a logarithmic gain characteristic. This logarithmic amplifier transformed the exponentially decreasing echo pattern into a linearly decreasing echo pattern. The output of the rf long-amplifier was diode detected and further amplified. The log-linear characteristics of this system were accurate over approximately a 35 dB variation in the amplitude of input signals. The amplitude versus time information generated in this way was digitized and recorded using a Biomation 8100 transient recorder under control

of an HP-9825A desktop calculator. All of the data were recorded on magnetic tape for subsequent analysis.

A series of pulse-echo patterns were recorded as a function of the electrical conductivity of the CdS crystal. The conductivity of the CdS crystal was modified by means of a tungsten filament lamp. Light intensity was adjusted through the use of neutral density optical filters. The level of optical excitation was measured using a conventional light meter as well as by recording the bulk resistance of the CdS crystal.

The attenuation coefficient in the CdS was estimated from the slope of a least squares line fit through the maxima of the echo amplitude versus time record. The electronic attenuation coefficient, i.e., that part of the total loss caused by the interaction of ultrasound with conductive electrons, was estimated by subtracting the background attenuation coefficient (measured at low conductivity in the dark) from the total observed attenuation coefficient. In Figure IV.7 we show the results of these experiments superimposed upon the predictions of the theory of Hutson and White.[37] The error bars represent the standard deviation of the least squares curve fitting routine. The standard deviation associated with the large values of the attenuation coefficient are large because of the small number of observable echoes present. Within the limit of experimental errors it appears that the weak coupling theory of the acoustoelectric effect[37] adequately describes the conductivity dependence of the attenuation coefficient.

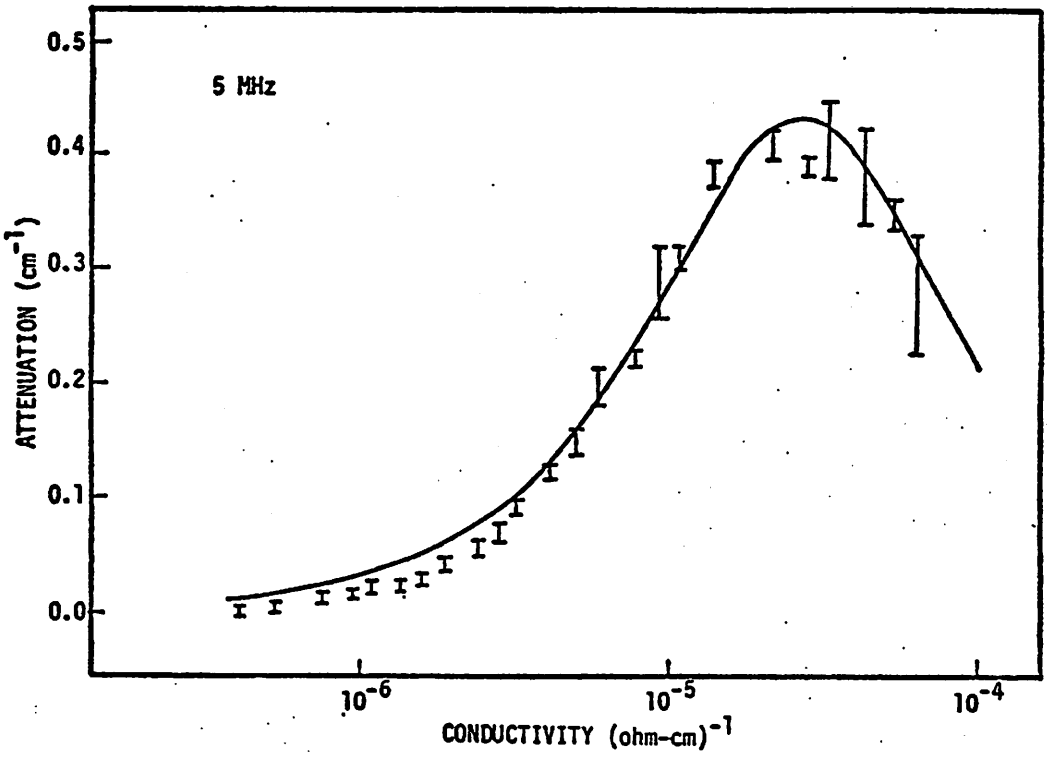

Figure VI.7. Electronic attenuation coefficient versus conductivity observed in crystal LJB. Measurements were made at 5 MHz using a pulse-echo technique. Crystal conductivity was determined from crystal resistance measurements and independent measurements of light intensity incident upon the crystal. Solid curve represents prediction of theory of the acoustoelectric effect in the weak coupling limit.

2. The Acoustoelectric Signal

In this section we discuss the observed time domain waveforms of the acoustoelectric signal produced by short ultrasonic pulses. We consider how this signal depends upon electrical as well as mechanical loading of the CdS crystal. We conclude this section by showing the steady state response of a thin CdS crystal to long burst of ultrasound. The piezoelectric and acoustoelectric resonator properties of this specimen are presented.

i) Short Pulses: Time Domain Response. Equation (III.41) which describes the time dependent acoustoelectric current density can be used to predict the time dependent acoustoelectric voltage produced by a CdS crystal under a variety of mechanical and electrical loading situations. The mechanical loading of the CdS crystal is handled explicitly by Eq. (III.41) by the reflection coefficients r_o and r_ℓ. The electrical loading of the CdS crystal can be incorporated with the Norton equivalent circuit shown in Figure VI.8. The acoustoelectric response of the crystal can be modeled as a time dependent acoustoelectric current source of strength $\langle J_{AE}(t) \rangle$ times the cross sectional area of crystal, in parallel with the bulk electrical properties of the crystal. The electrical loading the crystal is then simply treated as an arbitrary electrical impedance $Z_{e\ell}$ which additionally filters the acoustoelectric output of the CdS crystal.

To illustrate this approach we consider an example of a thick CdS crystal which is mechanically loaded on one face by water and which is unloaded (air backed) at the other face. Under these conditions ($r_o = 0.87$, $r_\ell = 1$) an acoustic pulse entering the crystal from the water

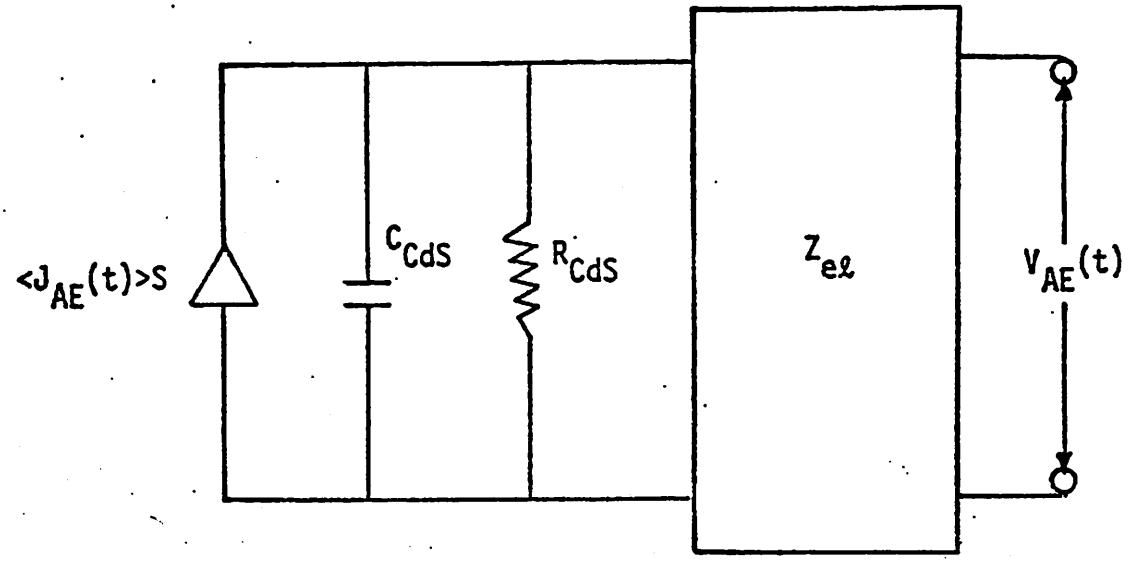

Figure VI.8. Norton equivalent circuit used to predict the acousto-electric voltage response of CdS specimens. The effects of mechanical loading are included in the expression for the time dependent current density from Eq. (III.41). The effects of electrical loading are accounted for by the general element $Z_{e\ell}$. A filtering approach is used to predict the time domain voltage waveform observed.

reverberates within the crystal. The electrical "load" which the CdS crystal is normally required to drive is the input impedance of the amplifier used to measure the electrical signal. The frequency dependent input impedance of most amplifiers can be approximated as a shunt resistance and a shunt capacitance. Typical values for the input resistance and capacitance of a signal amplifier with a field effect transistor input stage are $R_{in} \sim 10^{10}\,\Omega$ and $C_{in} = 15$ picofarads.

In Figure VI.9 we demonstrate a filtering approach which allows us to predict the time domain acoustoelectric waveform. In panel a) we show the time dependent acoustoelectric current density predicted using Eq. (III.41). The equation was evaluated assuming a crystal conductivity of $2 \times 10^{-6}\ (\Omega\,\mathrm{cm})^{-1}$, assuming the pulse length was equal to the crystal length, and using the theory presented in Chapter II to evaluate the electronic attenuation coefficient at a typical ultrasonic frequency of 5 MHz. The predicted time domain voltage was calculated by performing a Fourier transform of the acoustoelectric current and then multiplying these results by the frequency dependent impedance consisting of the crystal resistance and capacitance in parallel with the assumed input resistance and capacitance of the amplifier. Finally, an inverse Fourier transform was performed to predict the time domain voltage waveform presented in pabel b). It is interesting to note that the oscillating (bipolar) current waveform in panel a) has been low passed filtered in such a way to produce a nearly unipolar voltage waveform. The observed acoustoelectric waveform for crystal LJB-2 obtained under mechanical and electrical loading conditions essentially identical to those specified above is shown in panel c). We see that the

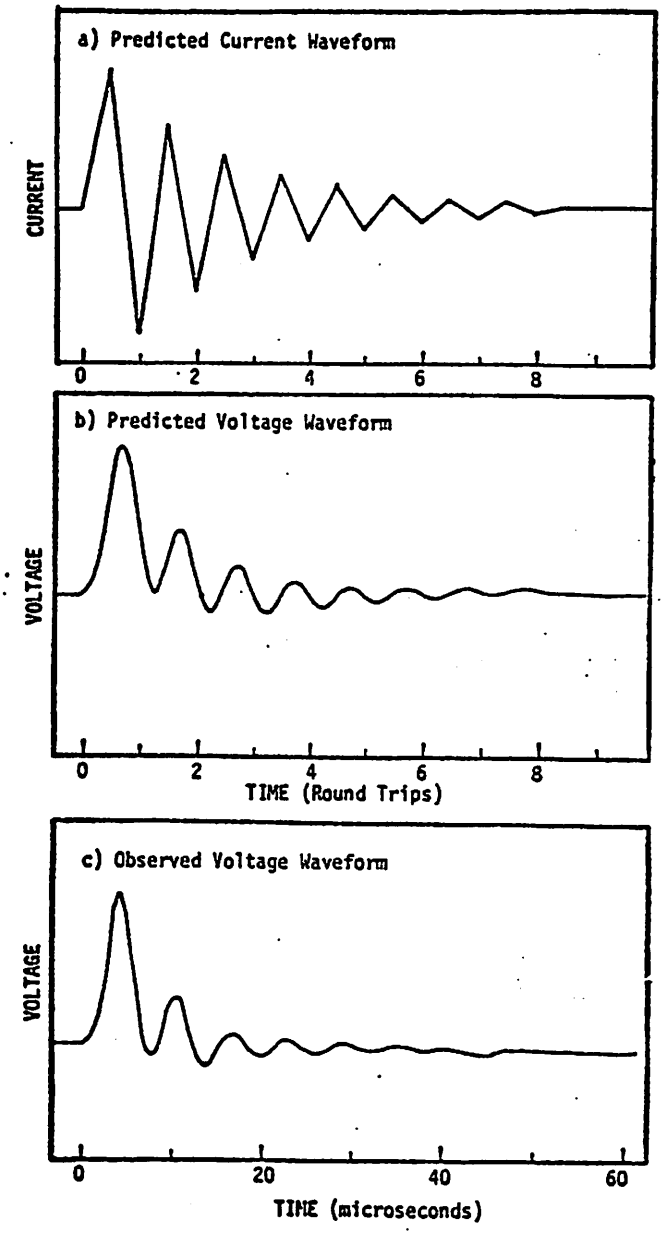

Figure VI.9. Predicted and observed time domain acoustoelectric response of CdS crystal LJB. In panel a) the acoustoelectric current generated by a pulse of length equal to the crystal length is shown. The crystal is assumed to be water loaded on one side and air loaded on the other [$r_o = 0.87$ and $r_\ell = 1.0$]; $\alpha\ell$ of the crystal is assumed to be approximately 0.62. The predicted voltage waveform shown in panel b) was calculated assuming $R_{CdS} = 5 \times 10^5 \Omega$, $C_{CdS} = 0.5$ pf, $R_{in} = 1 \times 10^{10} \Omega$ and $C_{in} = 15$ pf. The observed waveform from crystal LJB is shown in panel c) for identical mechanical and electrical loading conditions.

essential features of the signal are reproduced. In particular we note that a nearly unipolar voltage waveform is produced by the acoustic pulse reverberating within the crystal.

In order to produce a more compact time domain response one might consider backing the CdS crystal with a material of comparable mechanical impedance in order to eliminate the multiple reverberations of the acoustic pulse within the crystal. Under these conditions the acoustic pulse makes a single transit through the crystal and the current produced is shown in Figure VI.10 panel a). The resistance of the CdS crystal was chosen to be 80×10^3 ohms and a shunt capacitance of 150 picofarads was assumed. This large amount of shunt capacitance is representative of the capacitance present when about five feet of coaxial cable are used to connect the CdS crystal to an oscilloscope. The predicted acoustoelectric voltage waveform for these conditions is shown in panel b) of Figure VI.10. We see that the voltage produced is severely spread out in time primarily due to the shunt capacitance of the cable.

In Figure VI.11 we demonstrate how a more compact time domain response might be achieved even when such large values of shunt capacitance are present. The current waveform predicted in panel a) is associated with an air backed CdS crystal which has been mechanically matched to the water medium at the front surface of the crystal through the use of a quarter wave matching element ($r_o = 0$, $r_\ell = 1$). Under these conditions the acoustic pulse make a single round trip through the crystal and is then transmitted out of the CdS crystal back into the water. In panel b) we show the predicted voltage waveform, once again

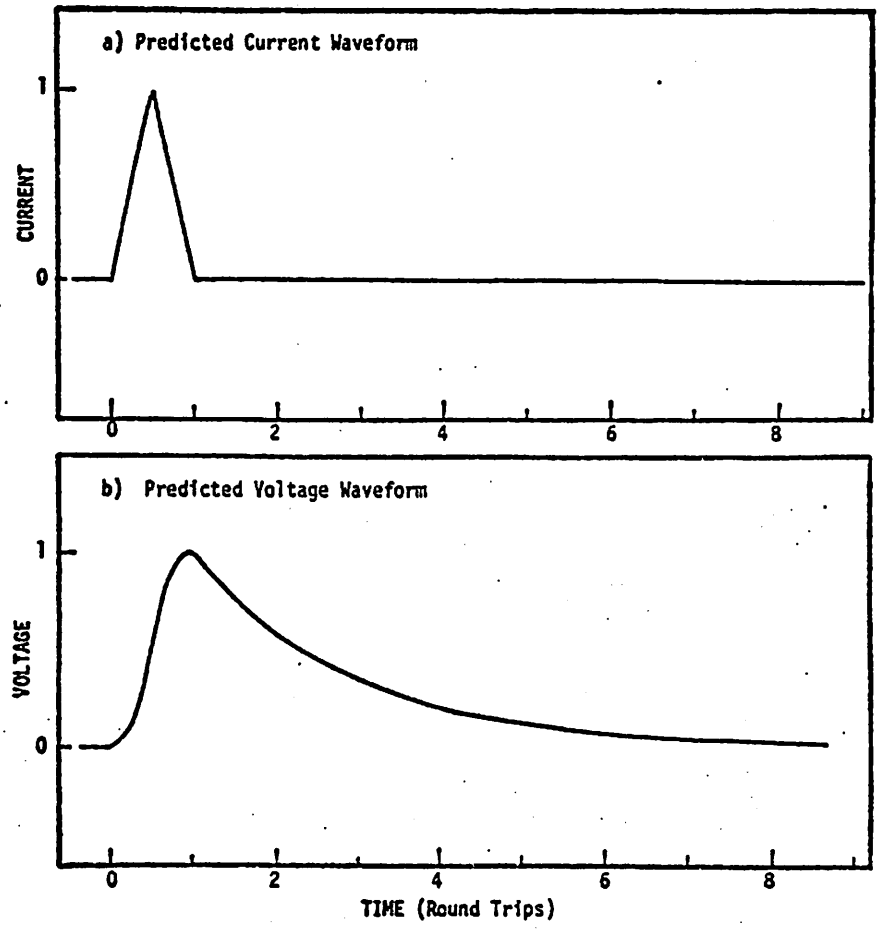

Figure VI.10. Predicted time domain acoustoelectric response of perfectly backed CdS crystal. In panel a) the acoustoelectric current generated by a single transit of a pulse with length equal to the crystal length is shown. The crystal is assumed to be perfectly backed [$r_\ell = 0$]; $\alpha\ell$ of the crystal is approximately 0.60. The predicted acoustoelectric voltage waveform shown in panel b) was calculated assuming $R_{CdS} = 8 \times 10^4 \Omega$, $C_{CdS} = 0.5$ pf, $R_{in} = 1 \times 10^6 \Omega$ and $C_{in} = 150$ pf. The large value of shunt input capacitance is typical of approximately five feet of coax cable.

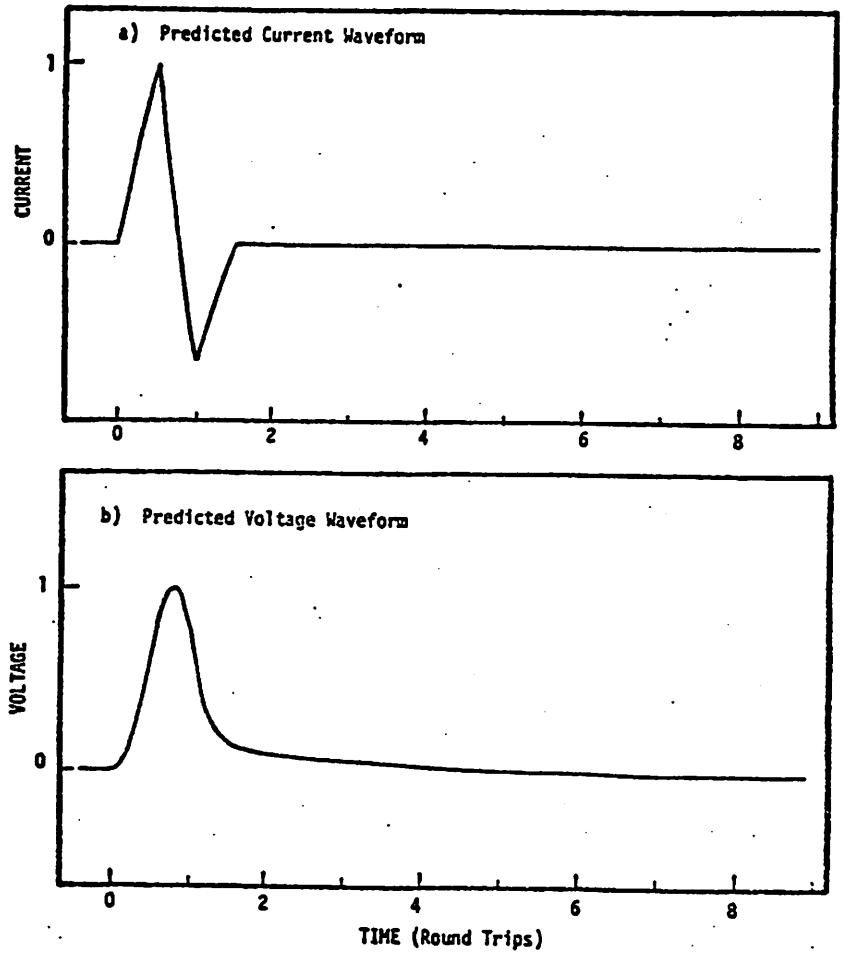

Figure VI.11. Predicted time domain acoustoelectric response of a matched and unbacked CdS crystal. In panel a) the acoustoelectric current generated by a single round trip of a pulse with length equal to the crystal length is shown. The crystal is assumed to be mechanically matched to the load at the front surface and unloaded at the back surface ($r_o = 0$, $r_\ell = 1$); $\alpha\ell$ of the crystal is approximately 0.60. Electrical loading conditions are the same as in Figure VI.10; however panel b) shows that better acoustoelectric pulse resolution has been attained.

assuming a crystal resistance of 80×10^3 ohms and a shunt capacitance of 150 pf. The time constant associated with the signal source is identical with that of the previous example, however the pulse definition has been improved and the time duration of the voltage signal has been reduced to approximately 2 pulse lengths.

In Figure VI.12 we show experimental results obtained with crystal JRK-2. This crystal exhibited electrical parameters comparable to those used in the predictions shown in Figure VI.11. This crystal was prepared with a matching layer on its front surface which was 5 quarter wavelengths thick at approximately 6 MHz. Therefore at this frequency $r_o \approx 0$. The crystal was imperfectly backed with a low impedance material ($r_\ell \approx 0.7$). Therefore reflection of the acoustic pulse at the back surface of the crystal was observed. As we see, the time domain acoustoelectric response of this crystal compares favorable with the prediction presented in Figure VI.11.

ii) Long Pulse: Frequency Domain Response. In this section we investigate the frequency dependence of the voltage response of an acoustoelectric and a piezoelectric resonator. Cadmium sulfide is a convenient material for this purpose because both these responses are simultaneously available when the crystal is mechanically resonant and can be monitored simultaneous using electrical filters. The experiment was performed using the quasi-continuous wave or long pulse, steady state response of the CdS resonator. The CdS crystal used in this experiment is identified as 470-1 and was prepared using the method outlined in Chapter V. This particular crystal was approximately 1 cm^2 in cross sectional area by 1.6 mm thick. Electrical contacts to this

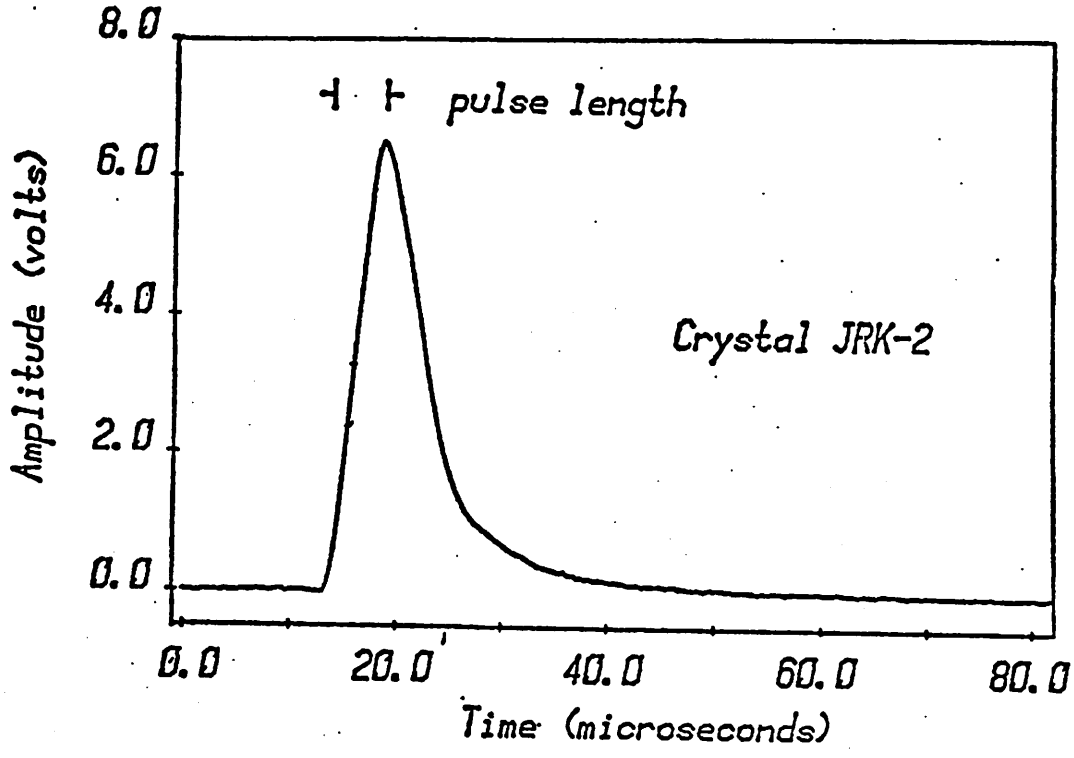

Figure VI.12. Observed time domain acoustoelectric voltage response of crystal JRK-2. The mechanical and electrical loading conditions on this crystal were essentially identical to those described in Figure VI.11. This crystal was provided with a quarter wave matching layer on its front surface so that $r_o \approx 0$.

crystal were indium and were shown to be ohmic by the methods previously described. Illumination was provided by a mercury-cadmium discharge lamp and fiber optic light ribbons. The experiment was performed in transmission in water tank using a broadband piezoelectric transmitter (Panametrics, V309) mounted coaxially with the CdS crystal approximately 15 cm away. The CdS crystal was mechanically backed with paraffin, and so the reflection coefficient at the rear surface was approximately 1. Gated rf pulses of approximately 35 μsec duration were applied to the transmitting transducer. This length of pulse was sufficiently long to produce a steady state response in the CdS plate but was sufficiently short so as not to produce any interference effects in the water delay medium. A voltage preamplifier (National Semiconductor LH0033) capable of responding to the total electrical signal produced by the plate was used. The acoustoelectric and piezoelectric response of the plate were monitored separately using the low and high pass filters described in Chapter V.

The results of these measurements of the piezoelectric response (triangles) and the acoustoelectric response (squares) as a function of frequency are shown in Figure VI.13. Both signals exhibit a resonant character. We note that the resonant acoustoelectric response of the plate has maxima twice as often in frequency as the piezoelectric response pattern. This observed behavior agrees with the resonator theory presented in Chapter III. The acoustoelectric response exhibits maxima for every harmonic of the plate fundamental, whereas the piezoelectric response exhibits maxima only at odd harmonics of the plate fundamental. Because the acoustoelectric signal is a response to the

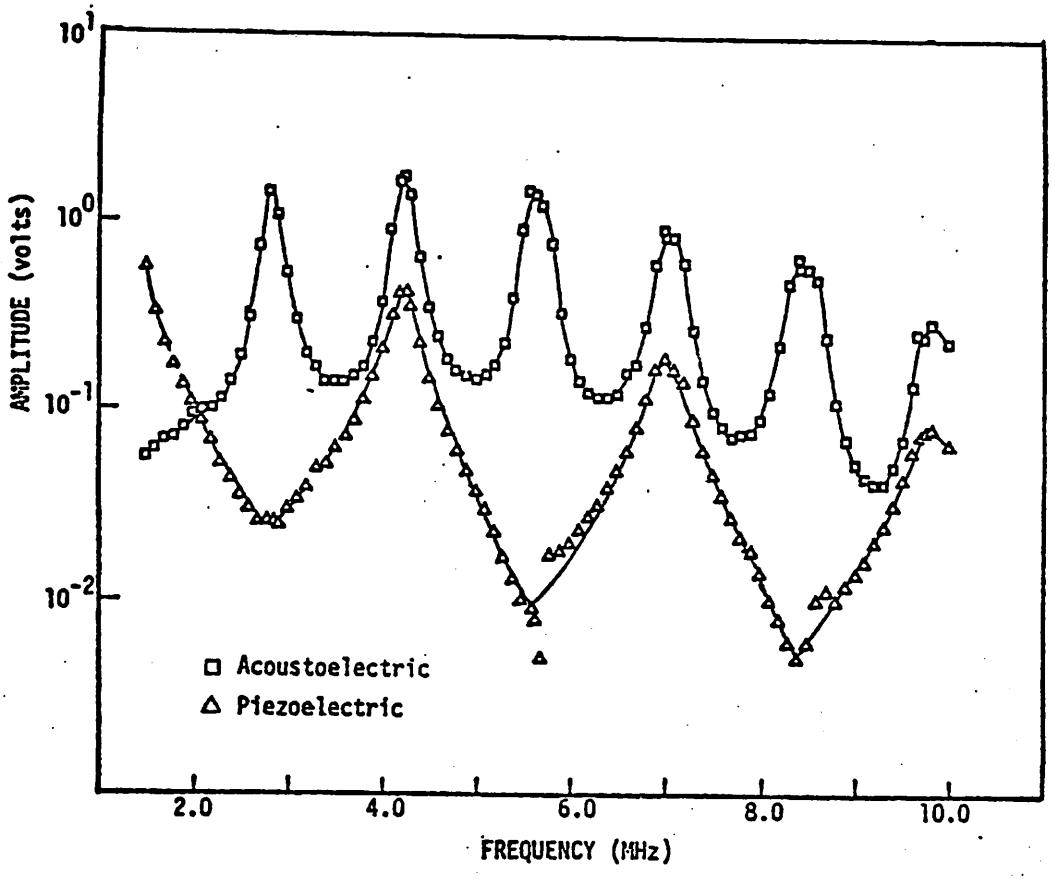

Figure VI.13. Acoustoelectric and piezoelectric resonator response of a thin plate piezoelectric semiconductor, CdS crystal 470-1. This crystal is approximately 1.6 mm in thickness with 1 cm^2 surface area. Crystal was illuminated with a long pulse (35 μsec) of ultrasound. Acoustoelectric and piezoelectric responses were monitored simultaneously using electrical filters to separate rf and low frequency signals.

net transfer energy within the bulk of the crystal, it reaches a maximum whenever the amount of mechanical energy stored in the resonator is maximized. In contrast, the piezoelectric response of the plate is the result of the net (i.e., relative) motion of the surfaces of the resonator plate. At even plate harmonics, the net motion of the surfaces is minimized.

3. Properties of Thick Piezoelectric Plate

In this section we demonstrate the low pass characteristics associated with a thick piezoelectric plate when it is used to detect a short ultrasonic pulse. For purposes of demonstration, a 1/4 inch thick plate of PZT-4 was used as the piezoelectric receiver. This material was chosen because the piezoelectric coupling constants which characterize it as a receiver are comparable to that of CdS. PZT-4, however, is an insulator; therefore any low frequency signals observed are not the result of the acoustoelectric effect. The dielectric permittivity of PZT-4 is much higher than that of CdS. Thus the low frequency response of PZT-4 is not as easily "shorted out" by the addition of load resistors as is that of CdS.

The experiment was performed with a combined reflection/transmission geometry. A short ultrasonic pulse was launched using a Panametrics A309 transducer driven by an electrical impulse supplied from Panametrics PR5052 pulser/receiver. The time domain signal caused by the reflected ultrasonic energy from the front surface of the PZT plate and the subsequent reverberations from within the plate were recorded using an HP-175A sampling oscilloscope under control of an HP-9825A calculator. The reflected time domain signals

were stored for subsequent processing. The electrical response of the PZT plate to the ultrasonic pulse was monitored directly using a voltage preamplifier whose input impedance was fixed at 10^5 ohms. The direct electrical response of the plate was also digitized and stored in a similar manner.

In Figure VI.14 we show the time domain record of the electrical signals. In panel a) we show the reflected ultrasonic signal as measured by the Panametric A309 transducer. The large echo is the signal caused by direct reflection from the water-PZT interface and the subsequent echoes correspond to reverberations of the pulse within the PZT plate. In panel b) we show the time domain record directly from the PZT plate. The electrical signals occur twice as often in time as those in panel a) because we are seeing the electrical response of each of the surfaces of PZT plate.[45,48-50] The alternating sign of the signals and the relative magnitude of each is in good agreement with the open circuit piezoelectric response expected from Eq. (III.11).

The frequency domain response of the front surface of the PZT-4 plate was determined by comparing the magnitude of the Fourier transform of the gated (dashed lines) portions each time domain record. By assuming that the transfer function ($T(\omega)$) of the Panametrics transducer is the same in either the transmit or receiver mode[70-75] we can determine the transfer function of the PZT plate, $P(\omega)$. The magnitude of the Fourier transform of the gated portion of panel a) corresponds to the square of the transmitter transfer function $|T(\omega)|^2$ because two transductions have taken place. The magnitude of the Fourier transform of the gated portion of panel b) then corresponds to $|T(\omega)||P(\omega)|$. The

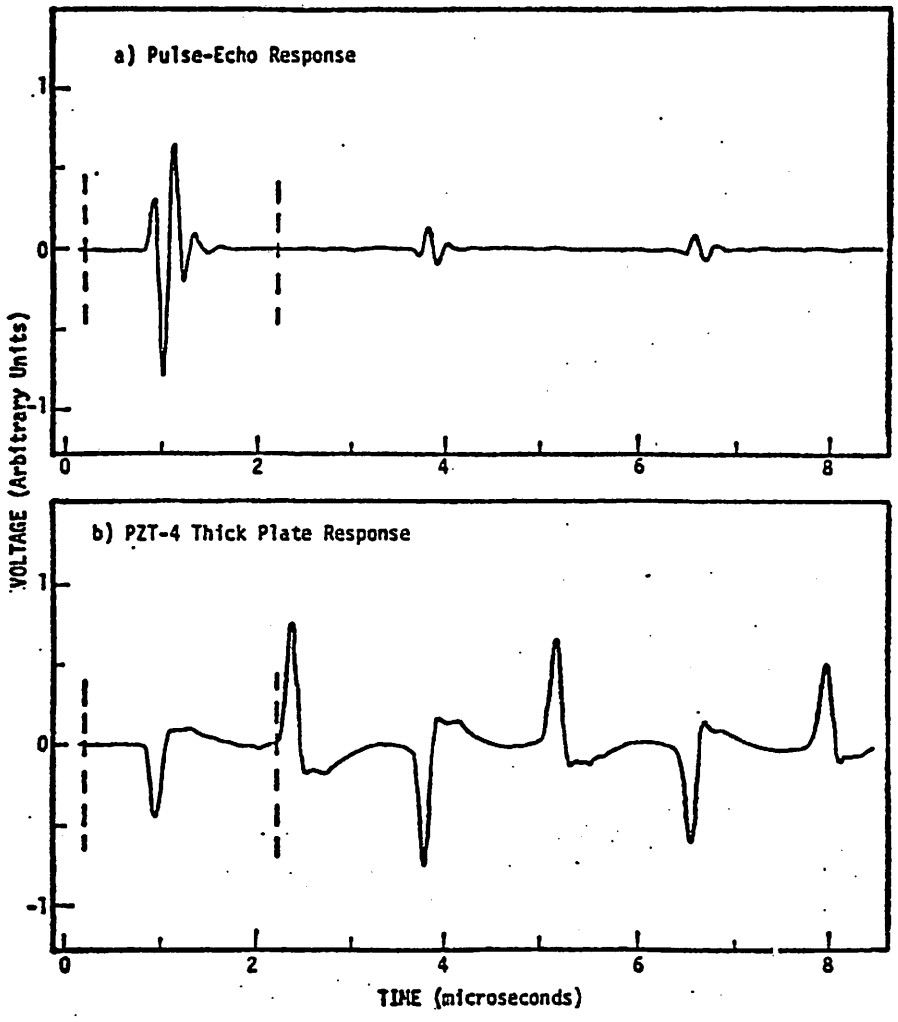

Figure VI.14. Time domain response of thick PZT-4 plate to a transient ultrasonic pulse. In panel a) the time domain response of acoustic signals reflected from the PZT-4 plate are shown. In panel b) the direct piezoelectric response of thick plate are shown. Note that electrical signals occur twice as often in panel b) as those in panel a) because we observe the electrical response of both front and back surfaces of PZT-4 plate.

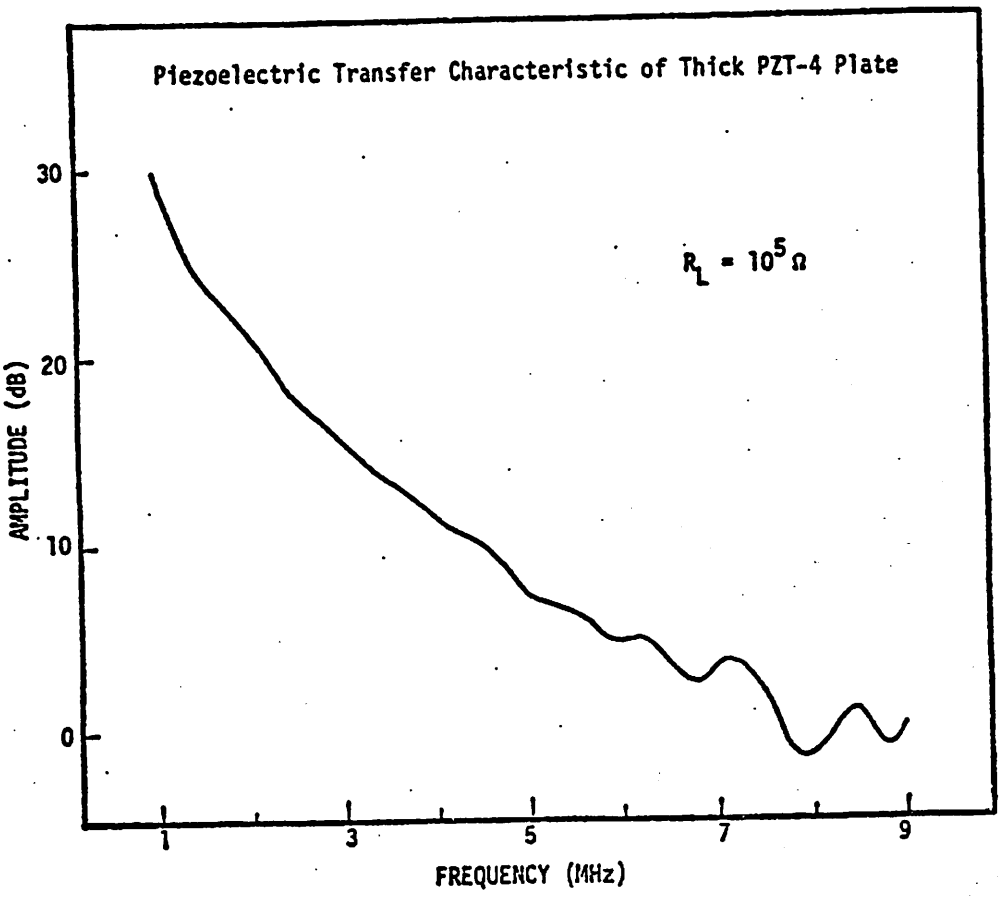

Figure VI.15. Spectral amplitude of nonresonant PZT-4 plate. The gated (dashed lines) portions of Figure VI.14 were Fourier transformed and logarithmically subtracted to yield the transfer characteristic of the thick PZT-4 plate.

frequency characteristics of the plate alone can be determined by logarithmic subtraction,

$$20 \log P(\omega) = 20 \log(|T(\omega)P(\omega)|) - 10 \log(|T(\omega)|^2) \ .$$

The results of this analysis are presented in Figure VI.15. A 30 dB enhancement of the low frequency components of the ultrasonic pulse is seen to be produced by the thick PZT plate. This is similar to the results predicted earlier in Figure III.4.

4. Calibration

In order to estimate the sensitivity and response characteristics of the acoustoelectric effect in cadmium sulfide it is necessary to have a means for estimating the amount of ultrasonic energy incident upon the CdS crystal. The approach employed consisted of calibrating a commercial piezoelectric transmitting transducer over a broad range of frequencies.

As discussed in Chapter V, a transducer calibration technique based upon the transient thermoelectric effect[78-80] was implemented. All measurements were done using a copper-constantan thermocouple in a 1/8 inch thick castor oil absorbing medium. The castor oil absorber was held at 10°C. The calibrations were performed upon a Panametrics A309 transducer (serial number 5066). This transducer was focused at 2 inches and had a nominal center frequency of 5 MHz.

An analysis of the errors associated with the transient thermoelectric calibration technique has been presented by Goss, et al.[80] They showed that a major source of error associated with this technique can be attributed to heat diffusion from the thermocouple probe due to insufficient ultrasonic beam width. For this reason, some preliminary measurements of the beam profile of the Panametrics A309 transducer were performed. Beam profiles were measured using a 1 mm diameter PZT probe. Figures VI.16 and VI.17 show representative beam profiles taken at an ultrasonic frequency of 3.5 MHz using 3 sec ultrasonic pulses. Measurements were made along a line perpendicular to the major axis of the transmitting transducer and intersecting the axis at distances of 5 and 8 cm respectively.

Figure VI.18 summarizes the beam profile data in terms of the measured beam width (-10 dB from maxima) versus distance along the axis of the transmitter. Measurements were made along 7 different lines through the ultrasonic beam and at 3 different ultrasonic frequencies. From these results we conclude that the beam width at 8 cm from the transmitter was sufficiently large for accurate thermoelectric measurements and yet sufficiently small to produce measurable heating. These conditions are satisfied over an ultrasonic bandwidth of $\sim$3.5 to 8.5 MHz.

Transient thermoelectric measurements were carried out on axis, at 8 cm from the transmitting transducer.

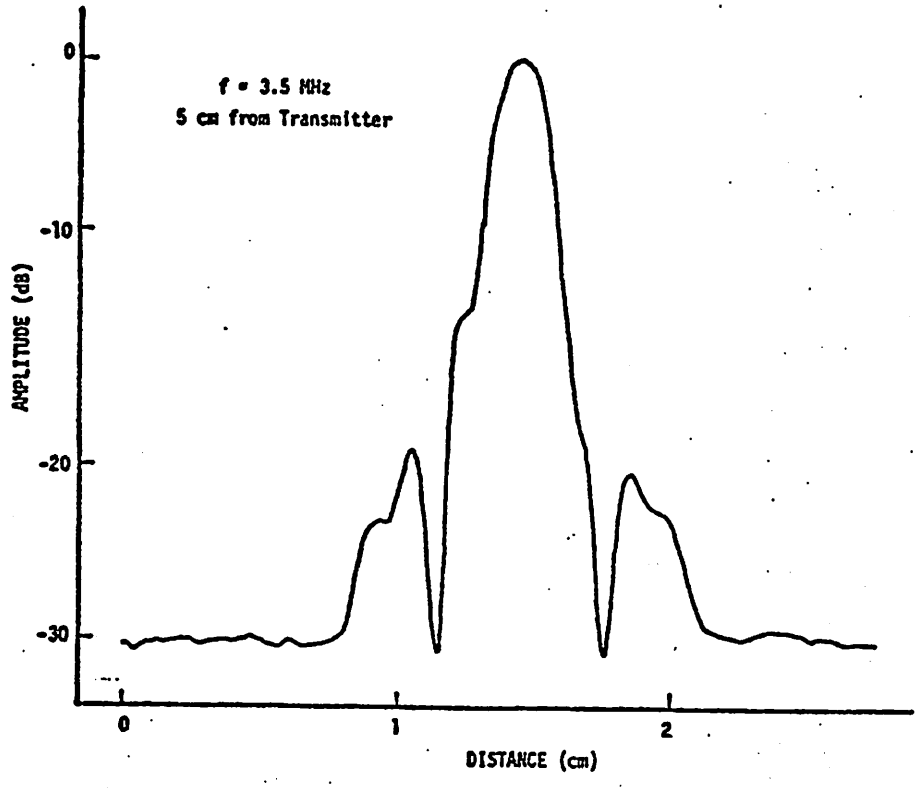

Figure VI.16. Beam pattern profile of calibrated Panametrics transducer measured at 3.5 MHz in the focal plane (5 cm focus). Measurements were made using a 3 μsec burst of rf to drive the transducer, and a 1 mm PZT probe was used to map the field.

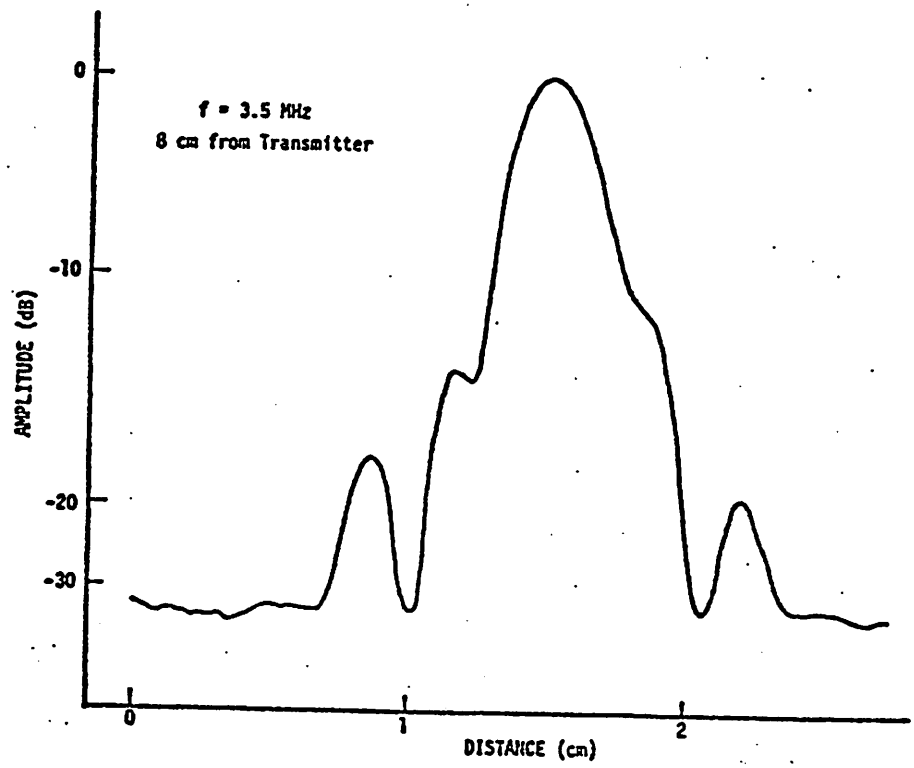

Figure VI.17. Beam pattern profile of calibrated Panametric transducer measured at 3.5 MHz in a plane located at 8 cm. Measurements were made using a 3 μsec burst of rf to drive the transducer, and a 1 mm PZT probe was used to map the field.

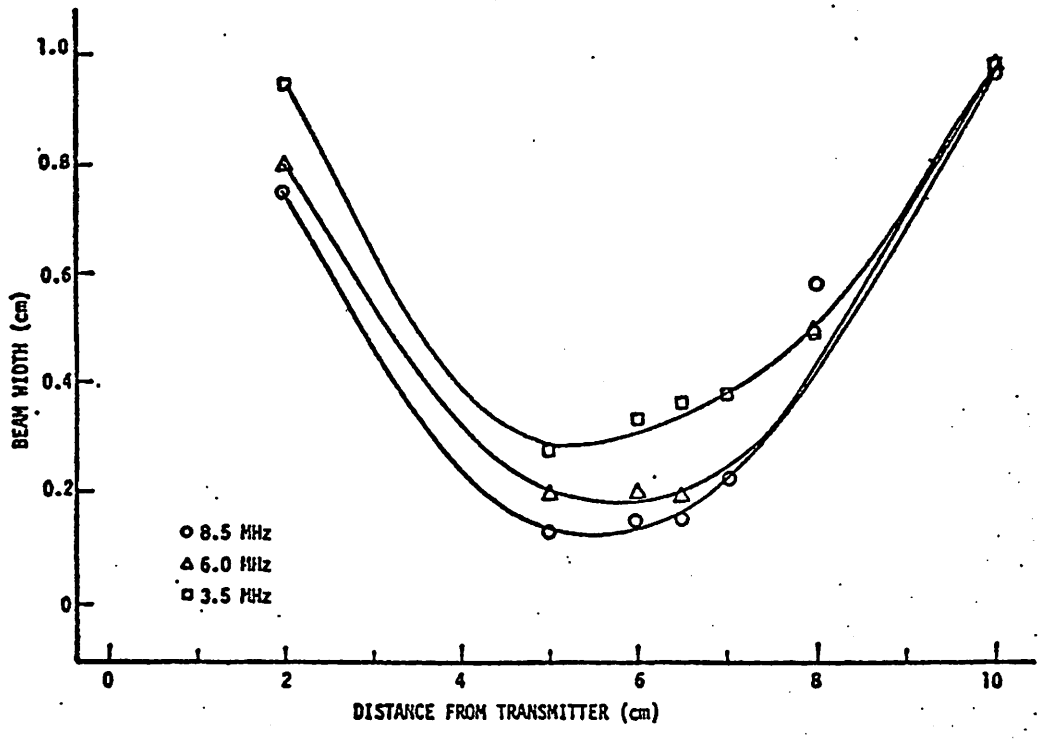

Figure VI.18. Ultrasonic beamwidth versus distance from calibrated Panametrics transducer. Measurements were made using 3 μsec bursts of 3.5, 6.0, and 8.5 MHz rf to drive the transmitting transducer. Beam widths were measured at -10 dB from central maximum.

A representative transient thermoelectric curve is shown in Figure VI.19. This curve was obtained using an ultrasonic pulse of approximately 1 sec duration at a frequency of 4.6 MHz. Two characteristic types of heating are observable on this transient thermoelectric curve.[79] Viscous heating, which is the result of the relative motion of the thermocouple and the castor oil, accounts for the sharp rise and fall in termperature at the beginning end of the ultrasonic pulse ($t = 0.5$ sec and $t = 1.5$ sec, respectively). Absorptive heating is observed as a more gradual and nearly linear increase in termperature. The instantaneous ultrasonic intensity is calculated from the observed rate of absorptive heating using Eq. (V.3).

Some of the results of this calibration work are depicted in Figure VI.20. The instantaneous intensity output of the Panametrics A309 is shown as a function of frequency for a constant transmitter drive level. Data of this sort were collected at three different transmitter drive levels to verify system linearity. These results were used subsequently to estimate the efficiency and bandwidth of the acoustoelectric effect.

i) Intensity Sensitive Nature of the Acoustoelectric Effect. A transmission experiment was performed to determine the dependence of the acoustoelectric voltage upon incident ultrasonic intensity. A three microsecond burst of 6 MHz ultrasound was transmitted from the calibrated piezoelectric transmitter and received by crystal LJB. The acoustoelectric waveform produced is shown in Figure VI.9. The amplitude of the first voltage peak was recorded as a function of

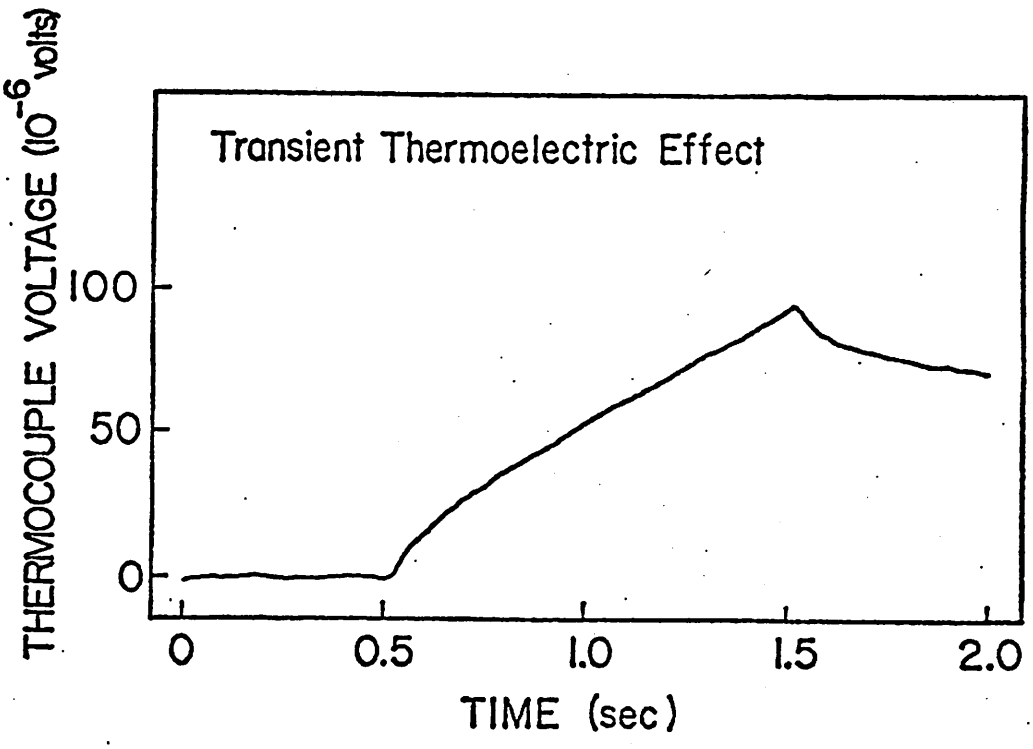

Figure VI.19. Representative transient thermoelectric measurement obtained at 4.6 MHz used for transducer calibration. A copper-constantan thermocouple imbedded in castor oil was used to measure the temperature rise caused by the absorption of ultrasound. Data of this sort were recorded at 3 different transmitter derive levels and at 200 KHz frequency intervals from 2.4 to 9.2 MHz.

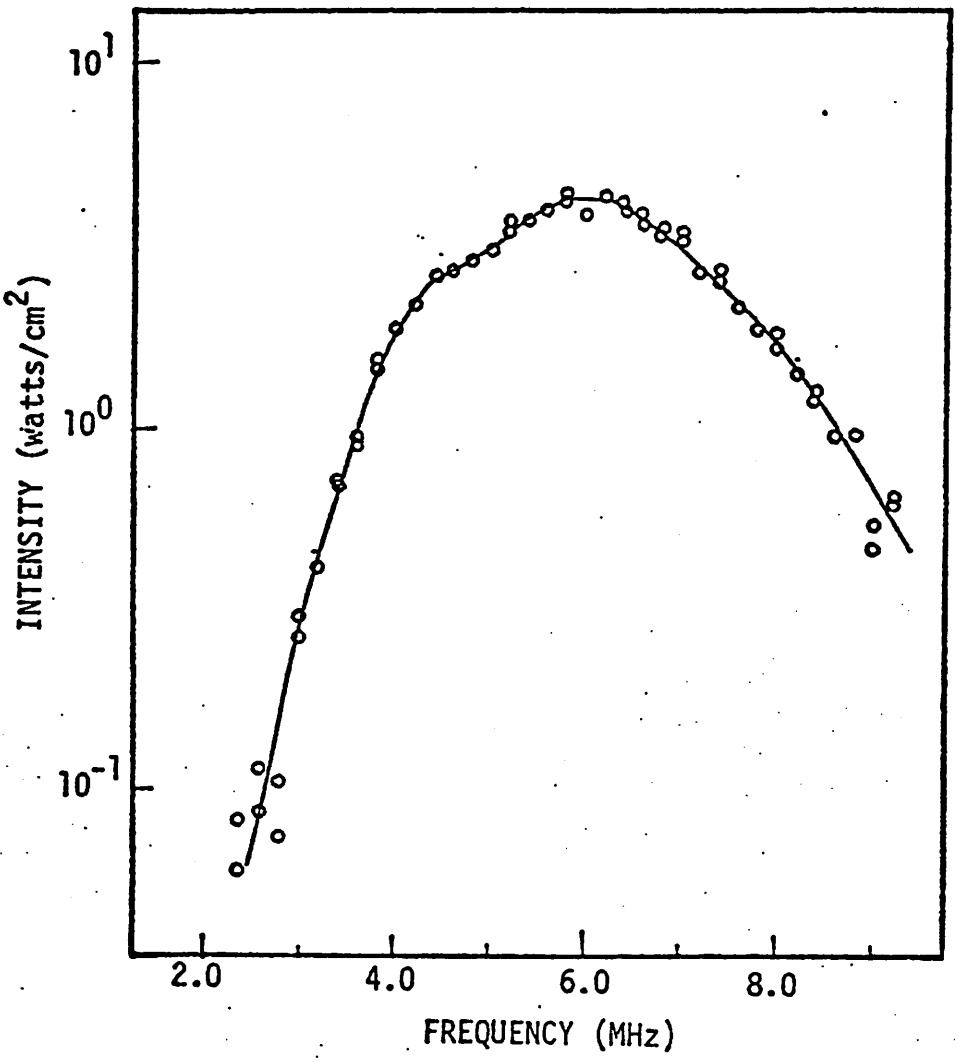

Figure VI.20. Instantaneous acoustic intensity produced by Panametric transducer versus frequency. Measurements were made on the axis of the transducer field pattern at 8 cm from the transducer. A constant voltage drive was applied to the input of the power amplifier. The 50 Ω output impedance of power amplifier was loaded by the transducer near the band center.

the amplitude of the transmitter drive voltage. The previous calibration results allowed us to determine the acoustic intensity output at each of these transmitter drive levels. In Figure VI.21 we show the acoustoelectric output as a function of incident ultrasonic intensity. We see that the acoustoelectric signal is indeed proportional to the ultrasonic intensity incident upon it. We also note that the observed signal is limited by noise at intensity levels lower than 8×10^{-6} watts/cm^2. For this crystal the observed noise level was approximately 50 microvolts rms.

ii) Broadband Responsivity and Sensitivity. The results of the calibration measurements can be used to estimate the broadband responsivity of the acoustoelectric receiver. By broadband responsitivity we mean the magnitude of the acoustoelectric voltage produce per unit ultrasonic intensity incident over a range of ultrasonic frequencies. The ultimate sensitivity, i.e., the minimum ultrasonic signal detectable against the noise background, can also be determined.

In Figure VI.22 we show the measured broadband voltage responsivity for crystal LJB. These data were obtained using 3 μsec pulses of ultrasound and were measured in transmission using the calibrated piezoelectric transducer as transmitter. The results of the transient thermoelectric calibrations were used to normalized the acoustoelectric voltage produced at each frequency to the voltage which would be produced for 0.5 watt/cm^2 of instantaneous or peak incident acoustic intensity. The nearly flat response of the crystal as a function of frequency agrees with expectations for the acoustoelectric voltage response discussed in Section III.G. For comparison the broadband

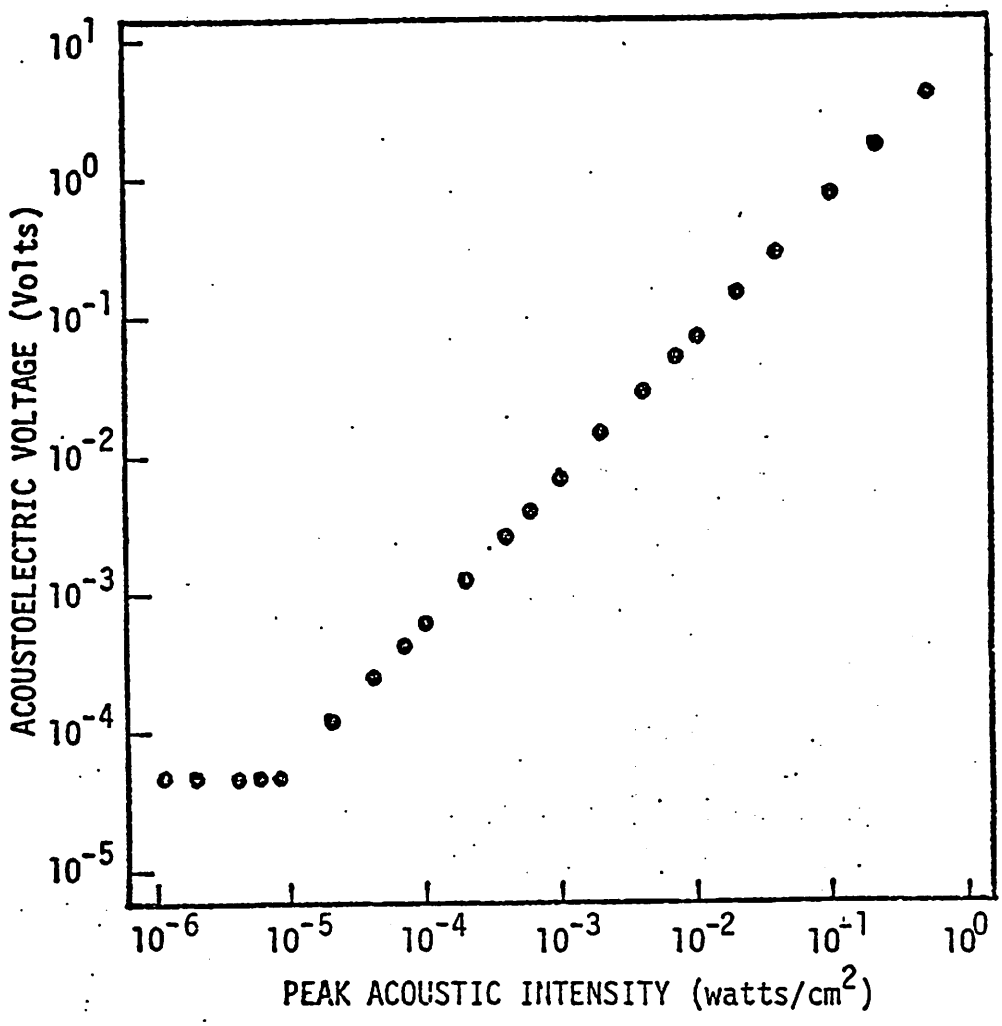

Figure VI.21. Acoustoelectric voltage response of crystal LBJ versus instantaneous incident acoustic intensity. Measurements were made at 5 MHz using the previously calibrated Panametrics transducer. The lower limit on the acousto-electric voltage is comparable to the Johnson noise produced the bulk resistance of the CdS crystal.

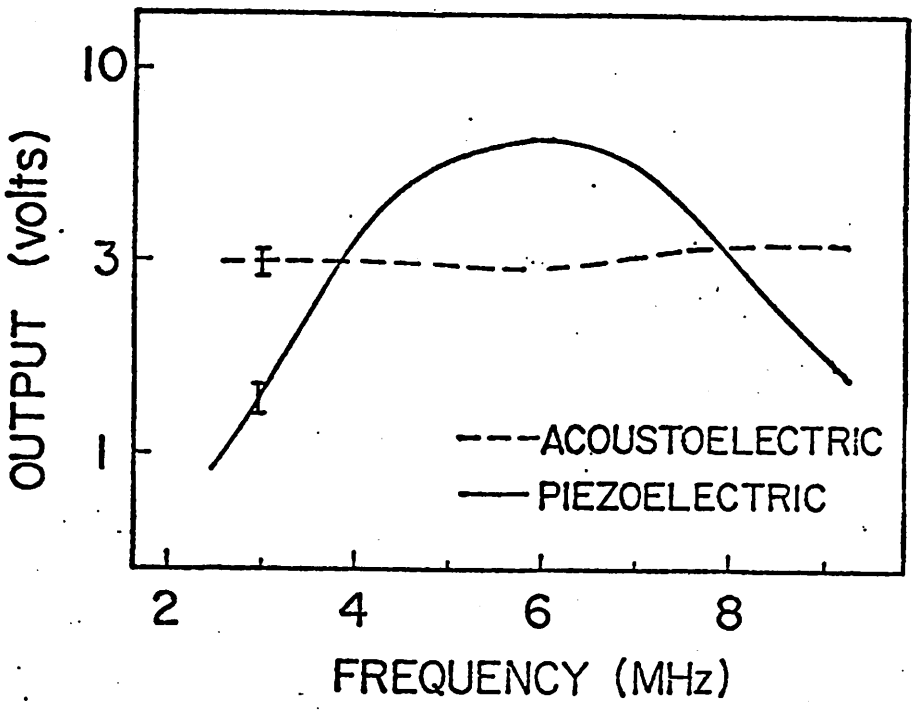

Figure VI.22. Broadband responsivity of the acoustoelectric voltage response of crystal LJB. The acoustoelectric output in volts (dashed line) is shown for an instantaneous acoustic intensity input of 0.5 watt/cm^2 at each ultrasonic frequency measured. The responsivity of the acousto-electric receiver is nearly frequency independent (varied by less than 1 dB) over the 2.5 to 9.5 MHz frequency range. The responsivity (solid line) of a commercially available broadband piezoelectric transducer over the same frequency range and for the same incident acoustic power level is shown for comparison.

responsivity of the calibrated piezoelectric transducer (A309, #5066) is shown with the solid curve. The piezoelectric transducer's responsivity was determined in reflection using a stainless steel reflector.

An estimate of the ultimate sensitivity of the acoustoelectric response in this mode of operation can be gained by estimating the noise equivalent power. If the noise background is primarily generated by the Johnson noise associated with the crystal resistance, then the minimum measureable signal corresponding to a one-to-one signal to noise ratio can be determined. With a crystal resistance of 5×10^5 Ω and an electronic bandwidth of 3×10^5 Hz, the rms noise level should be approximately 50 microvolts. This agrees well with noise level observed using crystal LJB and the field effect transistor preamp shown in Chapter V. With the observed responsivity shown in Figure VI.21, this corresponds to a noise equivalent power of approximately 8×10^{-6} watts/cm^2 of instantaneous acoustic intensity. This intensity corresponds to the ultrasonic intensity incident upon the cadmium sulfide crystal, not to the intensity present within the CdS crystal. The acoustic mismatch between CdS and water causes an intensity transmission coefficient of 25%. In other words, the noise equivalent power of this CdS specimen could be further reduced to 2×10^{-6} watts/cm^2 of incident acoustic intensity if care were taken to eliminate the acoustic mismatch between water and CdS. The observed noise equivalent power for this crystal makes it approximately an order of magnitude less sensitive than expected based upon the predictions of Section III.H. We also note that the intensity sensitive response of this crystal is not compromised by the low frequency direct piezoelectric response of the crystal which would be evident at low signal levels.

As a means of further increasing the sensitivity associated with the acoustoelectric response of crystal LJB-1, the transmitter modulation scheme discussed in Chapter V was implemented using a lock-in detector in the receiver circuitry. A block diagram of the system is shown in Figure VI.22. A high ultrasonic repetition rate of 100 KHz was used so that full advantage could be taken of the signal averaging properties provided by lock-in detection, while still maintaining a relatively short (100 millisecond) time constant at the lock-in. Two hundred percent (i.e., carrier suppressed) modulation of the 3 microsecond, 5 MHz pulsed ultrasonic signal was performed by the modulator. The modulation frequency was chosen to be 10 KHz. The acoustoelectric signal was therefore modulated at 20 KHz because the signal it produces is not sensitive to the absolute phase of the ultrasonic wave. By using a 100 millisecond averaging time at the lock-in this scheme provided a 100-fold increase in sensitivity with CdS crystal LJB-1, i.e., a noise equivalent power of approximately 8×10^{-8} watts/cm^2. The signal provided by the lock-in was proportional to the square of the transmitter drive level all the way down to the noise level. In other words, the acoustoelectric response of the CdS plate did not appear to be compromised by the low frequency direct piezoelectric response of the plate.

D. Applications of the Acoustoelectric Effect in CdS

The applicationsof ultrasonic measurement techniques in the area of medical imaging, as well as tissue and materials characterization, has grown substantially over the past two decades.[10,11] Many of these applications dictate that ultrasonic measurements be made in the near field (i.e.,

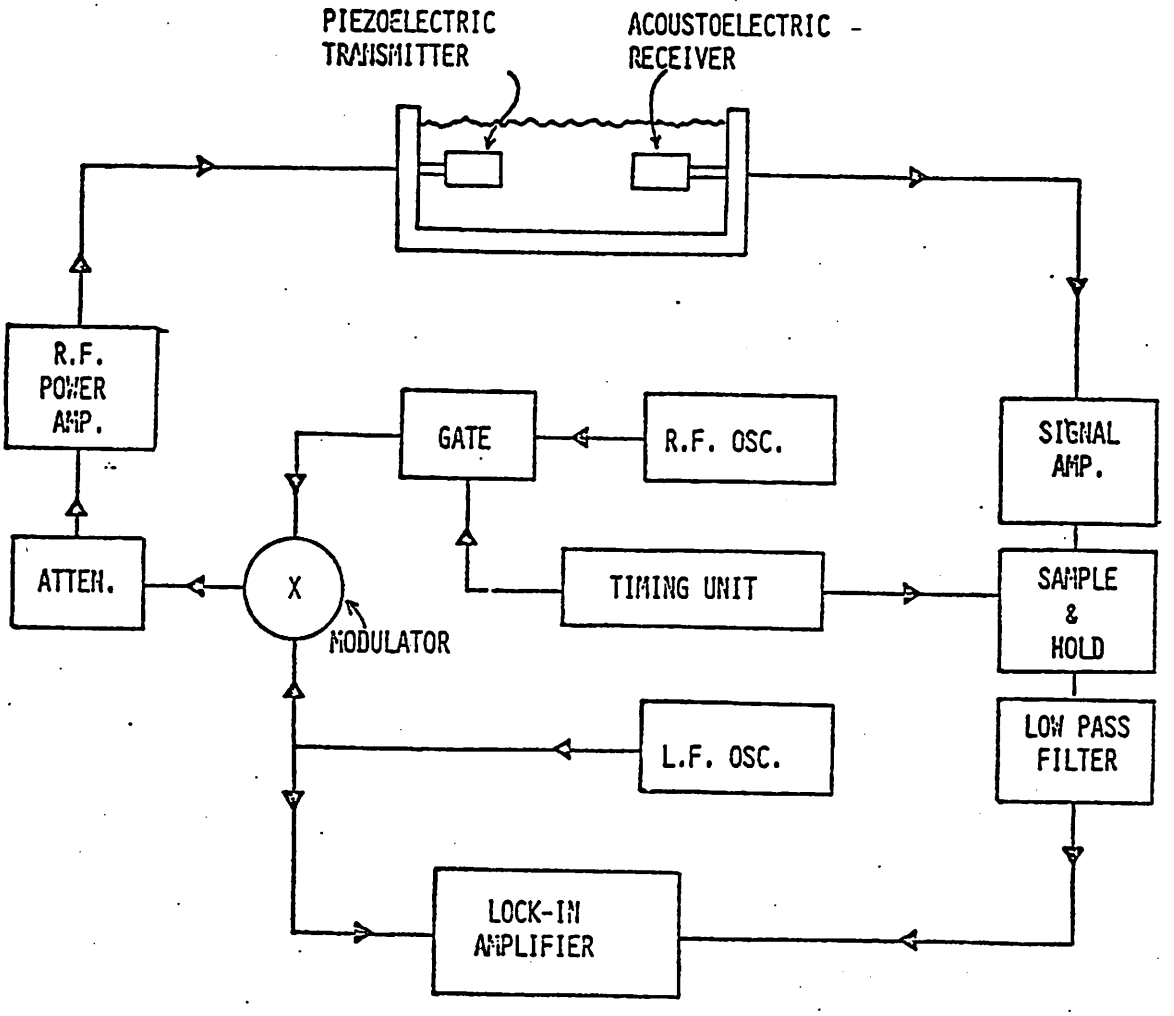

Figure VI.23. Block diagram of system used to increase the sensitivity of the acoustoelectric receiver. Two hundred percent amplitude modulation of the transmitted rf pulses was performed using the modulator described in Figure V.8. A PAR 126 lock-in amplifier was used to measure the modulated acoustoelectric signal. Using this approach the sensitivity of crystal LJB was improved by 100-fold over the measurements reported in Figure VI.21.

non-plane wave) region of either the transducer radiation pattern or in the near field of radiation pattern re-radiated (i.e., scattered or reflected) by the object under investigation. In this section we demonstrate the applicability and utility of the acoustoelectric effect in CdS for making quantitative measurements of acoustic fields under non-plane wave conditions. The benefits provided by the phase insensitive response of receiving transducer based on the acousto-electric effect in CdS are demonstrated in the context of quantitative ultrasonic transmission, scattering, and imaging experiments.

1. Broadband Attenuation Measurements with Inhomogeneous or Irregularly Shaped Objects

The acoustoelectric response of a thick plate of CdS provides a means for realizing the response characteristics of a phase insensitive receiver aperture as described in Chapter IV. The acoustoelectric response of CdS is also a very broadband response in the sense that a wide range of ultrasonic frequencies produce a useable acoustoelectric signal. In this section we show that both of these properties are desirable for making ultrasonic attenuation determinations on inhomo-geneous or irregular objects using transmitted ultrasound.

a) Transmission Measurements with Gated Bursts. To illustrate both the phase insensitive and broadband response properties of the acoustoelectric effect in CdS we made a series of attenuation versus frequency measurements of a homogeneous plate of plastic (polyester) which had a well defined surface irregularity: a step, of $\sim$1 mm depth, machined into one of its faces. To compare the response of identical phase sensitive and phase insensitive receiving apertures

a single crystal of CdS was used as both a piezoelectric and an acousto-electric receiver. By using appropriately chosen high and low pass filters these two responses could be measured simultaneously and independently.

A substitution technique[86] was used in conjunction with the acoustoelectric and piezoelectric response of the CdS crystal to determine the frequency dependence of the apparent attenuation coefficient $\alpha(\omega)$ for the plastic plate relative to an equivalent thickness of water.

Panel a) and c) of Figure VI.24 illustrate that measurements of the ultrasonic attenuation of the plastic were initially made through flat end parallel portions of the plate. Measurements of the apparent attenuation coefficient of the plate were subsequently made in the step position illustrated in panel b). With the step intersecting the ultrasonic beam we expect that a relative phase shift will be introduced into part of the beam and the ultrasonic field pattern at the receiver will be similar to those calculated in Figure IV.5 The results of measurements made using the piezoelectric response of the CdS crystal are shown in Figure 25a. We see that the observed frequency dependence of the attenuation coefficient with the piezoelectric receiver is a nearly linear function of frequency for measurements made through the flat portion of the plate. However, a scalloped spectrum results when the beam passes through the step discontinuity. At 5.7 MHz, the step discontinuity introduces a three half wavelength phase shift in the portion of beam which passes through the thicker portion of the plate relative to the portion of the beam which passes through a thinner

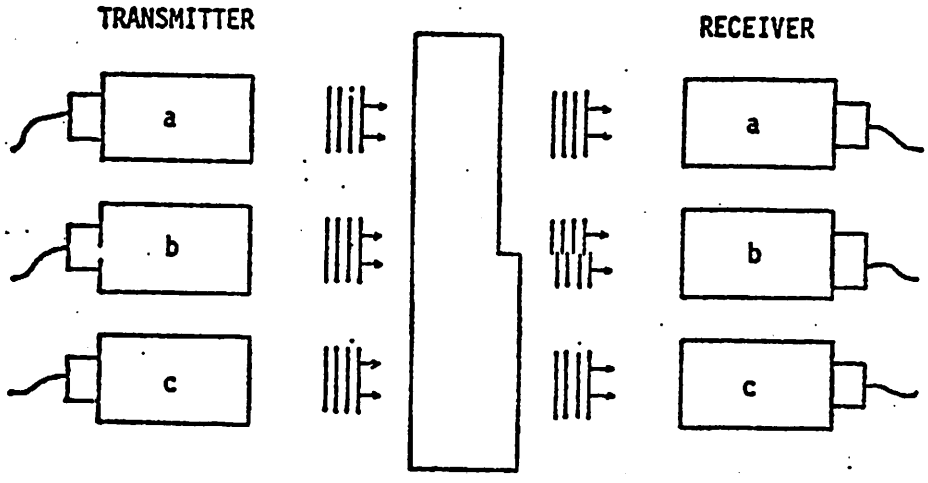

Figure VI.24. Schematic of ultrasound transmission experiment used to show the phase insensitive response of the acousto-electric receiver. Measurements of the apparent attenuation of the plastic plate made in positions a and c were made using the piezoelectric and acousto-electric response of crystal LJB. These measurements were compared with identical determinations made at position b which includes a step discontinuity.

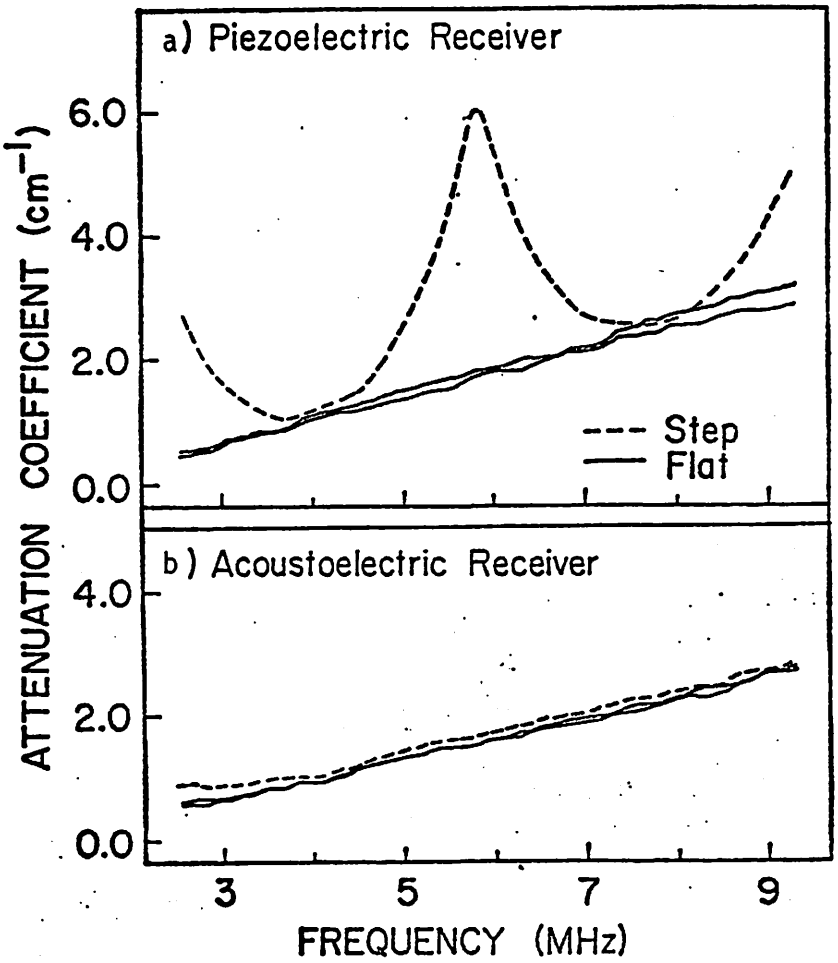

Figure VI.25. Demonstration of the phase insensitive response of the acoustoelectric response of crystal LJB. The apparent attenuation coefficients $\alpha(\omega)$ are shown as a function of frequency for the plastic plate as measured by the piezoelectric response of crystal LJB [panel a)] and the acoustoelectric response of crystal LJB [panel b)]. In panel a) the piezoelectric determination of $\alpha(\omega)$ through the stepped portion of the plate exhibits a scalloped pattern resulting from interference of electrical signals produced at different locations on the receiver aperture. In panel b) we see that the acoustoelectric determination of $\alpha(\omega)$ is not affected by the presence of the step discontinuity in the ultrasonic beam.

portion of the plate. As discussed in Chapter IV, this scalloped spectrum is the result of interference of the complex acoustic pressure field over the surface of a phase sensitive receiver aperture.

Figure VI.25b shows the results of measurements made using the acoustoelectric response of CdS receiver. Measurements made through flat and stepped regions of the plate are all mutually consistent, and in agreement with the piezoelectric measurements made through the flat portions of the plate. This result illustrates that the acoustoelectric response of the large CdS receiver can be used as a phase insensitive receiver aperture.

Another series of experiments were performed on specimens which processed irregularities which were more complex than those in the previous example. In this series, measurements were made on excised dog hearts. The apparent attenuation coefficient measured in transmission were compared for data obtained with phase sensitive (piezoelectric) and phase insensitive (acoustoelectric) responses of CdS. All measurements were made on contiguous and morphologically similar regions of the dog left ventricle. Results are shown in Figure VI.26. Panel a) depicts four attenuation-vs-frequency determinations obtained using a piezoelectric receiver and panel b) depicts the results from the same regions of dog heart using an acoustoelectric receiver. The piezoelectric determinations show a marked variability. In contrast, the data obtained with the acoustoelectric receiver, shown in panel b) exhibit uniformity and consistency.

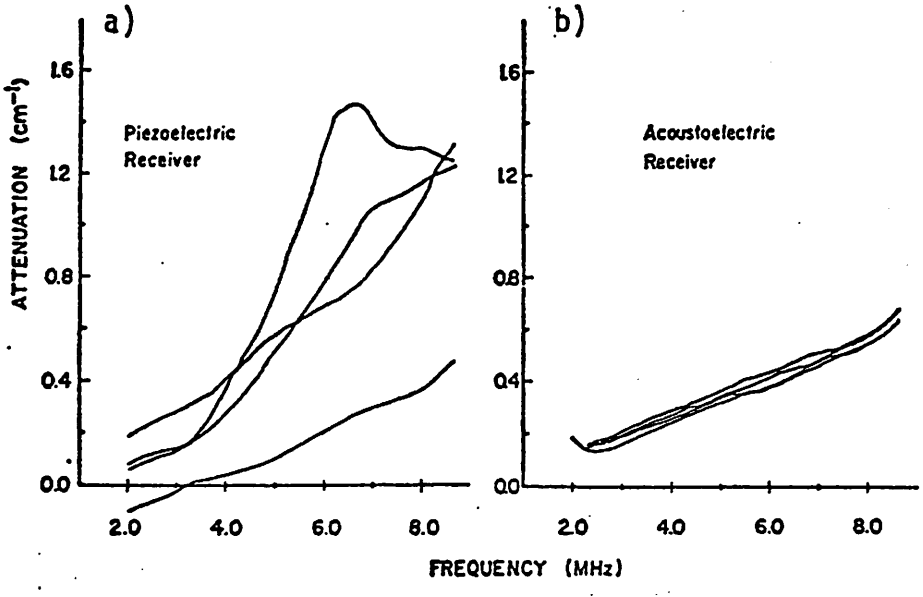

Figure VI.26. Apparent attenuation coefficient-frequency plots measured on four contiguous sites of normal dog heart. panel a) shows measurements made with the 1.3 cm diameter piezoelectric receiver while panel b) shows measurements obtained on the same four sites using the 1.3 cm diameter acoustoelectric receiver.

Reports of animal studies from several laboratories[83,86] suggest that the slope of the attenuation coefficient versus frequency provides a useful index for distinguishing between normal and diseased myocardium. From the results presented in Figure VI.26 it appears that a more reliable determination of the slope of the attenuation coefficient for the purpose of tissue characterization be achieved by making use of the acoustoelectric receiver.

b) Transmission Measurements Using Transient Pulses. As we showed in Section C of this chapter, the response of an acoustoelectric receiver to a high frequency burst of ultrasonic energy is a low frequency, video pulse (centered near dc) whose amplitude is proportional to the instantaneous acoustic intensity. Thus all ultrasonic frequencies are mapped into the same video bandwidth. In other words, frequency information about the ultrasonic pulse is lost unless special care is taken. In this section we describe how useful frequency information can be recovered (derived) from the acoustoelectric response of a CdS crystal to a single, transient acoustic pulse.

Broadband ultrasonic pulses can be achieved by driving a low Q ultrasonic resonator with a delta function stimulus. The ultrasonic pulse produced in this way exhibits a broad bandwidth of frequency components and these components are present "simultaneously" within the pulse.

When such a pulse is incident upon an acoustoelectric receiver, all of the ultrasonic frequency components within the pulse will therefore simultaneously contribute to the video signal produced. Thus, information about any particular frequency component is lost because

it is mixed with information from all other ultrasonic frequency components. Useful spectral information, however, can be recovered under these conditions. As illustrated earlier in Section C, the ultrasonic frequency response of the acoustoelectric receiver is flat. Thus all frequency components present within the acoustic pulse are treated equally. The output of an acoustoelectric receiver in response to a transient pulse should therefore be related to the area under the spectrum amplitude of the ultrasonic pulse.

To test this hypothesis, we compared the measured response of the acoustoelectric receiver with the calculated area under the spectrum amplitude of known ultrasonic pulses. A block diagram of the measurement system is shown in Figure VI.27 A Panametrics PR5052 was used to excite a V315 transducer (10 MHz center frequency). Well characterized specimens of polyethylene were then used to attenuate the transmitted ultrasonic pulse by known amounts. The low frequency acoustoelectric response was recorded as a function of polyethylene thickness. These measurements were then compared with the calculated area under the spectrum amplitude of the original signal and with the signal attenuated by the attenuation coefficient of polyethylene plates. In Figure VI.28 we plot the measure acoustoelectric signal loss versus the calculated area under the spectrum amplitude. There is a good agreement between the measured and the calculated results. Thus it appears that the response of an acoustoelectric receiver to a broadband pulse is closely related to the area under the spectrum amplitude of the pulse.

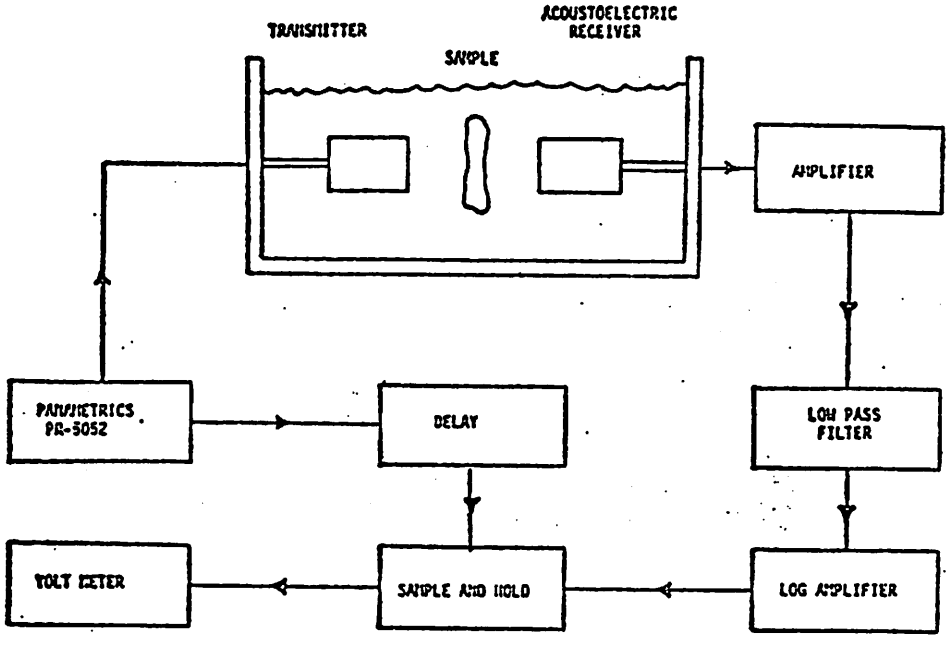

Figure VI.27. Block diagram of system used to measured the response of an acoustoelectric receiver to a transient ultrasonic pulse. A Panametrics V315, 10 MHz center frequency transmitting transducer was used to launch a well defined transient pulse. Samples of known ultrasonic properties (polyethylene plates) were used to attenuate the pulse in a known way.

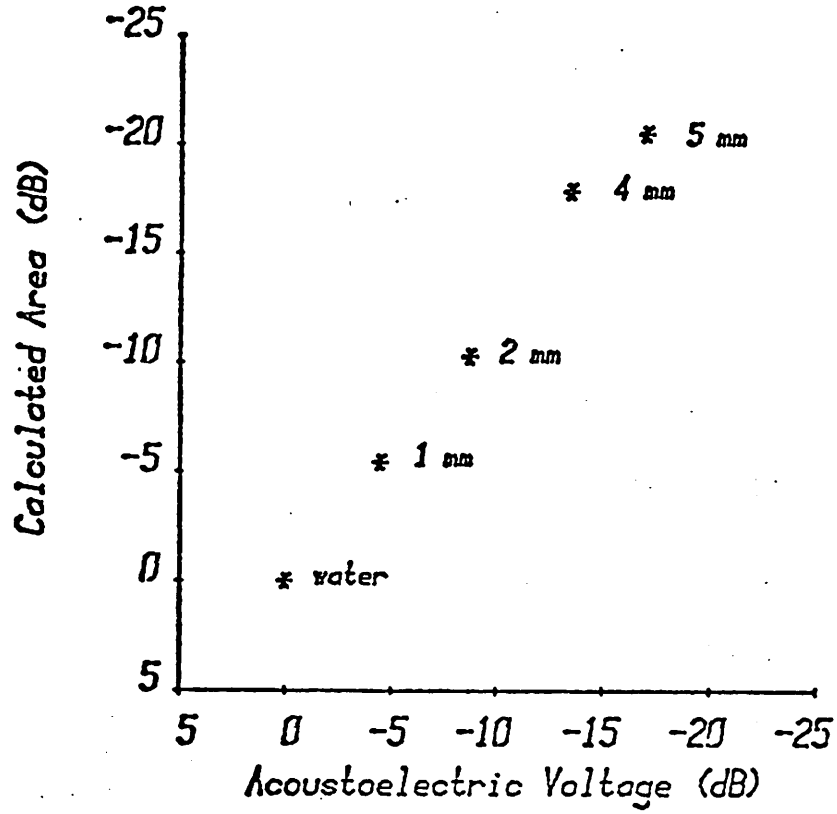

Figure VI.28. Measured acoustoelectric signal loss versus calculated area under spectral amplitude of a transient ultrasonic pulse. Measurements were performed by using different thicknesses of polyethylene to attenuate a transient ultrasonic pulse in a well defined way. The frequency dependence of the attenuation coefficient for polyethylene is nearly linear with a slope of 0.79 cm^{-1}/MHz.

Motivated by the apparent success of this initial evaluation of the acoustoelectric receiver to broadband, transient pulses, we evaluated this system as a means for monitoring the attenuation of unknown samples. For this work, a transmitting transducer with well defined and easily parameterized frequency response was needed. A Panametrics A305 transducer was chosen because its spectral response could be easily parameterized as a gaussian of the form

$$S_0(\omega) = Ae^{-(\omega-\omega_0)^2 T^2} \qquad \text{(VI.1)}$$

where ω_0 is the center frequency of the power spectrum and 1/T is the frequency at which the spectrum falls to e^{-1} of its maximum response and A is a frequency independent constant of proportionality.

Based on the hypothesis that the response of an acoustoelectric receiver to a broadband acoustic pulse is related to the area under the amplitude spectrum of the pulse, we model the acoustoelectric signal produced by this gaussian pulse as

$$V_0 = \int_{-\infty}^{\infty} S_0(\omega)d\omega = A\sqrt{\pi/T^2} \quad . \qquad \text{(VI.2)}$$

If the acoustic pulse is now attenuated by a sample which exhibits a frequency dependent attenuation coefficient of the form $\alpha(\omega) = \alpha'\omega$ and a thickness d, then the new amplitude spectrum presented to the acoustoelectric receiver will be of the form

$$S_1(\omega) = Ae^{-2\alpha'\omega d}\, e^{-(\omega-\omega_0)^2 T^2} \quad . \qquad \text{(VI.3)}$$

This expression can be rewritten as

$$S_1(\omega) = Ae^{+\alpha'^2 d^2/T^2} e^{-2\alpha' d\omega_o} e^{-(\omega-\omega_1)^2 T^2} \qquad \text{(VI.4)}$$

where $\omega_1 = \omega_o - \alpha' d/T^2$. The spectrum respresented by Eq. (VI.4) can be viewed as a skewed gaussian with maximum spectral amplitude at ω_1. As noted by other investigators,[87,88] the shift in maximum frequency response $(\omega_o - \omega_1)$ is directly proportional to the slope of the attenuation coefficient, α'.

The response of the acoustoelectric receiver to such a skewed gaussian spectrum is predicted to be

$$V_1 = \int_{-\infty}^{\infty} S_1(\omega)d\omega \qquad \text{(VI.5a)}$$

$$V_1 = A\sqrt{\pi/T^2}\, e^{+\alpha' d^2/T^2} e^{-2\alpha' d\omega_o} \qquad \text{(VI.5b)}$$

$$= A\sqrt{\pi/T^2}\, e^{+\alpha'^2 d^2/T^2} e^{-2\alpha(\omega_o)d} \,. \qquad \text{(VI.5c)}$$

By using a substitution technique to compare the sample response to an equivalent system response with no sample present we can take the quotient

$$\frac{V_1}{V_0} = e^{-2\alpha(\omega_o)d} e^{+\alpha'^2 d^2/T^2} \,. \qquad \text{(VI.6)}$$

For narrowband pulses, i.e., provided that 1/T is small,

$$\alpha'^2 d^2/T^2 < 2\alpha(\omega_o)d \qquad \text{(VI.7)}$$

and Eq. (VI.6) reduces to the form

$$\frac{V_1}{V_0} = e^{-2\alpha(\omega_0)d} \quad . \tag{VI.8}$$

Thus the ratio of the two voltages is simply related to the attenuation coefficient at the center frequency of the pulse. (This forms the basis for the way the gated cw measurements described in the previous section were made.)

Going back to Eq. (VI.6), and recalling that $\alpha(\omega_0) = \alpha'\omega_0$, we see that

$$\alpha'^2(d/T)^2 - 2\alpha'\omega_0 d - \ln V_1/V_0 = 0 \quad . \tag{VI.9}$$

This is a quadratic equation in the slope of the attenuation coefficient α' and has the solution

$$\alpha' = \left(\frac{T}{d}\right)\left(\omega_0 T - \sqrt{\omega_0^2 T^2 + \ln(V_1/V_0)}\right) . \tag{VI.10}$$

Equation (VI.10) permits the determination of the slope of the attenuation coefficient by measuring the response of the acoustoelectric receiver to two broadband pulses if some characteristics of the transmitting transducer are known.

This measurement scheme was implemented using a Panametrics A305 (1/2 inch diameter, 2 inch focus) transmitting transducer with the following characteristics $f_0 = \omega_0/2\pi = 6.5$ MHz and $1/T \simeq 2.4$ MHz. The slope of the attenuation coefficient was determined using this method on 60 different sites within a normal region of left ventricle

of an excised dog heart. The results of these measurements yield an average for the slope of 0.082 ± 0.013 cm^{-1}/MHz. This value agrees reasonably well with the value 0.075 ± 0.002 reported in previous studies. The most significant source of error may be caused by the departure of the transmitting transducer's spectrum from a true gaussian power spectrum which was assumed in the analysis of the problem. This means of determining the slope of the attenuation coefficient is very easily implemented since it requires the measurement of a single voltage per measurement site.

c) Chirp ("Linear fm") Pulses. Chirped ultrasonic pulses represent another means of encoding information about many frequencies upon a single ultrasonic pulse. By a chirped pulse we mean a relatively long, gated pulse of rf with the carrier frequency changing in a well defined way during the duration of the pulse. One common type of chirped pulse consists of the "linear fm" pulse in which the carrier frequency is a linear function of time for the duration of the pulse. Like broadband transient pulses, a broad range of ultrasonic frequencies can be present in a single chirp pulse; however, these frequencies are not all present simultaneously. For this reason, the time dependent wave form produced by an acoustoelectric receiver used to detect a chirped ultrasonic pulse might be used to determine ultrasonic amplitude versus frequency information.

We performed a number of experiments using acoustoelectric receivers to detect linearly chirped ultrasonic pulses. One series of measurements is presented here to demonstrate the response characteristics of the acoustoelectric receiver. This measurement was performed at the relative slow chirp rate of 69 KHz per microsecond because of limitations in the transmitter circuitry. The transmitted ultrasonic pulse consisted of a gated rf pulse, 128 μsec long, in which the carrier frequency was swept from 2 to 10 MHz. In Figure VI.29 we compare the response of the acoustoelectric receiver to a broadband piezoelectric receiver when each is used to detect this chirped pulse. In panel a), the envelope of the received signal seen by the piezoelectric receiver is illustrated. The amplitude as a function of time is representative of the spectrum amplitude of these piezoelectric transducers. In panel b) we show the received signal as seen by the acoustoelectric receiver. The amplitude versus frequency response of the acoustoelectric receiver is comparable to the piezoelectric receiver; however the turn on and turn off time of the pulse observed with the acoustoelectric receiver is somewhat broader. In panel c) and d) we illustrate the phase sensitive response of the piezoelectric receivers and the phase insensitive response of the acoustoelectric receiver when used to detect chirped ultrasonic pulses. In panel c) we show the amplitude versus time response of a piezoelectric receiver when it is used to detected a chirped pulse which has passed through a step in the otherwise flat and parallel plastic plate shown in panel e). As illustrated in panel c) there is one point in time, i.e., one frequency, at which the thickness of step is equal to an odd number of half wavelengths.

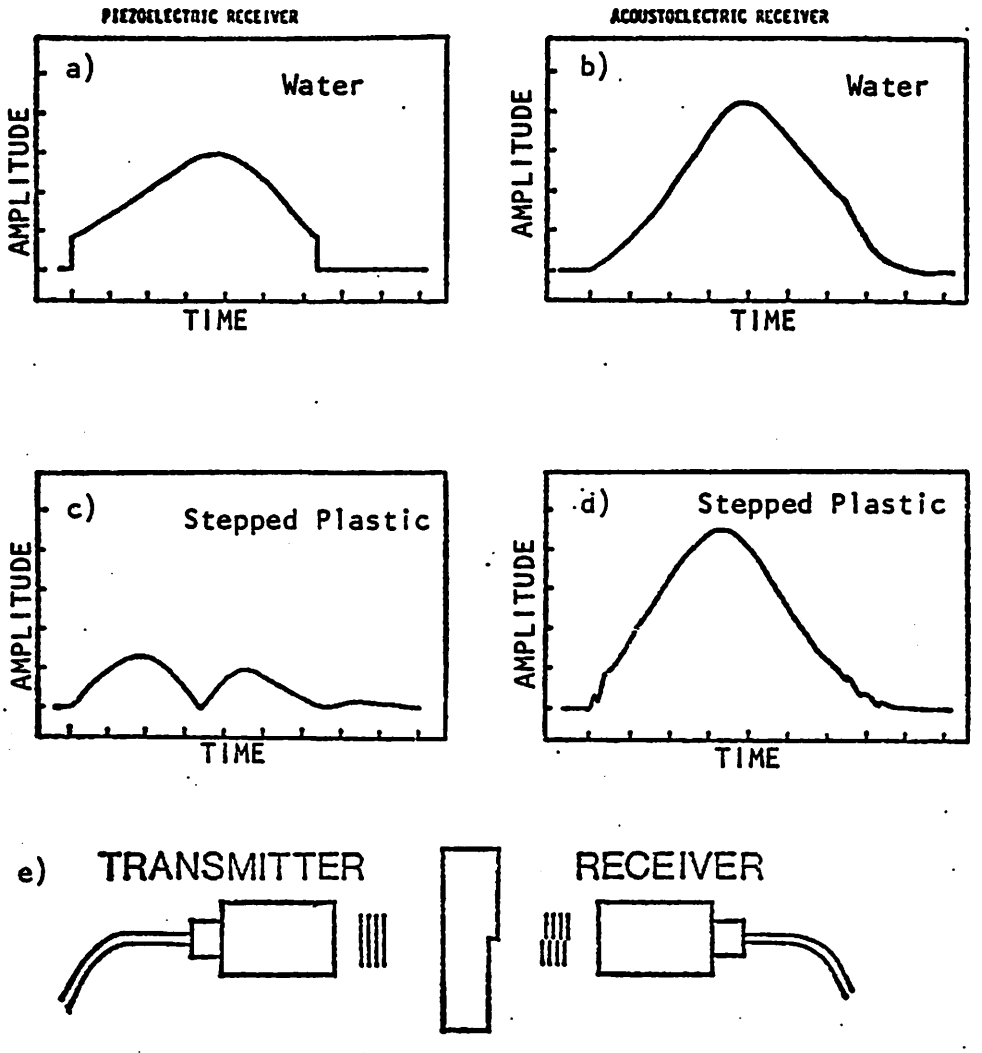

Figure VI.29. Detection of a chirped ("linear fm") ultrasonic pulse by broadband piezoelectric and acoustoelectric receiving transducers. Panels a) and b) show the response of the piezoelectric and acoustoelectric receivers to a chirped pulse transmitted through water. Panels c) and d) show the response of these transducers when the chirped pulse is transmitted through a stepped plastic plate shown in panel e). We note the phase insensitive response of the acoustoelectric receiver. (Ultrasonic pulse length = 128μsec, sweep from 2 to 10 MHz, horizontal scale = 20μsec/div, vertical scale = 0.1 v/div [panels a) and c)], 1 v/div [panel b)], 0.2 v/div [panel d)].

At this time (i.e., frequency) no output is generated by the piezoelectric receiver because of interference over the receiver aperture (phase cancellation). Panel d) shows the response of the acoustoelectric receiver when it is used to measure the same chirped pulse. No phase cancellation takes place. Instead, the center frequency of the pulse is shifted slightly downward; i.e., it occurs at an earlier time. This result is consistent with the discussion presented in the previous section for materials such as plastic which exhibit a linear attenuation versus frequency characteristic.

The use of chirped ultrasonic pulses appears to offer an alternate way of obtaining amplitude versus frequency information while maintaining the freedom from phase cancellation achieved with the acoustoelectric receiving transducer.

2. Scattering Measurements

A series of scattering measurements were performed to illustrate the basic difference between phase sensitive and phase insensitive detection in a simple scattering geometry. The geometry chosen was discussed in detail in Chapter IV. There we considered a plane wave incident upon two cylindrical scatterers and calculated the scattered field distributions in a plane situated at right angles relative to the direction of the incident ultrasonic wave.

In this section, we compare the observed output of various size phase sensitive and phase insensitive receivers as a function receiver position in a plane located 20 cm from the center of the scattering cylinders. We also look at right angle scattering as a function of the angle of incidence of the plane wave radiation upon the scattering cylinders.

The scattering cylinders used in these experiments consisted of a pair of brass rods, 2.4 mm in diameter. This large rod size was chosen to provide sufficient scattered ultrasonic energy so that acoustoelectric measurements would be possible. The rod separation (from center to center) was chosen to be 7.9 mm. The rods were illuminated by 2 μsec burst of 5 MHz ultrasound from a transmitting transducer located at a distance of approximately 18 cm from the rods. The output of the acoustoelectric receiver labeled JRK-2 and of 2 different piezoelectric receivers was digitized and recorded using a Biomation 8100 transient recorder and an HP-9825A calculator. The angle of the scatterers relative to the incident plane wave and the position of the receiver apertures within the receiver plane were manipulated with this calculator through the use of stepper motors.

The experimental results to be presented were obtained by post-processing the recorded time domain waveforms. All of the piezoelectric waveforms (rf signals) were processed by rectifying and integrating the first 1.6 μsec of the received acoustic pulse. This time was chosen to avoid any multiple scattering events or energy reradiated by the rods as a result of mode conversion. These scattering processes were not considered in the analysis presented in Chapter IV and can be eliminated from the experimental results because they are observed at later times. The acoustoelectric signals which are video or low frequency signals were analyzed by peak detecting the signal within the first four microseconds of the acoustoelectric time domain record. This time window was chosen because the delay associated with the acoustic transit time through crystal JRK-2 is 4 microseconds. Complications arising from the time-delayed modes discussed above are not significant under these

conditions. Both piezoelectric and acoustoelectric results presented are normalized relative to the measured response of the respective receiver apertures to a normally incident plane wave.

In Figure VI.30 we present the results of the right angle scattering measurements as a function of angle between the incident plane wave and the scattering rods. All measurements were made with the receiver centered at $x = 0$ in the receiver plane (see Figure IV.8). A comparison of large (12.7 mm) and small (3.2 mm) diameter circular piezoelectric receivers is shown in panel a). We see that the relative output of the small diameter phase sensitive receiver is always larger than the output of the large diameter phase sensitive receiver. At angles of incidence such as 45°, the phase distribution of the pressure field over the area of the 3.2 mm diameter receiver is nearly uniform and therefore nearly unity output is observed. In contrast, the phase distribution over the area of the 12.7 mm diameter receiver is not uniform. The complex pressure field begins to oscillate near the edges of the receiver aperture and therefore a reduced output is observed. We also see that there are angles where nearly zero output is produced by either phase sensitive receiver aperture. As noted earlier, these zeroes are the result of antisymmetric pressure distribution over the receiver aperture and should not be interpreted as zero incident ultrasonic energy.

In panel b) of Figure VI.30 we compare the results obtained for the right angle scattering measurement when a large aperture piezoelectric and a large aperture acoustoelectric receivers are used.

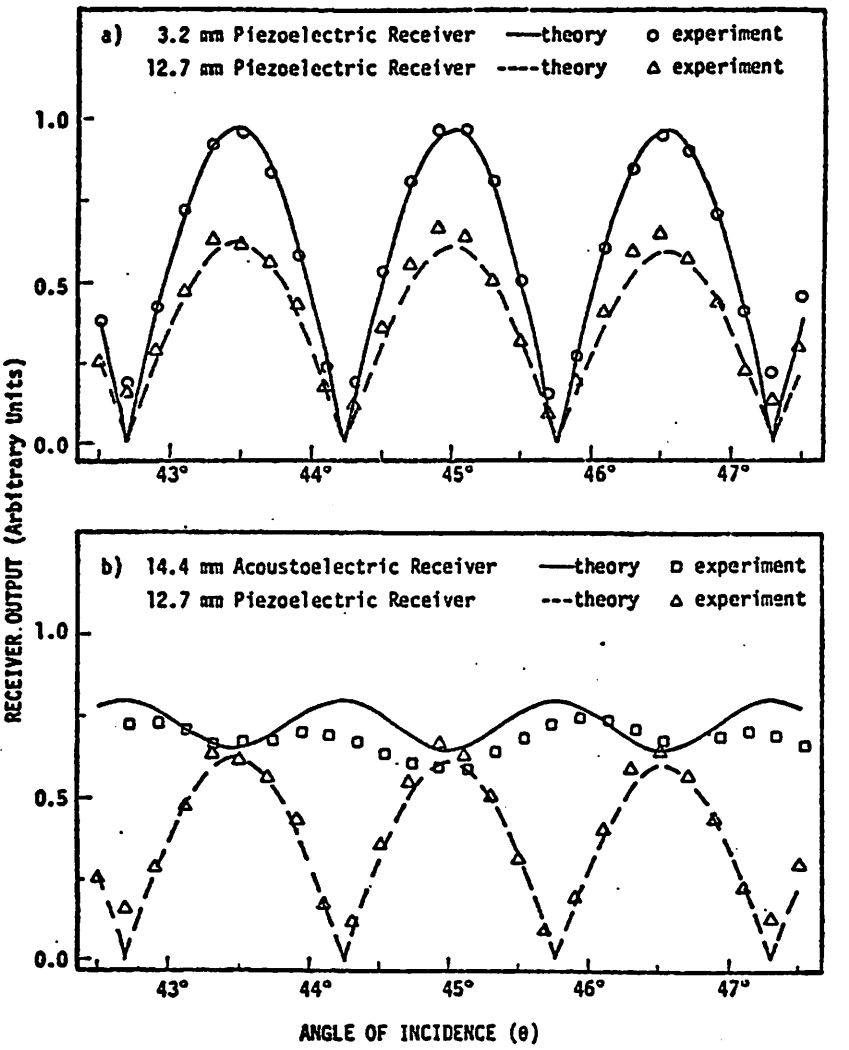

Figure VI.30. Results of right angle scattering experiment from cylindrical brass rods. Measurements were made at an ultrasonic frequency of 5 MHz and at a distance of 20 cm from the rods to the receiver. Results have been normalized relative to the result that would be observed for a plane wave incident upon the receiver. In panel a) we compare the results of measurement of scattered energy obtained using two different size phase sensitive (piezoelectric) receiver apertures. In panel b) we compare the results of measurement of scattered energy obtained using comparable size phase sensitive (piezoelectric) and phase insensitive (acoustoelectric) receiver apertures.

The acoustoelectric receiver used was crystal JRK-2. The active area of this receiver was 1.44 cm x 0.6 cm and the crystal was oriented with the long aperture dimension parallel to the x axis in the receiver plane. Measurements made with the phase insensitive receiver illustrated that the received acoustic energy is non-zero at all angles. This is in constrast with the results obtained with the comparable size piezoelectric receiver. (We note that for this geometry, the maxima in the output of the phase insensitive receiver is displaced in angle from the maxima in the phase sensitive receiver output. This displacement occurs because this phase insensitive receiver is approximately one and one-half fringe spacings wide. At angles such as 44.20, two interference fringe maxima are simultaneously within the receiver aperture and maximum output occurs. Under these conditions, however, the complex pressure field distribution is antisymmetric over the receiver aperture and zero output is produced by the phase sensitive receiver.)

Another series of scattering measurements were made by fixing the angle of incidence of the incoming plane wave upon the scattering rods at 45° and scanning the various receiver elements in the x direction in the receiver plane. The complex field pattern produced by the scattering rods should be similar to the field patterns shown in Figure IV.9. In panel a) of Figure VI.31 we show the normalized output as measured using a small aperture and large aperture phase sensitive receiver. We note that the output of either of these receivers is quickly diminished as it is displaced from $x = 0$ in the receiver plane. Rapid fluctuations in the phase of the complex pressure field causes cancellation of electrical signal over the receiver

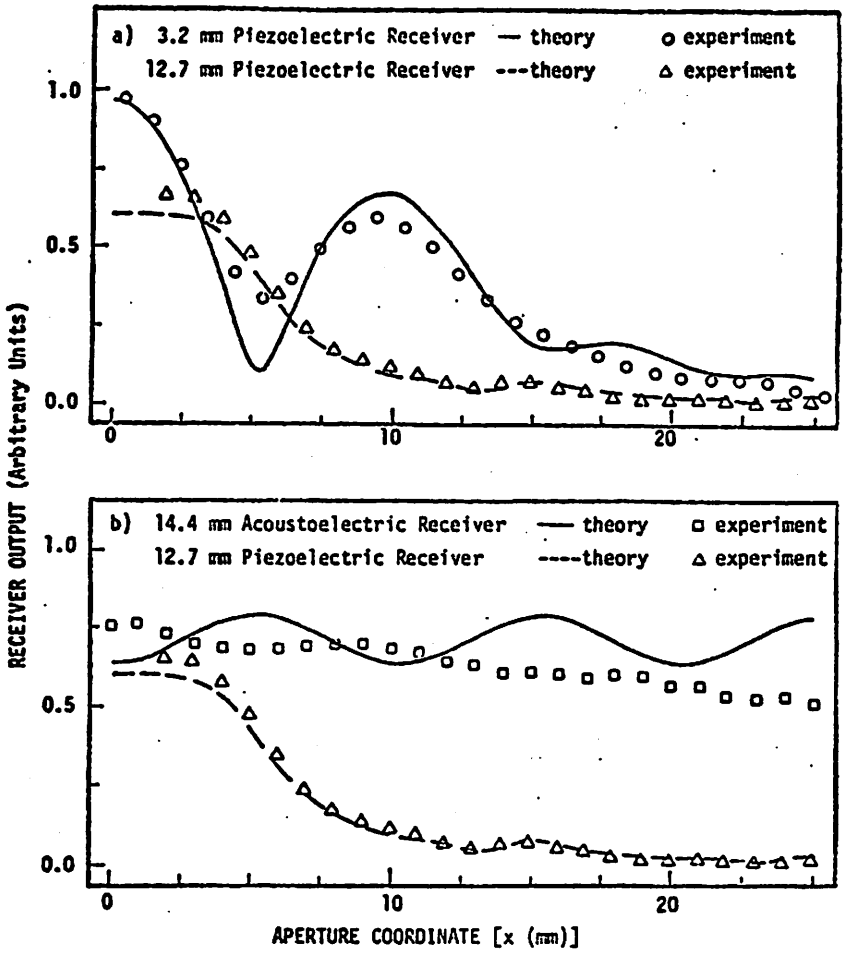

Figure VI.31. Results of measuring scattered energy as a function of position of receiver aperture. The receiver was located at Z = 20 cm from the scatterers. Measurements were made at an ultrasonic frequency of 5 MHz. The scattering rods were located in a plane oriented 45° with respect to the incident plane wave illumination. In panel a) we compare the results of measurement of scattered energy obtained using two different size phase sensitive (piezoelectric) receiver apertures. In panel b) we compare the results of measurement of scattered energy obtained using comparable size phase sensitive (piezoelectric) and phase insensitive (acoustoelectric) receiver apertures.

aperture as these phase sensitive receivers are displaced. In panel b) of Figure VI.31 we compare the output of a large aperture piezoelectric and acoustoelectric receiver as they are displaced in the x dimension of the receiver plane. We see that the output of the phase insensitive receiver remains nearly constant as it is displaced. A comparable size phase sensitive receiver output falls off quite rapidly for displacement greater than approximately 8 mm. The acoustoelectric receiver output shows that a finite amount of acoustic energy is incident upon it even when it is displaced by 20 mm in the receiver plane. In contrast the piezoelectric receiver output has fallen to nearly zero.

It should be noted that the predicted curves were calculated assuming infinitesimally thin strip sources rather than rods of finite width. We feel justified in taking this approach based upon the work of Wiener[89] and Faran.[90] They showed that the angular distribution of the acoustic radiation scattered from a rigid or nearly rigid brass rod under conditions similar to those presented here (i.e., $ka = 5$) was relatively uniform for angles in the 80° and 90° range. Therefore the uniform radiation pattern produced by an infinitesimal line source should be adequate for our particular geometry. The lack of detailed agreement between the measured and predicted signals can be attributed to our incomplete modeling of the scattering event. The general features of the experimental results are found to agree with the general features predicted. We see that the acoustoelectric and piezoelectric receiver measure fundamentally different properties of the scattered radiation field.

3. Tomographic Imaging

The application of an acoustoelectric receiver to the problem of making images based upon ultrasonic attenuation has also been investigated. The particular imaging system investigated was based upon transmission tomography and was implemented using computer reconstruction techniques.[91,92] A tomographic imaging system produces a cross sectional image through an object of any physical parameter which can be measured as a series of line integrals through the object. Greenleaf, et al.[93] demonstrated that the ultrasonic attenuation coefficient of an object is amenable to imaging in a tomographic system.

Reconstructions based upon ultrasonic attenuation are made from a series of measurements of the total signal loss suffered by an acoustic pulse as it travels from transmitter to receiver. As the transmitter and receiver are simultaneously scanned past an object of interest, a projection line of the ultrasonic signal loss is formed. The object (or equivalently the transmitter and receiver) is then rotated and a new view or projection line is then measured. The set of projection lines formed in this way are then filtered and back-projected to form of two dimensional spatial map of the ultrasonic attenuation coefficient within the plane scanned. The success of this type of imaging system therefore depends upon the accurate determination of the ultrasonic signal loss at each point on the projection line.

Because objects to be imaged cannot present flat and parallel surfaces at all angles of view and may, in addition, include some inhomogeneities, some distortion of the ultrasonic beam by the object of interest is inevitable. As we showed in Section C.1a, these

distortions can lead to errors in the determination of the attenuation coefficient if a phase sensitive receiving transducer is used. Errors caused by phase cancellation over the receiver aperture can be eliminated by using a phase insensitive receiving transducer based upon the acoustoelectric effect.

To demonstrate the effects of phase cancellation in an attenuation tomography system, a series of measurements and reconstructions were performed on test objects. A cylindrical specimen of castor oil in a 2 cm diameter finger cot immersed in a water bath was selected as one test object to illustrate the effects of phase cancellation. Because the speed of sound in castor oil is one percent higher than the speed of sound in water some distortion of the ultrasonic wavfronts takes place as the beam is scanned past the object. This effect is most pronounced near the edges of the object where the beam travels partially through the object of interest and partially through water.

In panel a) of Figure VI.32 we show a set of projection lines measured using a 12 mm diameter piezoelectric and a 12 mm diameter acoustoelectric receiver. The projection line consists of the apparent attenuation or total signal loss as a function of distance along the scan line. The projection line measured using the acoustoelectric receiver varies smoothly with distance along the scan line while the projection line measured with the piezoelectric receiver exhibits sharp "ears" near the edges of the attenuating object. At the edges of the object the variability in the ultrasonic pathlength over the spatial extent of the beam leads to wavefront distortion. As a result distortion and the subsequent phase cancellation at the receiver, the

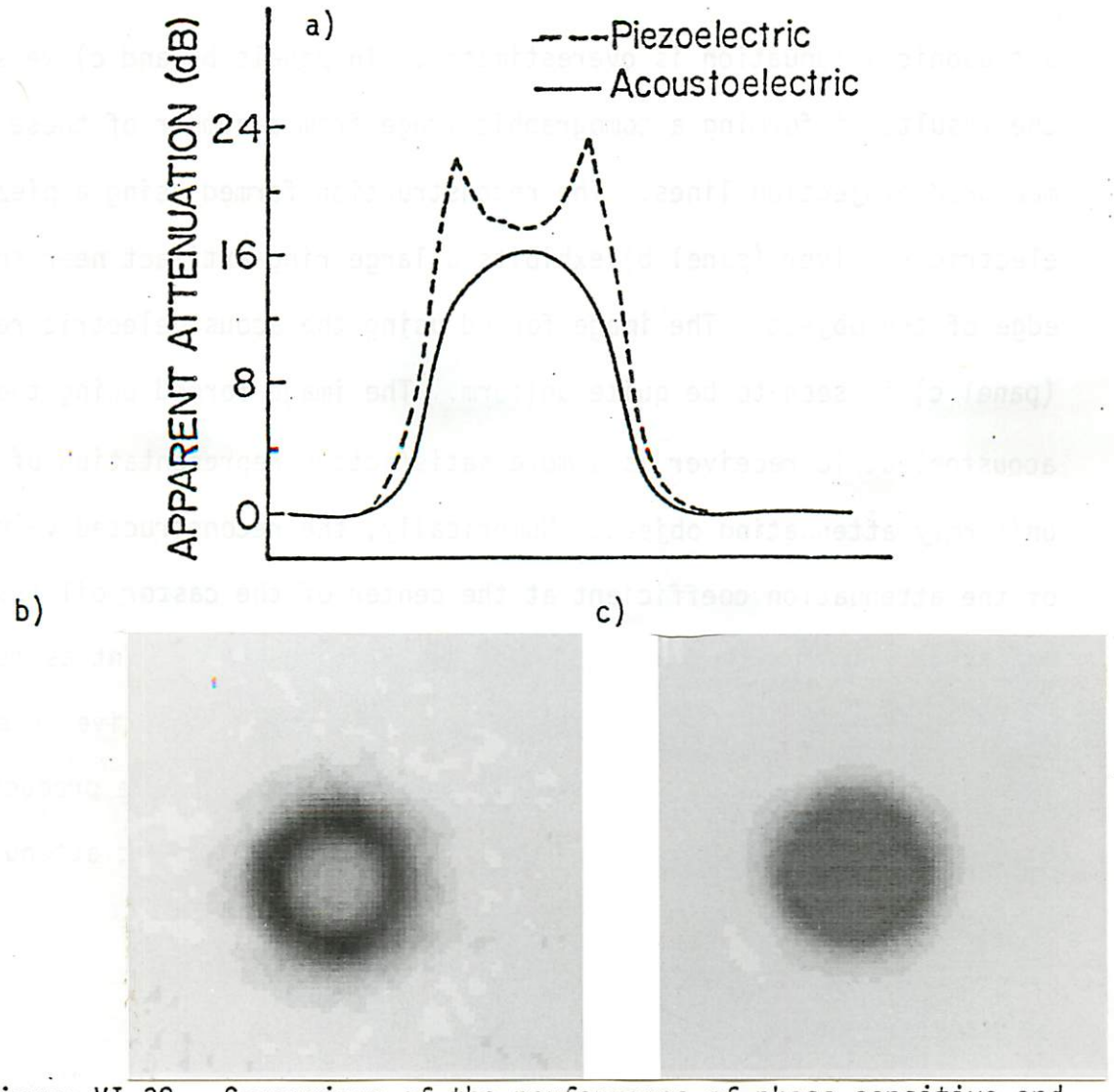

Figure VI.32. Comparison of the performance of phase sensitive and phase insensitive receiver apertures in the context of reconstructive tomography based on ultrasonic attenuation. Measurements were made upon a cylindrical test object consisting of a castor oil-filled finger cot. In panel a) we show a single projection line through the test object. Tomographic reconstruction made with piezoelectric measurements is shown in panel b) and reconstruction made with acoustoelectric measurements is shown in panel c). The value of the reconstructed attenuation coefficient obtained in panel c) is within 5% of the accepted value.

ultrasonic attenuation is overestimated. In panels b) and c) we show the results of forming a tomographic image from a number of these measured projection lines. The reconstruction formed using a piezoelectric receiver (panel b) exhibits a large ring artifact near the edge of the object. The image formed using the acoustoelectric receiver (panel c) is seen to be quite uniform. The image formed using the acoustoelectric receiver is a more satisfactory representation of a uniformly attenuating object. Numerically, the reconstructed value of the attenuation coefficient at the center of the castor oil test object is within five percent of the attenuation coefficient as measured by independent means. The application of a phase insensitive receiving transducer to a tomographic imaging system appears to have produced the first quantitatively accurate images based upon ultrasonic attenuation.[27]

VII. SUMMARY

The study and application of electron-phonon coupling in the piezoelectric semiconductor cadmium sulfide has made possible the realization of large aperture, phase insensitive ultrasonic detectors. We have demonstrated that a phase insensitive or noncoherent ultrasonic receiving transducer is capable of being used in a variety of ultrasonic systems to provide quantitative, reliable information about the physical properties of irregular and inhomogeneous material. Comparisons of measurements made with phase sensitive and phase insensitive receivers illustrated the susceptibility to error of the former when quantitative determinations of ultrasonic amplitude are attempted in the presence of wavefront distortion.

Many features associated with the operation of receiving transducers based upon the acoustoelectric effect were detailed in this work. We documented that the acoustoelectric voltage response of thick ($\sim$1 cm) CdS specimens to short bursts of ultrasound is nearly independent of frequency (varies by less than 1 dB) in the 2.5 to 9 MHz frequency range. The response time of thick CdS crystals to short ultrasonic bursts was shown to be good, i.e., on the order of the pulse transit time through the CdS specimen. Measurement of the ultimate sensitivity of the receiver when used to detect short acoustic pulses was determined to be on the order of 1×10^{-6} watts/cm^2 of instantaneous acoustic intensity. The resonant acoustoelectric voltage response of thin CdS specimens to long bursts of ultrasonic energy was documented. Unlike the piezoelectric response of a thin CdS plate, acoustoelectric voltage maxima were predicted

and observed for even as well as odd mechanical resonances. Substantial improvements in the responsivity of acoustoelectric receivers are available when this mode of operation is employed. This improvement in sensitivity, however, is gained at the expense of detector response time.

Using a variety of test objects to produce distorted or non-uniform ultrasonic wavefronts, we demonstrated that the acoustoelectric response of a thick CdS crystal is truly phase insensitive. This phase insensitive response has been applied to the problem of making quantitative determinations of the ultrasonic attenuation coefficient of inhomogeneous and irregular tissue specimens. The utility of a phase insensitive receiver aperture for making quantitative images of attenuation based upon reconstructive tomography was also demonstrated.

In conclusion, we observe that for a variety of reasons the acoustoelectric effect may not provide the ultimate noncoherent ultrasonic receiver. Future developments of miniature element piezoelectric arrays, for example, may lead to a different means for realizing a large aperture phase insensitive ultrasonic receiver. At present, however, the acoustoelectric receiver does provide a valuable means for illustrating the advantages of a noncoherent detection scheme when measurements must be made in the presence of wave distortion. In this sense, the acoustoelectric receiver represents a standard against which future noncoherent ultrasonic detection methods can be judged.

APPENDIX A

WAVE PROPAGATION IN PIEZOELECTRIC SEMICONDUCTOR

The following is a derivation after Kyame[35] and Hutson and White[37] which illustrates a general treatment of wave propagation in a piezoelectric material. Because of our interest in the hexagonal material, cadmium sulfide, we limit this treatment to plane wave propagation in the Z or x_3 direction. The other orthogonal crystalline axis are specified by x_1 and x_2. Standard tensor notation are used to define the strain S'_{ik} in terms of the particle displacement ξ_k:

$$S'_{ik} = S_{ik} + S_{ki} = \frac{\partial \xi_k}{\partial x_i} \tag{A.1}$$

where

$$S_{ik} = \frac{1}{2}\left(\frac{\partial \xi_i}{\partial x_k} + \frac{\partial \xi_k}{\partial x_i}\right) .$$

Because we are confining ourselves to plane wave propagation in the x_3 direction, partial derivatives with respect to the spatial variables x_1 and x_2 are zero. Under these conditions the piezoelectric constitutive relations reduce to

$$T_{3i} = c^E_{3i3k}\, S'_{3k} + e_{k3i}\, E_k \tag{A.2}$$

$$D_k = -e_{k3i}\, S'_{3i} + \varepsilon_{ik}\, E_i \tag{A.3}$$

where $c^E_{ijk\ell}$ is the elastic stiffness tensor at constant electric field e_{ijk} is the piezoelectric tensor and ε_{ik} is the permittivity matrix.

The electromagnetic constitutive relations are

$$B_i = \mu_o H_i \qquad \text{and} \qquad J_i = \sigma_{ik} E_k \tag{A.4}$$

where we have assumed isotropic magnetic permeability μ_o and have allowed for anisotropic electrical conductivity.

In order to describe the propagation of an acoustic wave in a piezoelectric material, electromagnetic field parameters must satisfy Maxwell's equations

$$\nabla \times \vec{H} = \frac{\partial \vec{D}}{\partial t} + \vec{J} \qquad \nabla \times \vec{E} = - \frac{\partial \vec{B}}{\partial t}$$

$$\nabla \cdot \vec{B} = 0 \qquad \nabla \cdot \vec{D} = - qn \tag{A.5}$$

and the mechanical field parameters must satisfy Newton's Law

$$\frac{\partial T_{3i}}{\partial x_3} = \rho \frac{d^2 \xi_i}{dt^2} \quad , \quad i = 1,2,3 \quad . \tag{A.6}$$

In the above equations q is the electronic charge and n represents the departure from equilibrium in the number density of electrons.

From the plane wave condition we find that $(\nabla \times \vec{H})_3 = 0$ and $(\nabla \cdot \vec{D})_3 = -qn$ lead us to the continuity equation.

$$q \frac{\partial n}{\partial t} = (\nabla \cdot \vec{J})_3 \quad . \tag{A.7}$$

From the curl E and curl H equations we find that

$$\frac{\partial^2}{\partial x_3^2} E_q = \mu \frac{\partial}{\partial t} \left[\frac{\partial}{\partial t} D_q + J_q \right] \qquad q = 1,2 \quad . \tag{A.8}$$

Differentiation of Eq. (A.3) with respect to time and substitution of Eqs. (A.4) and (A.8) allows us to write

$$\frac{\partial^2}{\partial x_3^2} E_q = \mu \frac{\partial}{\partial t}\left[e_{q3i} \frac{\partial^2 \xi_i}{\partial t\, x_3} + \varepsilon_{iq} \frac{\partial}{\partial t} E_i + \sigma_{iq} E_i\right] \quad \begin{matrix} i = 1,2,3 \\ q = 1,2 \end{matrix} \quad . \quad (A.9)$$

Differentiation of Eq. (A-2) with respect to x_3 and substitution into Eq. (A-6) allows us to write

$$\frac{\partial}{\partial x_3} T_{3i} = \rho \frac{\partial^2 \xi_i}{\partial t^2} = c_{3i3k} \frac{\partial^2 \xi_k}{\partial x_3^2} - e_{k3i} \frac{\partial E_k}{\partial x_3} \quad c,ik = 1,2,3 \quad . \quad (A.10)$$

Equation (A.9) represents two coupled wave equations and Eq. (A.10) represents three coupled wave equations describing the propagation of elastic particle displacements ξ_i and electric field E_i down the x_3 axis of the crystal. The solution of these five coupled wave equations will produce five different phase velocities which can be given the following interpretation: three of the phase velocities represent elastic modes of propagation (under appropriate conditions of symmetry, two shear polarizations and one longitudinal polarization) and two of the phase velocities represent the electromagnetic modes of propagation (two transverse polarizations).

A solution to these five equations can be found by assuming that

$$\xi_i = \xi_i^o e^{i(kx_3 - \omega t)} \quad \text{and} \quad E_i = E_i^o e^{i(kx_3 - \omega t)} \quad . \quad (A.11)$$

With these assumed solutions, $(\nabla \times H)_3 = 0$ and Eq. (A.3) we can solved explicitly for E_3,

$$E_3 = +\frac{ie_{33i}\,k}{\left(\varepsilon_{33} + \frac{i\sigma_{33}}{\omega}\right)}\,\xi_i - \frac{\left(\varepsilon_{q3} + \frac{i\sigma_{q3}}{\omega}\right)}{\left(\varepsilon_{33} + \frac{i\sigma_{33}}{\omega}\right)}\,E_q\,, \qquad q = 1,2 \quad . \quad (A.12)$$

Expansion of Eqs. (A.9) and (A.10) and substitution of Eq. (A.12) allows us to write

$$-i\frac{k^2}{\omega^2}\,E_q = \mu k\, e'_{q3i}\,\dot{\xi}_i - i\mu\,\varepsilon'_{pq}\,E_p\,, \quad i = 1,2,3;\ q,p = 1,2\,, \quad (A.13)$$

$$\omega^2\rho\xi_i = k^2\, c'_{3i3k}\,\xi_k + ik\, e'_{q3i}\,E_q\,, \quad i,k = 1,2,3,\ q = 1,2 \quad (A.14)$$

where the coupling constants have been modified as follows

$$C'_{3i3k} = C_{3i3k} + \frac{e_{33i}e_{33k}}{\varepsilon_{33} + i\,\frac{\sigma_{33}}{\omega}} \quad (A.15)$$

$$e'_{q3i} = e_{q3i} + e_{33i}\left\{\frac{\varepsilon_{q3} + i\,\sigma_{q3}/\omega}{\varepsilon_{33} + i\sigma_{33}/\omega}\right\} \quad (A.16)$$

$$\varepsilon'_{pq} = \left(\varepsilon_{pq} + \frac{i\sigma_{pq}}{\omega}\right) - \frac{(\varepsilon_{p3} + i\sigma_{p3}/\omega)(\varepsilon_{3q} + i\sigma_{3q}/\omega)}{(\varepsilon_{33} + i\sigma_{33}/\omega)} \quad . \quad (A.17)$$

From this set of equations we can see that the effect of piezoelectricity is to stiffen the effective elastic constants of the material.

A solution to the five coupled wave equations represented by Eqs. (A.13) and (A.14) must exist if the determinant of these coefficients

vanishes

$$\begin{vmatrix} \left(\frac{c'_{3131}}{\rho} - \frac{\omega^2}{k^2}\right) & \frac{c'_{3131}}{\rho} & \frac{c'_{3133}}{\rho} & \frac{\omega}{k} v'_{131} & \frac{\omega}{k} v'_{231} \\ \frac{c'_{3231}}{\rho} & \left(\frac{c'_{3232}}{\rho} - \frac{\omega^2}{k^2}\right) & \frac{c'_{3232}}{\rho} & \frac{\omega}{k} v'_{132} & \frac{\omega}{k} v'_{232} \\ \frac{c'_{3331}}{\rho} & \frac{c'_{3332}}{\rho} & \left(\frac{c'_{3333}}{\rho} - \frac{\omega^2}{k^2}\right) & \frac{\omega}{k} v'_{133} & \frac{\omega}{k} v'_{233} \\ \frac{\omega}{k} v'_{131} & \frac{\omega}{k} v'_{132} & \frac{\omega}{k} v'_{133} & \left(\frac{1}{\mu\varepsilon} - \frac{\omega^2}{k^2}\frac{\varepsilon_{11}}{\varepsilon}\right) & -\frac{\omega^2}{k^2}\frac{\varepsilon_{21}}{\varepsilon} \\ \frac{\omega}{k} v'_{231} & \frac{\omega}{k} v'_{232} & \frac{\omega}{k} v'_{233} & -\frac{\omega^2}{k^2}\frac{\varepsilon_{12}}{\varepsilon} & \left(\frac{1}{\mu\varepsilon} - \frac{\omega^2}{k^2}\frac{\varepsilon_{22}}{\varepsilon}\right) \end{vmatrix} \tag{A.18}$$

In order to form this secular determinant we have made use of the average dielectric constant of the material ε and have defined a new quantity with units of velocity

$$v'_{ijk} = \frac{e'_{ijk}}{\sqrt{\varepsilon\rho}} \quad .$$

At this point, we note that if the medium were not piezoelectric, i.e., if e'_{ijk}'s $\to 0$, then all of the v'_{ijk}'s would go to zero and the secular determinant would separate into a three by three secular determinant describing the acoustic properties and a 2 x 2 secular determinant describing the electromagnetic properties.

In the presence of piezoelectricity (e'_{ijk}'s $\neq 0$) we ask how large an error is made by ignoring the effect of the v'_{ijk}'s on our final phase velocities and decomposing the 5 x 5 determinant into two determinants, a 3 x 3 and a 2 x 2. In other words, how bad an approximation is it to say

that the only effect of piezoelectricity is to modify the elastic stiffness tensor. We can estimate the magnitude of the error this approximation causes by supposing that we have "solved" the 3 x 3 acoustic determinant for the phase velocity of the three elastic modes ($\omega/k = v_1, v_2, v_3$); i.e., that these velocities are the eigenvalues of the 3 x 3 acoustic problem. Presumably the velocity v_3 differs by some small amount from the velocity which would be the eigenvalue of the 5 x 5 problems. If we allow $c = 1/\sqrt{\mu\varepsilon}$ to be the average velocity of light in the medium then we can estimate the order of magnitude of the correction δ^2 to the velocity v_3^2. The secular determinant (A.18) can be written as

$$\begin{vmatrix} (v_1^2 - v_3^2 + \delta^2) & 0 & 0 & v'v_3 & v'v_3 \\ 0 & (v_2^2 - v_3^2 + \delta^2) & 0 & v'v_3 & v'v_3 \\ 0 & 0 & \delta^2 & v'v_3 & v'v_3 \\ v'v_3 & v'v_3 & v'v_3 & (c^2 - v_3^2) & -v_3^2 \\ v'v_3 & v'v_3 & v'v_3 & -v_3^2 & (c^2 - v_3^2) \end{vmatrix} = 0 \quad . \quad \text{(A.19)}$$

Expanding Eq. (A.19) we find that,

$$(v_1^2 - v_3^2 + \delta^2)\left[(v_2^2 - v_3^2 + \delta^2)(\delta^2 c^4 + \text{lower order term in } c)\right]$$
$$+ 2v'v_3\left[(v_2^2 - v_3^2 + \delta^2)c^2 + \text{lower order term in } c\right] = 0 \quad .$$

Therefore

$$\delta^2 \approx 2\left(\frac{v_3}{c}\right)^2 v'^2 \quad .$$

To summarize, the fact that the material is piezoelectric can be handled by modifying the elastic constants of the material. This modification introduces a correction term into the solution for ω^2/k^2 which is of order v'^2. The fact that the mechanical disturbance is accompanied by an electromagnetic wave introduces further correction terms which are of order $[v_3^2/c^2]v'^2$ or smaller. Thus, we are certainly justified in ignoring these electromagnetic corrections to the complex acoustic wave velocity. This simplification allows us to decouple the wave propagation problem and describe the acoustic wave propagation with a single 3 x 3 secular determinant.

Our acoustic problem is further simplified when we realize that we are propagating our acoustic wave along a six fold symmetry axis in CdS. Under these conditions, all three modes of propagation are pure modes and the shear modes are degenerate.[43,94] The 3 x 3 secular determinant now reduces to:

$$\begin{vmatrix} \left(\frac{c_{3232}}{\rho} - \frac{\omega^2}{k^2}\right) & 0 & 0 \\ 0 & \left(\frac{c_{3232}}{\rho} - \frac{\omega^2}{k^2}\right) & \\ 0 & 0 & \left(\frac{c'_{3333}}{\rho} - \frac{\omega^2}{k^2}\right) \end{vmatrix} = 0 \quad .$$

Note also that the prime has been omitted from c_{3232} because these modes are not piezoelectrically active. Because of the particularly simple form of secular determinant, the problem of longitudinal acoustic wave propagation along the "c" axis is cadmium sulfide can be described using a one dimensional analysis.

REFERENCES

1. I. S. Bowen, "Final Adjustment and Test of the Hale Telescope," Pub. A.S.P. 62, 91 (1950). Also see H. W. Babcock, "The Possibility of Compensating for Astronomical Seeing," Pub. A.S.P. 65, 229 (1953).

2. R. Hanbury Brown and R. Q. Twiss, "A New Type of Interferometer for Use in Radio Astronomy," Phil. Mag. 45, 663 (1954). Also see R. Hanbury Brown, R. C. Jennison and M. K. Das Gupta, "Apparent Angular Sizes of Discrete Radio Sources, Nature 170, 1061 (1952).

3. S. L. McCall, T. R. Brown, and A. Passner, "Improved Optical Stellar Imaging A Using Real-Time Phase-Correction System: Initial Results," The Astrophysical Journal 211, 463-467 (1977).

4. A. Labeyrie, "Attainment of Diffraction Limited Resolution in Large Telescopes by Fourier Analysing Speckle Patterns in Star Images," Astron. & Astrophys. 6, 85-87 (1970).

5. L. N. Mertz, "Speckle Imaging, Photon by Photon," Applied Optics 18, 611-614 (1979).

6. H. Seki, A. Granato, and R. Truell, "Diffraction Effects in the Ultrasonic Field of a Piston Source and Their Importance in the Accurate Measurement of Attenuation," J. Acoust. Soc. Am 28, 230-238 (1956).

7. R. Truell and W. Oates, "Effect of Lack of Parallelism of Sample Faces on the Measurement of Ultrasonic Attenuation," J. Acoust. Soc. Am. 35, 1382-1386 (1963).

8. R. Truell, C. Elbaum and B. B. Chick, Ultrasonic Methods in Solid State Physics (Academic Press, New York, 1969), pp. 89-120

9. E. P. Papadakis, "Ultrasonic Diffraction from Single Apertures with Application to Pulse Measurements and Crystal Physics," Physical Acoustics, Vol. XI, Chapter 3, Warren P. Mason, ed., (Academic Press, New York, 1975)

10. Acoustical Holography, Vols. 1-8, (Plenum Press, New York, 1969).

11. E. P. Papadakis, "Ultrasonic Velocity and Attenuation: Measurement Methods with Scientific and Industrial Applications," Physical Acoustics, Vol. XII, W. P. Mason, ed., (Academic Press, New York, 1976).

12. R. H. Parmenter, "The Acousto-Electric Effect," Phys. Rev. 89, 990-998 (1953).

13. G. Weinreich, T. M. Sanders, Jr., and Harry G. White, "Acousto-electric Effect in n-Type Germanium," Phys. Rev. 114, 33-44 (1959).

14. A. R. Hutson, J. H. McFee, and D. C. White, "Ultrasonic Amplification in CdS," Phys. Rev. Letters 7, 237 (1961).

15. D. L. White, "Amplification of Ultrasonic Waves in Piezoelectric Semiconductors," J. Appl. Phys. 33, 2547 (1962).

16. A. R. Moore, R. W. Smith, P. Worcester, "Amplification of Non-Pure Transverse or Longitudinal Waves in CdS," IBM J. Res. Devel. 13, 503 (1969).

AE
17. R. K. Route and G. S. Kino, "Acoustoelectric Amplification in InSb," IBM J. Res. Devel. 13, 507-9 (1969).

18. K. Blotekjaer and C. F. Quate, "The Coupled Modes of Acoustic Waves and Drifting Carriers in Piezoelectric Crystals," Proceedings of the IEEE 52, 360-377 (1964).

19. V. E. Henrich and G. Weinreich, "Pulsed Ultrasonic Studies of the Acoustoelectric Effect, Ultrasonic Attenuation, and Trapping in CdS," Phy. Rev. 178, 1204-1217 (1969).

20. H. D. Nine and R. Truell, "Photosensitive-Ultrasonic Properties of Cadmium Sulfide," Phys. Rev. 123, 799-803 (1967).

21. R. K. Lomnes and F. L. Weichman, "Use of Ultrasonic Attenuation to Study Photoconduction and Optical Properties of CdS," J. Appl. Phys. 43, 590 (1972).

22. J. H. Gibson, "Self-Interaction of Acoustic Waves in Cadmium Sulfide," Ph.D. Thesis, University of Michigan, 1968.

(2) AE
23 P. D. Southgate, "Use of a Power-Sensitive Detector in Pulse-Attenuation Measurements," J. Acoust. Soc. Am. 39, 480-483 (1966).

(3)
24. J. G. Miller, J. S. Heyman, D. E. Yuhas, A. N. Weiss, "A Power Sensitive Transducer for Echocardiography and Other Medical Applications," in Ultrasound in Medicine, Vol. 1, New York, Plenum Press, 1975, pp. 355-404.

25. P. N. Marcus, E. L. Carstensen, "Problems with Absorption Methods of Inhomogeneous Solids," J. Acoust. Soc. Am. 58, 1334-1335 (1975).

26. L. J. Busse, J. G. Miller, D. E. Yuhas, J. W. Mimbs, A. N. Weiss and B. E. Sobel, "Phase Cancellation Effects: A Source of Attenuation Artifact Eliminated by a CdS Acoustoelectric Receiver," in Ultrasound in Medicine, Vol. 3, D. White, ed. (Plenum, New York, 1977), pp. 1519-1535.

(6)

27. J. R. Klepper, G. H. Brandenburger, L. J. Busse, and J. G. Miller, "Phase Cancellation, Reflection, and Refraction Effects in Quantitative Ultrasonic Attenuation Tomography," 1977 Ultrasonics Symposium Proceedings, IEEE Cat. #77CH1264-1SU, pp. 182-188.

28. J. S. Heyman and J. H. Cantrell, "Application of an Ultrasonic Phase Insensitive Receiver to Materials Measurements," 1977 Ultrasonic Symposium Proceedings, IEEE Cat. #77CH1264-1SU, pp. 124-128.

29. J. S. Heyman, "Phase Insensitive Acoustoelectric Transducer," J. Acoust. Soc. Am. 64, 243 (1978).

30. G. Weinreich, "Ultrasonic Attenuation by Free Carriers in Germanium," Phys. Rev. 107, 317 (1957).

31. H. Gohecht and A. Bartschat, "Uber den Einfluss des Aktivators und der Speiherung von Strahlunepenergie auf das piezo-elektrische und elastische verhalten von Cadmiumsulfid-Einkristallen Z. Physik 153, 529 (1959).

32. A. R. Hutson, "Piezoelectricity and Conductivity in ZnO and CdS," Phys. Rev. Letters 4, 505 (1960).

33. Wen-Chung Wang, "Strong Acoustoelectric Effect in CdS," Phys. Rev. Letters 9, 443-445 (1962).

34. R. Frerichs, "The Photoconductivity of 'Incomplete Phosphors'," Phys. Rev. 72, 594 (1947).

35. D. R. Boyd and Y. T. Sihvonen, "Vaporization-Crystalization Method for Growing CdS single Crystals," J. App. Phys. 30, 176 (1959).

36. J. J. Kyame, "Conductivity and Viscosity Effects on Wave Propagation in Piezoelectric Crystals," J. Acoust. Soc. Am. 26, 990-993 (1954).

37. A. R. Hutson and D. L. White, "Elastic Wave Propagation in Piezoelectric Semiconductors," J. Appl. Phys. 33, 40 (1962).

38. C. Fischler and S. Yando, "Amplification of Acoustic Waves in Coupled Semiconductor-Piezoelectric System," Appl. Phys. Letters 13, 351-53 (1968).

39. C. Fischler, "Acoustoelectric Amplification in Composite Piezo-electric and Semiconducting Structures," IEEE Trans. Electron Devices ED-17, 214-218 (1970).

40. Y. V. Gulyaev and A. Y. Karabanov, "Amplification of Ultrasonic Waves in a Layered Structure Consisting of a Piezoelectric Dielectric and Semiconductor," Soviet Phys. Semiconductors 1, 626 (1967).

41. L. A. Coldren and G. S. Kino, "Monolithic Surface-Wave Acoustic Amplifier," Appl. Phys. Letters. 18, 317-319 (1971).

42. J. B. Moore, "A Convergent Algorithm for Solving Polynomial Equations," Journal of the Association of Computing Machinery 14, 311-315 (1967).

43. D. A. Berlincourt, D. R. Curran, and H. Jaffe, "Piezoelectric and Piezomagnetic Materials and Their Function in Transducers," Physical Acoustics, Vol. 1A, Chapter 3, W. P. Mason, ed. (Academic Press, New York, 1964).

44. R. T. Beyer and S. V. Letcher, Physical Ultrasonics (Academic Press, New York, 1969), pp. 50-59.

45. M. Redwood, "Transient Performance of a Piezoelectric Transducer," J. Acoust. Soc. Am. 33, 527-536 (1961).

46. D. I. Bolef and J. G. Miller, "High-Frequency Continuous Wave Ultrasonics," Physical Acoustics, Vol. 8, Chapter 3, W. P. Mason, ed. (Academic Press, New York, 1961).

47. K. N. Baranskii, "The Excitation of Hypersonic Frequencies in Quartz," Doklady Akad. Nauk S.S.S.R. 114, 517 (1957) [translation: Soviet Phys. Doklady 24, 237 (1958)].

48. E. H. Jacobsen, "Sources of Sound in Piezoelectric Crystals," J. Acoust. Soc. Am. 32, 949 (1960).

49. H. E. Bommel and K. Dransfeld, "Excitation and Attenuation of Hypersonic Waves in Quartz," Phys. Rev. 119, 1245 (1960).

50. W. P. Mason, "Electromechanical Transducers and Wave Filters," 2nd ed., D. Van Nostrand, Princeton, N.J., (1948).

51. A. Rose, "Performance of Photoconductors," Proc. of the IRE 43, 1850-1869 (1955).

52. C. I. Shulman, "Measurement of Shot Noise in CdS," Phys. Rev. 98, 384 (1955).

53. K. M. Van Vleit, J. Blok, C. Ris, and J. Steketec, "Measurements of Noise and Response to Modulated Light of Cadmium Sulfide Single Crystal," Physica 22, 723-740 (1956).

54. E. P. Papadakis, "Correction for Diffraction Losses in the Ultrasonic Field of a Piston Source," J. Acoust. Soc. Am. 31, 150-152 (1959).

55. H. J. McSkimin, "Empirical Study of the Effect of Diffraction on Velocity of Propagation of High Frequency Ultrasonic Waves," J. Acoust. Soc. Am. 32, 1401-1404 (1960).

56. E. P. Papadakis, "Diffraction of Ultrasound in Elastically Anisotropic NaCl and in some Other Materials," J. Acoust. Soc. Am. 35, 490-495 (1963).

57. E. P. Papadakis, "Diffraction of Ultrasound Radiating into an Elastically Anisotropic Medium," J. Acoust. Soc. Am. 36, 414-422 (1964).

58. A. E. Lord, "Geometric Diffraction Loss in Longitudinal and Shear-Wave Attenuation Measurements in an Isotropic Half Space," J. Acous. Soc. Am. 39, 650 (1966).

59. E. P. Papadakis, "Ultrasonic Diffraction Loss and Phase Change in Anisotropic Materials," J. Acous. Soc. Cem. 40, 863-876 (1966).

60. G. C. Benson and O. Kiyohara, "Tabulation of Some Integral Functions Describing Diffraction Effects in the Ultrasonic Field of a Circular Piston Source," J. Acoust. Soc. Am. 58, 184 (1974).

61. Lord Rayleigh, "The Theory of Sound," 2nd Ed. Vol. 2, (Dover, New York, 1945).

62. I. S. Gradshteyn and I. M. Ryzhik, "Table of Integral, Series and Products," Fourth ed., p. 957 (Academic, New York, 1965).

63. Eagle Picher Electronics Division, Miami, Oklahoma 74354.

64. W. L. Bragg, "Structure of Some Crystals as Indicated by Their Diffraction of X-Rays," Proc. Roy. Soc. (London) A89, 248 (1913).

65. W. M. Buttler and W. Muscheid, "Die Bedeutung des elektrischen Kontaktes bei Untersuchungen an Kadmiumsulfid-Einkristallen I," Ann. Phys. 14, 215 (1954).

66. W. M. Buttler and W. Muscheid, "Die Bedeutung des elektrischen Kontaktes bei Untersuchungen an Kadmiumsulfid-Einkristallen II," Ann. Phys. 15, 82 (1954).

67. R. W. Smith, "Properties of Ohmic Contacts to Cadmium Sulfide Single Crystals," Phys. Rev. 97, 1525-1530 (1955).

68. Y. T. Sihvonen and D. R. Boyd, "Ohmic Probe Contacts to CdS Crystals," J. Appl. Phys. 29, 1143 (1958).

69. T. L. Zapf, "Calibration of Quartz Transducers as Ultrasonic Power Standards by an Electrical Method," 1974 Ultrasonic Symposium Proceeding, IEEE Cat. #74CH0896-1SU, p. 45-50 (1974).

70. L. L. Foldy and H. Primakoff, "A General Theory of Passive Linear Electroacoustic Transducers and the Electroacoustic Reciprocity Theorem. I," J. Acoust. Soc. Am. 17, 109 (1945).

71. H. Primakoff and L. L. Foldy, "A General Theory of Passive Linear Electroacoustic Transducers and the Electroacoustic Reciprocity Theorem. II," J. Acoust. Soc. Am. 19, 50 (1947).

72. W. R. MacLean, "Absolute Measurement of Sound Without a Primary Standard," J. Acoust. Soc. Am. 12, 140 (1940).

73. E. L. Carstensen, "Self-Reciprocity Calibration of Electro-acoustic Transducer," J. Acoust. Soc. Am. 19, 961 (1947).

74. G. A. Sabin, "Calibration of Piston Transducers at Marginal Test Distances," J. Acous. Soc. Am. 36, 168 (1964).

75. J. M. Reid, "Self-Reciprocity Calibration of Echo-Ranging Transducers," J. Acoust. Soc. Am. 55, 862 (1974).

76. C. Schaefer, "Zur Theorie des Schallstrahlungsdruckes," Ann. Phys. 35, 473-491 (1939).

77. F. Dunn, A. J. Averbuch, and W. D. O'Brien, Jr., "A Primary Method for the Determination of Ultrasonic Intensity with the Elastic Sphere Radiometer," Acustica 38, 58-61 (1977).

78. W. J. Fry and R. B. Fry, "Determination of Absolute Sound Levels and Acoustic Absorption Coefficients by Thermocouple Probes--Theory," J. Acoust. Soc. Am. 26, 294-310 (1954).

79. W. J. Fry and R. B. Fry, "Determination of Absolute Sound Levels and Acoustic Absorption Coefficients by Thermocouple Probes--Experiment," J. Acoust. Soc. Am. 26, 311-317 (1954).

80. S. A. Goss, J. W. Cobb, and L. A. Frizzell, "Effect of Beam Width and Thermocouple Size on the Measurement of Ultrasonic Absorption using the Thermocouple Technique," 1977 Ultrasonic Symposium Proceedings, IEEE #77CH1264-1SU, pp. 206-211.

81. F. Dunn, P. D. Edmonds, and W. J. Fry, "Absorption and Dispersion of Ultrasound in Biological Media," Biological Engineering, H. P. Schwan, ed., (McGraw-Hill, New York 1969), p. 214.

82. R. H. Bube, "Photoconductivity of the Sulfide, Selenide, and Telluride of Zinc or Cadmium," Proceeding of the IRE 43, 1836-1849 (1955).

83. D. E. Goldman and T. F. Heuter, "Tabular Data of the Velocity and Absorption of High-Frequency Sound in Mammalian Tissues," J. Acoust. Soc. Am. 28, 35 (1956); 29, 655 (1957).

84. J. G. Miller, D. E. Yuhas, J. W. Mimbs, S. B. Dierker, L. J. Busse, J. S. Laterra, A. N. Weiss, and B. E. Sobel, "Ultrasonic Tissue Characterization: Correlation Between Biochemical and Ultrasonic Indices of Myocardial Injury," 1976 Ultrasonics Symposium Proceedings, IEEE Cat. #76CH1120-5SU, 33-43 (1976).

85. S. A. Goss, R. L. Johnston and F. Dunn, "Comprehensive Compilation of Empirical Ultrasonic Properties of Mammalian Tissues," J. Acoust. Soc. Am. 64, 423-457 (1978).

86. M. O'Donnell, J. W. Mimbs, and J. G. Miller, "The Relationship Between Collagen and Ultrasonic Attenuation in Myocardial Tissue," J. Acoust. Soc. Am. 65, 512-517 (1979).

87. R. Kuc, M. Schwatz, and L. Von Miesky, "Parametric Estimation of the Acoustic Attenuation Slope for Soft Tissue," 1976 Ultrasonics Symposium Proceedings, IEEE Cat. #76CH1120-5SU, 44-47 (1976).

88. A. C. Kak and K. A. Dines, "Signal Processing of Broadband Pulsed Ultrasound: Measurement of Attenuation of Soft Biological Tissues," IEEE Trans on Biomed. Eng. 25, 321-344 (1978).

89. F. M. Wiener, "Sound Diffraction by Rigid Spheres and Circular Cylinders," J. Acoust. Soc. Am. 19, 444-451 (1947).

90. J. A. Faran, "Sound Scattering by Solid Cylinders and Spheres," J. Acoust. Soc. Am. 23, 405 (1951).

91. R. N. Bracewell and A. C. Riddle, "Inversion of Fan-Beam Scans in Radio Astronomy," The Astrophysical Journal 150, 427 (1967).

92. R. A. Brooks and G. Di Chiro, "Principles of Computer Assisted Tomography (CAT) in Radiographic and Radioisotopic Imaging," Phys. Med. Biol. 21, 689-732 (1976).

93. J. F. Greenleaf, S. A. Johnson, S. L. Lee, G. T. Herman and E. H. Wood, "Algebraic Reconstruction of Spatial Distributions of Acoustic Absorption within Tissue from Their Two-Dimensional Acoustic Projections," Acoustical Holography, Vol. 5, P. S. Green, ed., (Plenum, New York, 1973), p. 591.

94. B. A. Auld, "Acoustic Fields and Waves in Solids," Vol. I (Wiley, New York, 1973).